AER

ATMOSPHERIC & ENVIRONMENTAL RESEARCH, INC.
Cambridge, Massachusetts

OUTER SATELLITE ATMOSPHERES: THEIR NATURE AND PLANETARY INTERACTIONS

Annual Report for Period
March 15, 1980 to May 31, 1981

Prepared for
NASA Headquarters
Washington, DC 20546

Prepared by
William H. Smyth
Atmospheric and Environmental Research, Inc.
840 Memorial Drive
Cambridge, Massachusetts 02139

TECHNICAL REPORT STANDARD TITLE PAGE

1. Report No.	2. Government Accession No.	3. Recipient's Catalog No.
Four		

4. Title and Subtitle	5. Report Date
Outer Satellite Atmospheres: Their Nature and Planetary Interactions	July 1981
	6. Performing Organization Code
7. Author(s) William H. Smyth	8. Performing Organization Report No.
9. Performing Organization Name and Address	10. Work Unit No.
Atmospheric & Environmental Research, Inc. 840 Memorial Drive Cambridge, Massachusetts 02139	11. Contract or Grant No. NASW-3387
	13. Type of Report and Period Covered
12. Sponsoring Agency Name and Address	Annual Report, March 15, 1980 to May 31, 1981
NASA Headquarters Headquarters Contract Division Washington, DC 20546	14. Sponsoring Agency Code HW-2

15. Supplementary Notes

16. Abstract

New modeling capabilities developed and initial model calculations performed are reported for the peculiar directional features of the Io sodium cloud discovered by Pilcher (1980a) and the extended atomic oxygen atmosphere of Io discovered by Brown (1980). Model results to explain the directional feature by a localized emission from the satellite are encouraging, but as yet, inconclusive, whereas for the oxygen cloud, an escape rate of 1-2 x 10^{27} atoms sec^{-1} or higher from Io is suggested. Preliminary modeling efforts have also been initiated for the extended hydrogen ring-atmosphere of Saturn detected by the Voyager spacecraft and for possible extended atmospheres of some of the small satellites located in the E-ring. Continuing research efforts reported for the Io sodium cloud include further refinement in our modeling of the east-west asymmetry data, the asymmetric line profile shape, and the intersection of the cloud with the Io plasma torus. In addition, the completed pre-Voyager modeling of Titan's hydrogen torus is included and the near completed model development for the extended atmosphere of comets is discussed.

17. Key Words (Selected by Author(s))	18. Distribution Statement
satellite atmospheres planetary magnetospheres comets	

19. Security Classif. (of this report)	20. Security Classif. (of this page)	21. No. of Pages	22. Price*
Unclassified	Unclassified	119	

*For sale by the Clearinghouse for Federal Scientific and Technical Information, Springfield, Virginia 22151.

Table of Contents

List of Figures

List of Tables

I. INTRODUCTION

Research efforts this year have been characterized by a strong emphasis in development of new topics while maintaining and continuing the refinement and advance of several important topics established during the last few years. For Jupiter, new modeling capabilities have been developed for the peculiar directional features of the Io sodium cloud discovered by Pilcher (1980a) and for the extended atomic oxygen atmosphere of Io discovered by Brown (1980). For Saturn, preliminary modeling efforts have been initiated for the extended ring atmosphere detected by the UV instrument of the Voyager spacecraft (Broadfoot, et al. 1981) and for possible extended atmospheres of some of the smaller satellites located in the E-ring. Continuing research for Jupiter included a further refinement in the analysis of the east-west asymmetry of the Io sodium cloud (see the attached preprint; Smyth, 1981a), additional exploratory modeling of the shape of the sodium line profile, and improvement in the modeling of the interaction of the Io plasma torus with the Io sodium cloud. Continuing research for Saturn consisted of refinements in the modeling of Titan's hydrogen torus (see the attached reprint; Smyth, 1981b), while continuing research for comets has resulted in the assembly and testing of the computer code for the extended coma atmosphere.

The research reported for the Jupiter and Saturn systems is part of our overall program effort that has been designed not only to make full use of the new data provided by the Voyager and Pioneer 11 spacecrafts in 1979, 1980 and 1981, but also to consider the consistency and relationship of this new data to the substantial data base already available from ground-based, rocket, and Earth-orbiting-satellite observations. For the Jovian planets, model interpretation of these data may be used to obtain important information about the spatial and temporal distribution of extended satellite and ring atmospheres, to characterize and investigate the interaction of the satellites and rings with each other and with the magnetospheres of their parent planets, and to aid in understanding the concentration, energy density and spatial distribution of charged particles in the planetary magnetospheres.

The research effort reported for comets describes our progress in developing a general exospheric model to describe both the gaseous and dust coma. The development of this model was begun in FY 1980 and is now nearing completion. Application of the computer model to cometary data is important since it is one of the primary exploratory methods used to gain information about the composition, chemistry and structure of the comet nucleus.

II. EXTENDED ATMOSPHERES OF IO

Interest in understanding the atmospheres of the outer satellites, their extended natures and their planetary interactions, has grown significantly in the last decade. Major motivation and emphasis of the past few years have been focused upon understanding the extended atmospheres of Io, the innermost Galilean satellite of Jupiter. To date, three different extended neutral atmospheres have been observed for Io: (1) sodium, discovered in 1972 by Brown (1974), (2) potassium, discovered later by Trafton (1975), and (3) atomic oxygen, discovered very recently by Brown (1980). Other extended atmospheres may also exist for Io. The existence of an atomic hydrogen cloud, initially suggested from the measured UV emission near the satellite by the Pioneer 10 spacecraft (Judge and Carlson, 1974; Carlson and Judge, 1974; Judge et al., 1976), remains uncertain (Mekler and Eviatar, 1980) in the light of the more recently discovered UV emissions from the Io plasma torus measured by the Voyager spacecrafts (Broadfoot et al., 1979; Sandel et al., 1979). The detection from Voyager data of gaseous SO_2 on Io (Pearl et al., 1979) and the detection from Voyager data (Broadfoot et al., 1979; Bridge et al., 1979; Warwick et al., 1979) and Earth-based observations (Kupo et al., 1976; Brown, 1978; Pilcher and Morgan, 1979; Pilcher, 1980b; Trauger et al., 1980) of a plasma torus of sulfur and oxygen ions encircling Jupiter, suggest in addition that neutral clouds of SO_2 or

its chemical fragments, other than atomic oxygen, may also be present in the circumplanetary space.

Large numbers of observations of Io's sodium cloud have been obtained during the last seven years from ground-based measurements and this substantial data set is continuing to grow. Our past modeling program for Io has, until this year, concentrated largely upon studying this data set. Several of these studies are important and have been continued. The scope of these original sodium studies has, in the last year, however, been broadened to include the larger spacecraft and ground-based data base now available. This broadened base of modeling serves to both strengthen our past research goals and improve our future capacity to answer fundamental questions about the escape of gases from Io and the energy balance mechanisms operative in the Io plasma torus.

To provide insight and interpretation of these data sets for the extended atmospheres of Io, an active modeling program has been pursued at AER during the past two and one half years. This modeling effort has, however, been in development for about seven years, having its origin at Harvard University in 1973 (see Fang, Smyth and McELroy, 1976; Smyth and McElroy, 1977 and 1978), following the discovery of the Io sodium cloud by Brown (1974). A condensed summary of this past and our future projected research program for the extended atmospheres of Io is given in Table 1.

Table 1

Research Program: Extended Atmospheres of Io

	Past AER Effort			Proposed AER Effort
1. Io Sodium Cloud	1978	1979	1980	1981–1984
(i) 2-D Intensity Distribtuion	Model analysis of 56 2-D images (Smyth & McElroy, 1978)	Discovered solar radiation pressure mechanism (Smyth, 1979)	Constructed 3-D model for solar radiation pressure effects	Investigate effects of the Io plasma torus on 2-D distribution with solar radiation pressure effects
(ii) Line Profile Studies	–	Studied effects of solar radiation pressure and satellite phase angle	Studied correlation of spectral and spatial effects of high-speed sodium emission from Io	Perform model calculation and compare with new data
(iii) Interaction with the Io Plasma Torus	–	Preliminary model calculations for neutral cloud and ion source	2-D plasma torus description developed for sodium cloud model	Improve torus description in sodium cloud model and evaluate its effect
(iv) Peculiar Directional Features	–	–	Developed model to describe local enhanced ejection of sodium	Refinement of model and comparison with data
2. Io Potassium Cloud	–	–	–	Develop and compare model results with new data
3. Other Gas Clouds of Io				
(i) 2-D Intensity Distribtuion of Oxygen and Sulfur; Satellite Ion Source	–	–	Constructed 3-D model for oxygen cloud and its ion source	Continuation under JDAP support
(ii) Exploratory Modeling of new Clouds	–	–	–	Model development and application

A discussion of the progress made in each area of this research during the last year is presented below.

2.1 Io Sodium Cloud

In the past year, modeling of the sodium cloud has continued our past program strategy of emphasizing calculations that are exploratory in nature. These exploratory calculations have addressed four main interrelated areas: (1) modeling the two-dimensional intensity pattern of the cloud as a function of satellite phase angle, (2) modeling the shape of the sodium D-line profiles as a function of satellite phase angle, (3) modeling the interaction of the sodium cloud with the Io plasma torus, and (4) modeling the peculiar directional features of the sodium cloud recently discovered by Pilcher (1980) and also observed by Goldberg et al. (1980). A condensed summary of the past three-year history and the future three-year effort of our research in these four areas is presented in Table 1.

(i) Two-Dimensional Intensity Distribution

The longest and most active sector of our sodium cloud modeling has been in the first area indicated in Table 1, that of describing the two-dimensional spatial intensity of the region B cloud observed in the sky plane (see Figure 1 for an illustration of regions A, B, C1 and C2 of the sodium cloud). During the last two years, modeling efforts for the two-dimensional spatial intensity of the region B cloud

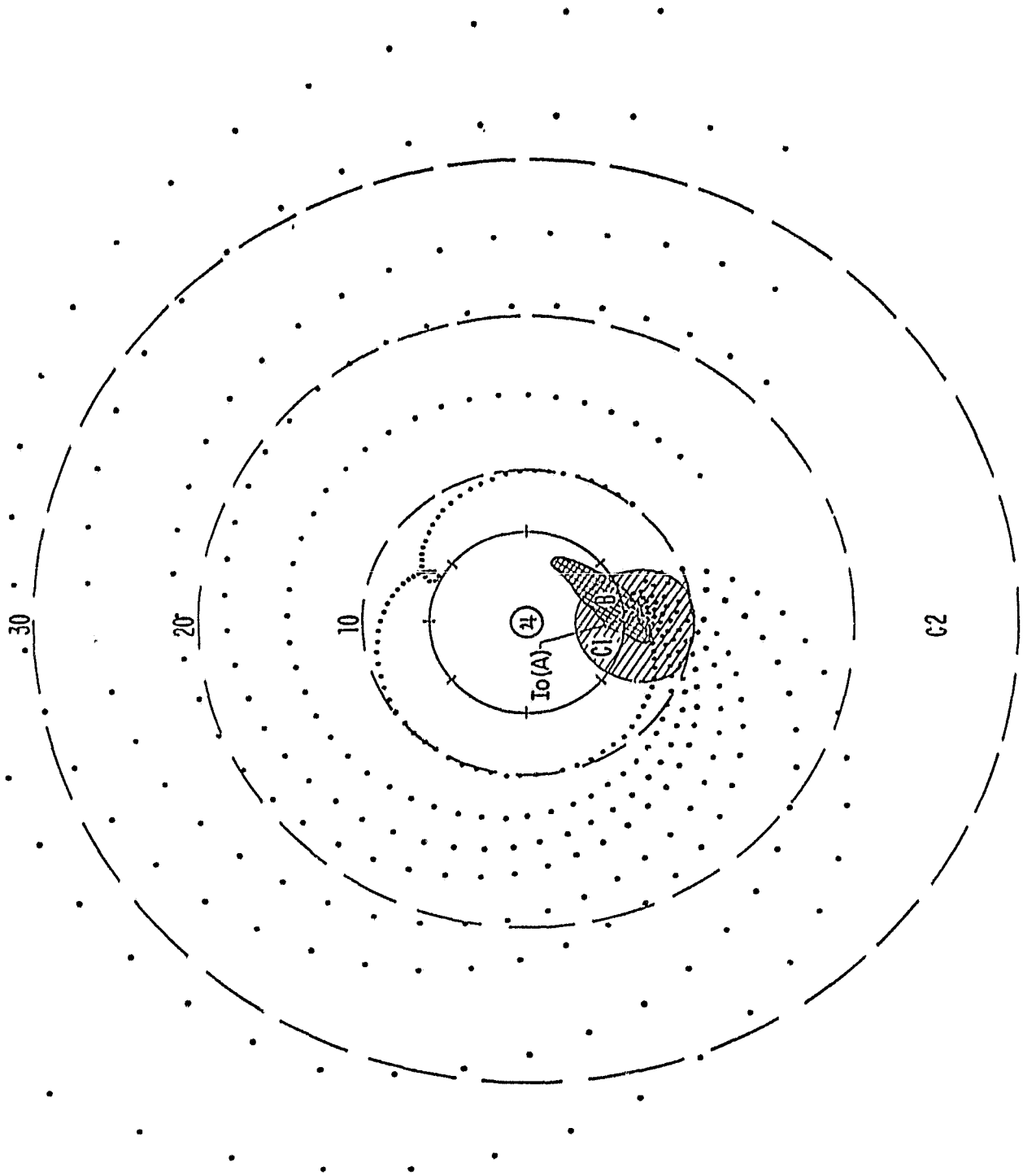

Figure 1: Regions of the Sodium Cloud. Region A (the satellite disc seen from Earth), B, C1 and C2 (the region beyond C1) are depicted in relation to Jupiter, Io's orbit, and the reference circles of radius 10, 20 and 30 Jupiter radii. The dot-plot orbits are for sodium atoms ejected from Io in the forward orbital direction with velocities between 3 and 20 km sec^{-1}.

have been focused upon understanding certain observed spatial east-west asymmetries that occur when data are compared for satellite orbital phase angles separated by 180 degrees. These asymmetries in the absolute intensity (Bergstralh et al., 1975 and 1977) as well as the distribution of spatial intensity (Goldberg et al., 1978; Goldberg, 1979; Goldberg et al., 1981) revealed a small periodic modulation of the sodium cloud about the earlier deduced steady state cloud description of Smyth and McElroy (1978). A significant discovery of our modeling in our previous research year (Smyth, 1979) was that this periodic modulation could be explained by the force extended on sodium cloud atoms as they resonantly scatter sunlight. Since this discovery, the mechanism has been incorporated in our three-dimensional sodium cloud model and calculations have been performed and analysis applied to verify in considerable detail the earlier reported results. The results of this last two years of modeling effort is presented in the paper (Smyth, 1981a), for which a preprint is included in the appendix, and will not be discussed further here. Future modeling efforts, to include the spatial and time dependent sodium cloud sink introduced by the oscillation of the Io plasma torus about the satellite orbit plane, are also discussed in the preprint. This remains as the only major improvement to the model before proper inversion of the east-west asymmetry data may be undertaken.

(ii) Line Profile Studies

The second area of investigation for the sodium cloud in Table 1 is that of studying the shape of the line profiles for D1 and D2 wavelength emissions measured by Earth-based observers. Studies of the line profile data are actually complementary to studies of the two-dimensional spatial intensity data discussed above. This is true since information about different velocity components of the initial velocity distribution of atoms emitted by Io may be more easily obtained from different data sets. The east-west absolute intensity asymmetry data are sensitive to the very low velocity components (Smyth, 1980a), while the line profile data are sensitive to the high velocity components (Smyth and McElroy, 1977; Carlson et al., 1978; Trafton and Macy, 1978; Macy and Trafton, 1980). The two-dimensional sodium cloud image data (which includes the east-west intensity distribution asymmetry data) are sensitive to the intermediate velocity components (Smyth and McElroy, 1978). A balanced approach is required to consistently unlock the velocity distribution from these data.

Our line profile modeling during the past two years has been divided into two parts. The first part is to provide, as a function of satellite phase angle, consistent modeling for both the line profile data and the two-dimensional intensity data (i.e., the region B cloud) within the common emission velocity range where overlap of data exists.

The second part, which has been our major emphasis this year, is to understand, as a function of satellite phase angles, the distribution of higher velocities required, beyond the lower-velocity components needed in describing the region B cloud, to accurately reproduce the larger Doppler shifts observed in the asymmetric line profile skirts. Model results reported last year (Smyth, 1980a) had already shown that the region B cloud (with initial emission velocities less than 3 km sec^{-1}) produces sizeable contributions ($\lesssim$200 ma) to the asymmetric skirt for phase angles less than 70 degrees in the east and less than 250 degrees in the west. These contributions result directly from viewing the velocity dispersion in the forward portion of the region B cloud which, geometrically, is somewhat along the line of sight for these phase angles (see Figure 1). For larger phase angles, however, inherent higher velocity components are required in the initial velocity distribution to match the observed asymmetric line profile skirt. These inherent higher velocity components may be an extension of the normal low-velocity, inner-hemisphere emission mechanism associated with the region B cloud, or may indicate the presence of a collisional-sweeping mechanism driven by the Jupiter magnetospheric wind moving past Io. Both mechanisms, illustrated in Figure 2, are capable of producing the general shape of the line profile for a suitably chosen but different velocity distribution. The performing of model calculations to investigate these two mechanisms has been

Inner Hemisphere Emission

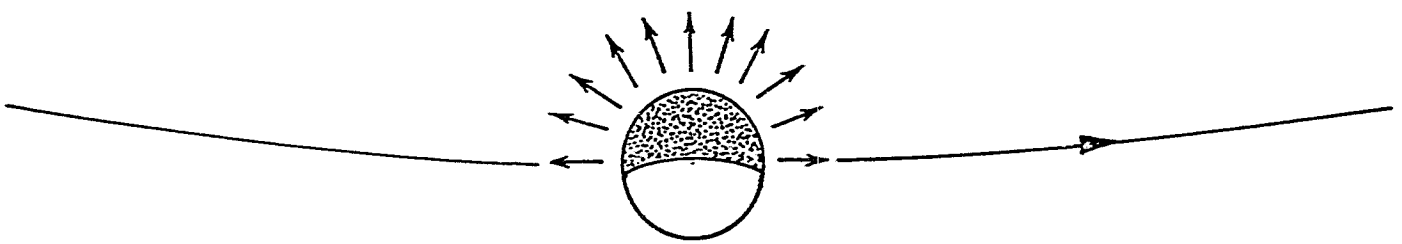

Magnetospheric Wind Emission

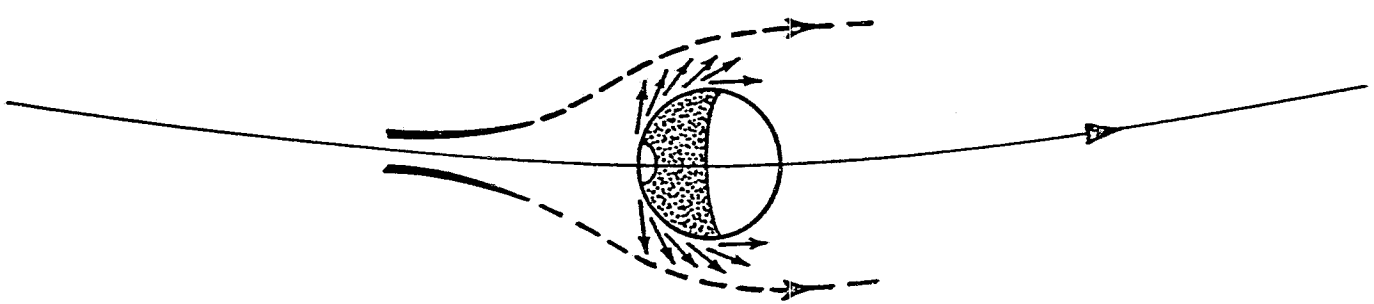

Figure 2: High Speed Emission of Sodium From Io. Two different velocity emission patterns of sodium atoms are illustrated; both of which are capable of producing an asymmetric shirt to the line profile.

our primary emphasis during the past year. Future line profile modeling will continue to examine line profile data to better understand the nature of the inherent higher velocity emission mechanism operative at Io.

(iii) Interaction with the Io Plasma Torus

The third area of investigation for the sodium cloud in Table 1 is that of describing its interaction with the Io plasma torus. The presence of an Io related plasma torus was discovered previous to the Voyager 1 encounter with Jupiter by Kupo et al. (1976) through ground-based measurements of excited state emission from S^+ ions. The presence of a much more complex plasma torus, approximately centered about the centrifugal equatorial plane with the orbital radius of Io, was revealed by the Voyager 1 spacecraft experiments (Broadfoot et al., 1979; Bridge et al., 1979; Warwick et al., 1979) during its encounter with Jupiter. The plasma torus extends radially from about 5 R_J to 7.5 R_J and provides a strong sink for sodium atoms, emitted by Io at 5.9 R_J, through electron impact ionization. The thermal electron component dominates the lifetime process for sodium in the plasma torus. Electrons in the outer warm region (>5.7 R_J), with a number density at 5.9 R_J of order 2000 cm^{-3} and a temperature of about 10^{5}° K (8.6 ev), can easily ionize sodium, with an ionization potential of 5.14 ev, in a time of about one hour. Within the cold inner region (>5.7 R_J), however, the lifetime is significantly larger, having a value

of about 5 hours at 5.5 R_J and increasingly very rapidly for small radial distances from Jupiter. A spatially asymmetric lifetime sink is thus produced in the radial direction near Io's orbit by the plasma torus.

Efforts to incorporate the interaction of the Io plasma torus in our sodium cloud model were initiated during the past year and a half. To date spatial variations of the electron number density within the torus have been described in two-dimensions, radially along and normal to the centrifugal equilibrium plane, with angular symmetry assumed about Jupiter. For simplicity the centrifugal and satellite planes have thus far been assumed to be co-planar. The plasma data (Bagenal and Sullivan, 1981) for Jupiter's magnetosphere, deduced from the Voyager 1 measurements (Bridge et al., 1979), are being used to currently update the plasma properties of Bagenal, Sullivan and Siscoe (1980) adopted earlier in our sodium model. A significant improvement to the sodium model will also result by adopting the more accurate description for the spatial variation of the electron energy distribution deduced by Scudder and Bridge (1981). Efforts to incorporate the oscillation of the plasma torus about the satellite plane will also be initiated in the coming year. These refinements in the description of the plasma torus are necessary in order to correctly specify the spatial and time dependent ionization history of the cloud atoms in the model calculations of the density and D-line intensities of the sodium cloud. Upon completion of these refinements,

definite conclusions about the magnitude of the flux of sodium atoms emitted by Io and the location of preferred areas of enhanced sodium emission from the satellite's exosphere can be deduced by comparison of the model calculations and the cloud data.

(iv) Peculiar Directional Features

The fourth area of investigation for the sodium cloud in Table 1 is that of studying the peculiar directional features recently detected by Pilcher (see Hartline, 1980; Pilcher, 1980a). These features, somewhat faint compared to the bulk of the region B cloud and usually observed outside of Io's orbit, are transient in nature and extend at times over 2.5 Jupiter radii from the satellite. Other feather-like extensions of the B cloud observed by Goldberg et al. (1980) are probably observations of the same phenomena. The features observed by Pilcher suggest that localized regions of the satellite may eject enhanced high-speed streams of sodium atoms with velocities of order 9 km sec^{-1}.

To facilitate study of these directional sodium features a cooperative effort has been established with Pilcher this past year. Upon examination of raw data (Pilcher, 1980c), our standard region B sodium cloud model was modified by adding a localized jet of enhanced high-speed sodium. The intensity of the sodium cloud on the sky plane, as would be seen by an Earth-observer, was calculated using this simple model for various assumptions about the enhanced sodium

stream. Some of these results (see Smyth, 1980b; an attached copy of the presentation is in the appendix, are similar in character to a recurring transient feature observed by Pilcher and strengthen the hypothesis that enhanced streams of sodium may be emitted by Io. The raw data of Pilcher are presently being reduced and will, in the near future, be available for direct comparison with our model results.

2.2 Io Potassium Cloud

The potassium cloud of Io was discovered by Trafton (1975) by observing its emission in the 7665 Å and 7699 Å resonance lines. The detection of potassium emissions was confirmed by measurements of Münch, Trauger and Roesler (1976) and Trauger, Roesler and Münch (1976). Later observations of the potassium cloud by Trafton (1977) suggested that it may be similar to the sodium cloud in many respects, but that its intensity is less bright and also more modulated by the location of the magnetic equator. More recent data for the potassium cloud were reported by Porco, Trauger and Karlson (1980). A significant number of observations (199 spectra) were very recently reported by Trafton (1980) who concluded from preliminary analysis that the potassium cloud and sodium cloud are very similiar in character and may be ejected from the same region of the satellite by the same physical mechanism.

Modeling of the potassium cloud in the past year has not been undertaken because of the lack of available

measurements. The recent number of observations reported by Trafton (1980), however, provides the necessary incentive for developing a potassium cloud model and performing interpretive model calculations. This will be the focus of our potassium cloud research in the coming year.

2.3 New Gas Clouds of Io

In addition to sodium and potassium, several other neutral gas clouds associated with SO_2 and its chemical fragments are likely to exist for Io. To date only an atomic oxygen cloud has been detected from ground-based observation of its 6300 Å emission (Brown, 1980). Exploratory modeling at AER for the oxygen cloud has already been undertaken during the past year. A model for the cloud has been developed to calculate its brightness on the sky plane for oxygen emission lines, both in the visible and ultraviolet, that are excited by electron impact. Preliminary modeling results for the visible 6300 Å emission of the oxygen cloud have already been obtained (see Smyth, 1980b; an attached copy of the presentation is in the appendix) and suggest an atomic oxygen source rate from Io of about $1\text{-}2 \times 10^{27}$ atoms sec^{-1} to explain the observations of Brown (1980). This value of the source rate is, however, only preliminary, and may be larger when proper account of an appropriate velocity dispersion for the oxygen atoms expected from Io is included in the model calculation.

The continuation of this exploratory modeling for oxygen and its expansion to include atomic sulfur will be supported in the future by NASA through the Jupiter Data Analysis Program. Exploratory modeling for other, yet undiscovered gas clouds of Io, will, however, be incorporated as part of our continuing research program here.

III. EXTENDED ATMOSPHERES OF THE SATURN SYSTEM

Interest in extended atmospheres associated with planetary rings and satellites began with studies of the Saturn system over ten years ago. Early ground-based measurements initiated by Franklin and Cook (1969) to search for an atmosphere enveloping Saturn's rings yielded negative results. More recent rocket measurements by Weiser, Vitz and Moos (1977) have detected a hydrogen Lyman-α emission in the vicinity of the planet which may be associated with a hydrogen atmosphere associated with the Saturnian ring system. Such an atmosphere could be produced by photo-sputtering of water ice from the ring material (Carlson, 1980). Very recent measurements of the Saturn system by the UV instrument of the Voyager 1 spacecraft (Broadfoot et al. 1981) confirm the earlier rocket measurements of Weiser, Vitz and Moos (1977) and establish the existence of a hydrogen ring atmosphere.

In addition to Saturn's rings, Titan, the largest satellite of this planet, has been thought capable of generating an extended atmosphere of hydrogen, since it has a local atmosphere containing methane (Kuiper, 1944). Photodissociation of this atmospheric methane followed by atmospheric chemistry and finally thermal escape from Titan of both atomic and molecular hydrogen (Hunten, 1973, 1974; Sagen, 1973; Pollack, 1973) would provide the source, and the gravitational capture of this source by Saturn would

produce a substantial hydrogen torus about the planet (Dennefeld, 1973 and 1974; McDonough and Brice, 1973a and 1973b). A marginal detection of the Titan hydrogen torus was made in 1976 and 1977 and reported by Barker (1977) and Barker et al. (1980) from Lyman-α data obtained from the Earth-orbiting Copernicus satellite. A positive detection of the Titan torus was reported more recently by Judge, Wu, and Carlson (1980) from Lyman-α data obtained by the ultraviolet photometer aboard the Pioneer 11 spacecraft. Very recent confirmation of these two previous measurements has now been established from the very recently obtained UV data of the Voyager 1 spacecraft (Broadfoot et al., 1981).

Additional interest in extended atmospheres of the Saturn system has been generated by the presence of an enhanced plasma density in the vicinity of the Saturn E-ring satellites (Enceladus, Tethys, Dione, and Rhez), which was detected by the plasma and UV instruments of Pioneer 11 (Wolfe et al. 1980; Wu, Judge and Carlson, 1980). The source of these ions could result from sputtering or photodissociation of ices from these satellites (Wolfe et al. 1980). In this case, a situation similar to Io in the Jupiter system may occur for one or more of these E-ring satellites.

Our past modeling program for extended atmospheres in the Saturn system, has until the last year, been limited to describing the extended hydrogen atmosphere of Titan. Our best modeling results, previous to the Voyager 1 encounter with Saturn, were recently reported by Smyth (1980b; 1981b,

see the attached reprint in the appendix). During the past year, development of a model for Saturn's hydrogen ring atmosphere has been initiated and preliminary exploratory modeling for possible extended atmosphere of the E-ring satellites has begun. The efforts reported here represent logical developments of these three areas of investigation. Discussion of progress in each of these areas is presented below and a condensed summary of how this related to our past and future projected research program is included in Table 2.

3.1 Titan's Hydrogen Torus

The three phases of our past modeling of the Titan hydrogen torus are indicated in Table 2. The first phase was the development of the model in 1978. This model represented an improvement over the earlier model of Fang, Smyth and McElroy (1976) by removing their restrictions of a circular symmetric torus about Saturn (the limit of long-lived collisionless gas clouds) and of a massless satellite point source. Results for this new model were first reported by Smyth (1978) and were later refined in 1979. With the encounter of Pioneer 11 with Saturn in the latter part of 1979, new data were available to improve the model calculations. New model results reflecting the Pioneer 11 encounter data were calculated in 1980 and were reported by Smyth (1980b; 1981b, see the attached reprint). These model results suggest that the escape flux of hydrogen atoms from

TABLE 2

RESEARCH PROGRAM: SATURN SYSTEM AND COMETS

	Past AER Effort			Proposed AER Effort
	1978	1979	1980	1981-1984
Extended Atmospheres of the Saturn System				
1. Titan Hydrogen Torus	Model Development	Pre-Pioneer Encounter Model Calculation for Cloud and Ion Source	Post-Pioneer Encounter Model Calculation for Cloud and Ion Source (Smyth, 1981)	Comparison of Model with Voyager Data
2. Saturn Rings	--	--	Model under Development	Comparison of Model with Pioneer and Voyager Data
3. E-Ring Satellite	--	--	Exploratory Calculation Performed	Consider Exploratory Calculation where Warranted by Voyager Data
Extended Atmospheres of Comets	--	--	Model under Development	Incorporation of Model Refinements and Application to Observations

Titan is about $1\text{-}3\times10^{9}$ atoms $cm^{-2}sec^{-1}$ and that the torus is essentially cylindrically symmetric about Saturn, except near the satellite where an enhancement in gas density is indicated. Future modeling efforts will provide interpretative analysis of the Lyman-α observations recently obtained for the Titan torus from the UV instrument of the Voyager 1 spacecraft (Broadfoot et al., 1981) and similar data anticipated from the encounter of Voyager 2 with Saturn.

3.2 Saturn Ring Atmosphere

Saturn's rings have been suspected for many years of having an atmosphere produced by loss of atoms and molecules from surface ices and rocky material. To search for such an atmosphere, Franklin and Cook (1969) observed the rings when the Earth was near the plane of Saturn's ring in 1966. Sunlight reflected from a satellite and passing just over the ring surface, was analyzed for absorption or enhancements by the ring atmosphere. These measurements yielded negative results, providing only an upper limit for the density of sodium vapor surrounding the ring. Estimates for the brightness and abundances of hydrogen atoms and OH radicals in a ring atmosphere were made later by Dennefeld (1973, 1974) assuming various measurements for release and dissociation of surface water ice. Lyman-α brightness for hydrogen of 1.3 Rayleigh, and 3090 Å emission brightness for OH radicals of 6.5 Rayleighs were suggested and based upon production

rates of 7.5×10^{23} atoms sec^{-1} and 3×10^{24} radicals sec^{-1}, respectively.

Detection from rocket measurements of a 200 Rayleigh Lyman-α emission in the vicinity of Saturn was reported by Weiser, Vita and Moos (1977) and provided the first evidence for a hydrogen ring atmosphere. Carlson (1980) indicated that the source rate of about 3×10^{28} atoms sec^{-1}, necessary to explain this observation, could be produced by the mechanism of photo-sputtering of ring water-ice and suggested that the dominant loss process for hydrogen was collision with the rings. He also estimated the mean number density of the ring atmosphere to be about 400 H atoms cm^{-3}, assuming the Lyman-α emission was produced by resonance scattering under optically thin conditions. Very recent measurements of the Saturn system by the UV instrument of the Voyager 1 spacecraft (Broadfoot et al. 1981) also detected the Lyman-α emission of the hydrogen ring atmosphere, with brightness measurements comparing favorably to those of Weiser, Vita and Moos (1977).

To better understand the spatial variation and structure of the hydrogen ring atmosphere and the supply of ring gases to this atmosphere, preliminary modeling efforts have been initiated during the last six months. A model for the extended ring atmosphere has been under construction in which hydrogen is assumed to be emitted from the ring surface, with a prescribed radial flux distribution having

angular symmetry around Saturn. This model is an adaptation of the Titan torus model discussed above. The initial velocity distribution of H atoms at the rings may be prescribed in the model and will depend upon the ejection mechanism operative. Different ejection mechanisms are under evaluation. The lifetime of the ejected hydrogen atoms is also under evaluation, It may depend upon absorption by multi-ring encounters or upon a chemical or ionization loss process. Future efforts will be directed toward completion of the model development and application of the model to ring-atmosphere data.

3.3 E-Ring Satellite Atmospheres

The possibility of the existence of extended atmospheres for the E-ring satellites Tethys and Dione has been raised by analysis of plasma data (Wolf et al. 1980; Frank et al. 1980) and extreme ultraviolet data (Wu, Judge, and Carlson 1980) obtained in the passage of the Pioneer 11 spacecraft through the magnetosphere of Saturn. The plasma data indicated the presence of an enhanced ion density extending from $\sim 4R_S$ to $9R_S$ and approximately bounded by the orbits of Enceladus ($3.97R_S$) and Rhea ($8.78R_S$). Within this plasma torus, two distinct maxima of the ion densities occur, one at the orbit of Tethys ($4.92R_S$) and one at the orbit of Dione ($6.28R_S$). The dominant ion species in the radial intervals from the planet of 4.1-7.1 R_S and 7.1-8.2 R_S have been

identified as O^{2+} and O^{3+}, respectively (Frank et al., 1980). Extreme ultraviolet emissions in the radial interval between 5 and 7 R_S have, in addition, been measured by the UV photometer of Pioneer 11 and associated with excitation of these oxygen ions by electron impact (Wu, Judge and Carlson, 1980). Beyond the plasma torus, in the radial interval 8.2-16 R_S, the dominant ion is H^+.

The source of atoms for the oxygen plasma torus and the proton plasma beyond the torus is not known. Since both Tethys and Dione have water ice on their surfaces (Cruikshank 1979) and the oxygen ion densities are observed to be maximum at the orbital radius of these two satellites, a satellite source is a likely candidate. This suggestion is reinforced by the similarity of the overall nature of the density and temperature of the oxygen plasma torus in the Saturn magnetosphere and the Io plasma torus in the Jupiter magnetosphere. Particularly striking in this regard is the steep gradient in the ion temperature at the inner portion of each torus (Frank et al. 1980; Bagenal and Sullivan 1981). For a satellite source, an extended atmosphere of oxygen or OH molecules, provided by dissociation of surface water and gravitational escape of its chemical products, could upon ionization (or dissociative ionization) be the intermediate link between the satellite and the magnetosphere.

Analysis of the extreme ultraviolet data of Pioneer 11 by Wu, Judge and Carlson (1980) indicated that an ion source

rate of about 8 x 10^{25} sec^{-1} would be required to sustain the oxygen plasma torus emission rate. If the primary source of this oxygen is the satellite Dione, a surface flux of O atoms or OH molecules of about $3x10^{9}$ $cm^{-2}sec^{-1}$ would be required. Such a high flux value is not readily supplied by estimated photo-sputtering surface rates of about $1x10^{8}$ $cm^{-2}sec^{-1}$ (Carlson 1980), but may possibly result by electron impact processes (Wu, Judge, and Carlson 1980), although laboratory data is required to evaluate this physical process. In contrast to the UV data, analysis of the plasma data of Pioneer 11 by Frank et al. (1980) suggested a much lower plasma torus source rate of $1.5x10^{23}$ to $1.5x10^{24}$ oxygen ions sec^{-1}. The analysis of Frank et al. (1980) also favors the Saturn rings as the primary source of the torus plasma and the satellites, Tethys and Dione, as the secondary sources. Preliminary analysis of the newly acquired plasma data from the Voyager 1 spacecraft encounter with Saturn (Bridge et al., 1981) indicates a magnetospheric structure similar to that deduced by Frank et al. (1980), confirming an enhanced density of heavy ions (with a mass-to-charge ratio of 14 to 16 atomic mass units) in the radial interval from 5 to 7 R_S from the planet. Further analysis of Voyager 1 data and future analysis of anticipated Voyager 2 data for the Saturn system should be very useful in better understanding the source of plasma in this planetary magnetosphere.

In the past year, efforts to understand the source of heavy ions in the plasma torus have been restricted to preliminary analysis relating the spatial envelopes of extended atmospheres for the E-ring satellites to the energetics of possible ejection processes. Future efforts for the E-ring satellites will focus upon further analysis to evaluate (1) the existence and structure of extended satellite atmosphere, (2) the importance of these extended atmospheres as a source of magnetospheric ions, and (3) the initial distribution and energy of these satellite ions to the planetary magnetosphere.

IV. EXTENDED ATMOSPHERES OF COMETS

Cometary research represents a broadening and natural extension of our previous modeling of extended satellite atmospheres and was recently undertaken for NASA in FY 1980 Large outer satellites and comets actually represent two extreme cases of solar system bodies which may have extended atmospheres. The large satellites are sufficiently massive that the scale height of a light atmospheric gas such as hydrogen is nearly equal to the satellite radius, so that gravitational escape and formation of an extended atmosphere is just thermally possible. Comets, on the other hand, with their small size and mass, have enormously large hydrogen scale heights compared to their radius, and cannot retain molecules released from their nucleus by solar heating when near the sun. Comets, therefore, create an atmosphere which is by nature always extended. Solar system objects with sizes immediate to the large satellites and comets, such as Tethys and Dione in the Saturn system, may also have extended atmospheres if a source of gaseous material is available from their surfaces.

The extended gaseous atmospheres of comets may be divided into two parts: the inner coma and the outer coma. Each part of the atmosphere has received considerable theoretical investigation. Hydrodynamic models have been constructed to describe the outward flow in the inner coma, since in this region intermolecular collisions dominate.

Exospheric models, based on collision-free trajectories of gas atoms and molecules, have been developed to describe the flow in the outer coma. The thrust of our research effort has been to develop improved exospheric models with sufficient flexibility and accuracy for useful analysis and interpretation of cometary data.

The development of our general exospheric model for comets during the last year has involved the testing and careful assembly of several individually constructed subroutines to form the overall desired computer model. This effort is part of our overall program objective as summarized in Table 2. The model at present is about 90% complete, with the remaining 10% of the program development dependent primarily upon the particular comet atmosphere and the emission scenario to be explored. The general atmospheric model is based upon exact orbit calculations in three dimensions and is suitable for interpretative analysis of both the dust and neutral gaseous components of extended cometary atmospheres. Preliminary test calculations of the assembled model are currently in progress for an extended gaseous atmosphere of comet Halley. The completed exospheric model has been developed to predict the density, column density and intensity of the coma for arbitrary viewing geometry and as a function of heliocentric distance for given source and lifetime conditions. The model should be useful both in refinement of analysis of past cometary data and in

investigation of new data anticipated in future studies of comets. Future efforts will continue implementation of model improvements and subsequent application to comet observations.

V. REFERENCES

Bagenal, F. and Sullivan, J.D. (1981) Direct Plasma Measurement in the Io Torus and Inner Magnetosphere of Jupiter. Preprint (to appear in JGR special Voyager issue).

Bagenal, F., Sullivan, J.D. and Siscoe, G.L. (1980) Spatial Distribution of Plasma in the Io Torus. Geophys. Res. Lett., 7, 41.

Barker, E.S. (1977) Progress Report: Copernicus Observations of Solar System Objects. Presented at the 9th Annual Meeting of AAS/DPS, Honolulu, HI, January 19-22.

Barker, E., Cazes, S., Emerich, C., Vidal-Madjar, A. and Owen, T. (1980) Lyman-Alpha Observations in the Vicinity of Saturn with Copernicus. accepted for publication in Ap. J.

Bergstralh, J.T., Matson, D.L. and Johnson, T.V. (1975) Sodium D-Line Emission from Io: Synoptic Observations From Table Mountain Observatory. Ap. J. Lett., 195, L131.

Bergstralh, J.T., Young, J.W., Matson, D.L. and Johnson, T.V. (1977) Sodium D-Line Emission from Io: A Second Year of Synoptic Observation from Table Mountain Observatory. Ap. J. Lett., 211, L51.

Bridge, H.S. et al. (1979) Plasma Observations Near Jupiter: Initial Results from Voyager 1. Science, 204, 47.

Bridge, H.S. et al. (1981) Plasma Observations Near Saturn: Initial Results from Voyager 1. Science, 212, 217.

Broadfoot, A.L. et al. (1981) Extreme Ultraviolet Observations from Voyager 1 Encounter with Saturn. Preprint (to be published in Science special Voyager issue).

Broadfoot, A.L. et al. (1979) Extreme Ultraviolet Observations from Voyager 1 Encounter with Jupiter. Science, 204, 979.

Brown, R.A. (1980) The Jupiter Hot Plasma Torus: Observed Electron Temperature and Energy Flow. Preprint.

Brown, R.A. (1978) Measurement of SII Optical Emission from Jupiter's Thermal Plasma. Ap. J. Lett., 224, L97.

Brown, R.A. (1974) Optical Line Emission from Io. In Exploration of the Planetary System. Proceedings IAU Symp. No. 65. Torun, Poland, September 5-8, 1973. Woszczyk and Iwaniszewska (eds.) D. Reidel Publ. Co., Dordrecht, pp. 527-531.

Carlson, R.W. (1980) Photo-Sputtering of Ice and Hydrogen Around Saturn's Ring. Nature, 283, 461.

Carlson, R.W. and Judge, D.L. (1974) Pioneer 10 Ultraviolet Photometer Observations at Jupiter Encounter. J. Geophys. Res., 79, 3623.

Carlson, R.W., Matson, D.L., Johnson, T.V. and Bergstralh, J.T. (1978) Sodium D-Line Emission from Io: Comparison of Observed and Theoretical Line Profiles. Ap. J., 223, 1082.

Cruikshank, D.P. (1979) The Surface and Interiors of Saturn's Satellite. Rev. Geophys. Space Phys., 17, 165.

Dennefeld, M. (1974) Theoretical Studies of an Atmosphere Around Saturn's Rings. in Exploration of the Planetary System. Proceedings IAU Symp. No. 65, Torun, Poland, September 5-8, 1973. Woszczyk and Iwaniszewska (eds.) D. Reidel Publ. Co., Dordrecht, pp. 471-481.

Dennefeld, M. (1973) Ph.D. Thesis, University of Paris.

Eddington, A.S. (1910) The Envelopes of Comet Morehouse (1980c). Mon. Not. Roy. Astron. Soc., 70, 442.

Fang, T.-M., Smyth, W.H. and McElroy, M.B. (1976) The Spatial Distribution of Long-Lived Gas Clouds Emitted by Satellites in the Outer Solar System. Planet. Space Sci., 24, 577.

Frank, L.A. Burek, B.G. and Ackerson, K.L. (1980) Plasmas in Saturn's Magnetosphere. J. Geophys. Res., 85, 5695.

Franklin, F.A. and Cook, A.F. II (1969) A Search for an Atmosphere Enveloping Saturn's Rings. Icarus, 10, 417.

Goldberg, B.A. (1979) Private communication.

Goldberg, B.A., Carlson, R.W., Matson, D.L. and Johnson, T.V. (1978) A New Asymmetry in Io's Sodium Cloud. Bull. AAS, 10, 579.

Goldberg, B.A., Mekler, Yu., Carlson, R.W., Johnson, T.V. and Matson, D.L. (1980) Io Sodium Emission Cloud and the Voyager 1 Encounter. Icarus, 44, 305.

Goldberg, B.A., Carlson, R.W., Johnson, T.V., Lorre, J., Matson, D.L., and Young, J.W. (1981) Io Sodium Cloud Revisited. EOS, 62, 316.

Hartline, B.K. (1980) Voyager Beguiled by Jovian Carrousel. Science, 208, 384.

Hunten, D.M. (1974) Blowoff and Escape of H_2. in The Atmosphere of Titan. NASA SP-340, p. 110.

Hunten, D.M. (1973) The Escape of H_2 from Titan. J. Atmos. Sci., 30, 726.

Judge, D.L. and Carlson, R.W. (1974) Pioneer 10 Observations of the Ultraviolet Glow in the Vicinity of Jupiter. Science, 183, 317.

Judge, D.L., Carlson, R.W., Wu, F.-M. and Hartmann, U.G. (1976) Pioneer 10/11 Ultraviolet Photometer Observations of the Jovian Satellites. In Jupiter, Studies of the Interior, Atmosphere, Magnetosphere and Satellites. Gehrels (ed.) The University of Arizona Press, Tucson, AZ, p. 1068.

Judge, D.L., Wu, F.-M., Carlson, R.W. (1980) Ultraviolet Photometer Observations of the Saturnian System. Science, 207, 431.

Kuiper, G.P. (1944) Titan: A Satellite with an Atmosphere. Ap, J., 100, 378.

Kupo, I., Mekler, Yu. and Eviatar, A. (1976) Detection of Ionized Sulfure in the Jovian Magnetosphere. Ap. J., 205, L51.

Macy, W. and Trafton, L. (1980) The Distribution of Sodium in Io's Cloud: Implications. Icarus, 41, 131.

McDonough, T.R. and Brice, N.M. (1973a) New Kind of Ring and the Recycling of Titan's Atmosphere. Icarus, 20, 136.

McDonough, T.R. and Brice, N.M. (1973b) A Saturnian Gas Ring and the Recycling of Titan's Atmosphere. Icarus, 20, 136.

Mekler, Yu. and Eviatar, A. (1980) Time Analysis of Volcanic Activity on Io by Means of Plasma Observations. J. Geophys. Res. (in press).

Münch, G., Trauger, J. and Roesler, F. (1976) Interferometric Studies of the Emissions Associated with Io. Bull. AAS, 8, 468.

Pearl, J. et al. (1979) Identification and Gaseous SO_2 and New Upper Limits for Other Gases on Io. Nature, 280, 755.

Pilcher, C.B. (1980a) Transient Sodium Ejection from Io. Bull. AAS, 12, 675.

Pilcher, C.B. (1980b) Images of Jupiter's Sulfur Ring. Science, 207, 181.

Pilcher, C.B. (1980c) Private communication.

Pilcher, C.B. and Morgan, J.S. (1979) Detection of Singly Ionized Oxygen around Jupiter. Science, 205, 297.

Pollack, J.B. (1973) Greenhouse Models of the Atmosphere of Titan. Icarus, 19, 43.

Porco, C., Trauger, J. and Karlson, R.W. (1980) A Comparison of Sodium and Potassium Velocity Dynamics near Io. Presented at The Satellites of Jupiter IAU Collog. No. 57, Kailua-Kona, HI, May 13-16.

Sagan, C. (1973) The Greenhouse of Titan. Icarus, 18, 649.

Sandel, B.R. et al. (1979) Extreme Ultraviolet Observations from Voyager 2 Encounters with Jupiter. Science, 206, 962.

Scudder, J.D. and Bridge, H.S. (1981) A Survey of the Plasma Electron Environment of Jupiter: A View from Voyager. Preprint (to appear in JGR special Voyager issue).

Smyth, W.H. (1981a) Io's Sodium Cloud: Explanation of the East-West Asymmetries II. Submitted to Ap. J.

Smyth, W.H. (1981b) Titan's Hydrogen Torus. Ap. J. 246, 344.

Smyth, W.H. (1980a) The Extended Sodium Atmosphere of Io. Presented at The Satellites of Jupiter IAU Collog. No. 57, Kailua-Kona, HI, May 13-16.

Smyth, W.H. (1980b) Modeling of Neutral Satellite Gas Clouds - Recent Advances. Bull. AAS, 12, 674.

Smyth, W.H. (1979) Io's Sodium Cloud: Explanation of the East-West Asymmetries. Ap. J., 234, 1148.

Smyth, W.H. (1978) Extended Hydrogen Atmospheres of the Outer Satellites. Bull. AAS, 10, 577.

Smyth, W.H. and McElroy, M.B. (1978) Io's Sodium Cloud: Comparison of Models and Two-Dimensional Images. Ap. J., 226, 336.

Smyth, W.H. and McElroy, M.B. (1977) The Sodium and Hydrogen Gas Clouds of Io. Planet. Space Sci., 25, 415.

Trafton, L. (1980) Observations of Potassium Emission Near Io. Bull. AAS, 12, 673.

Trafton, L. (1977) Periodic Variations in Io's Sodium and Potassium Clouds. Ap. J., 215, 960.

Trafton, L. (1975) Detection of a Potassium Cloud Near Io. Nature, 258, 690.

Trafton, L. and Macy, W. (1978) On the Distribution of Sodium in the Vicinity of Io. Icarus, 33, 322.

Trauger, J.T., Münch, G. and Roesler, F.L. (1980) A Study of the Jovian [SII] Nebula at High Spectral Resolution. Ap. J., 236, 1035.

Trauger, J., Roesler, F. and Münch, G. (1976) Velocity Structure in the Sodium Emission from Io. Bull. AAS, 8, 468.

Warwick, J.W. et al. (1979) Voyager 1 Planetary Radio Astronomy Observations Near Jupiter. Science, 204, 55.

Weiser, H. Vita, R.C. and Moos, H.W. (1977) Detection of Lyman-α Emission from the Saturnian Disk and from the Ring System. Science, 197, 755.

Wolfe, J.H., Mihalov, J.D., Collard, H.R., McKibbin, D.D., Frank, L.A. and Intriligator, D.S. (1980) Preliminary Results on the Plasma Environment of Saturn from the Pioneer 11 Plasma Analyzer Experiment. Science, 207, 403.

Wu, F.M., Judge, D.L. and Carlson, R.W. (1980) Observations of Extreme Ultraviolet Emissions from the Saturnian Plasmasphere. J. Geophys. Res., 85, 5853.

APPENDIX A

TITAN'S HYDROGEN TORUS

THE ASTROPHYSICAL JOURNAL, 246:344–351, 1981 May 15

TITAN'S HYDROGEN TORUS

WILLIAM H. SMYTH
Atmospheric and Environmental Research, Inc., Cambridge, Massachusetts
Received 1980 September 24; accepted 1980 December 2

ABSTRACT

A new model is presented for Titan's hydrogen torus, capable of describing its time evolution under the influence of the gravitational fields of both the satellite and planet. This description is valid when there are no collisions between cloud atoms. It represents an improvement over earlier models, where attention was restricted to a long-lived, collisionless gas cloud exhibiting circular symmetry about Saturn and to a massless, satellite point source. In this model, the lifetime of the gas cloud is limited by ionization impact of hydrogen atoms with the solar wind and planetary magnetospheric plasma and is estimated from *Pioneer 11* data to be of the order of 10^7 s. For this lifetime value, measurements of the solar-resonance–scattered Lα intensity of the torus, obtained both by the Earth-orbiting *Copernicus* satellite and by the UV instrument of *Pioneer 11*, suggest that the hydrogen torus completely surrounds Saturn but that it is not cylindrically symmetric about the planet. This lack of symmetry is caused by the finite lifetime of hydrogen atoms in the planetary magnetosphere/solar-wind environment. The time-evolution torus model is thus introduced for data interpretation. The measured vertical extent of the torus suggests that hydrogen atoms are emitted from Titan's exosphere with velocities near, and only slightly in excess of, the satellite escape speed. Titan's gravitational field is therefore explicitly included. Modeling results presented provide an explanation for the basic features present in both Lα measurements and suggest a satellite escape flux of $1-3\times10^9$ atoms cm^{-2} s^{-1} and a hydrogen torus containing of the order of 10^{34} atoms.

Subject headings: planets: magnetospheres — planets: satellites — planets: Saturn

I. INTRODUCTION

Titan, the largest satellite of Saturn, is known to have an atmosphere containing large detectable concentrations of CH_4 (Kuiper 1944) and perhaps H_2 (Trafton 1972), although more recent measurements (Münch, Trauger, and Roesler 1977) make the latter detection less certain. Infrared spectra of Titan's atmosphere by Gillett, Forrest, and Merrill (1973), showing a pronounced peak at 12 μm, also suggest the presence of C_2H_6. Photochemical processes in Titan's atmosphere, in addition to being able to produce C_2H_6 and other heavy hydrocarbons (Strobel 1974), may also provide large escape fluxes of hydrogen atoms and molecules to the space around Saturn (Hunten 1973, 1974; Sagan 1973; Pollack 1973; McDonough and Brice 1973).

McDonough and Brice (1973) first noted that most of the hydrogen escaping Titan would be gravitationally bound to Saturn and would form a toroidal-shaped gas cloud around the planet. They suggested that this hydrogen torus might be optically detectable from Earth orbit and estimated its density to be between 1 and 10^3 atoms or molecules cm^{-3}. They also noted that the actual density and spatial distribution of the torus were functions of the Titanian atmospheric escape flux, the radius and temperature of the exosphere, and the size and strength of Saturn's magnetosphere, which, through charged-particle collisions, could provide the dominant loss process for hydrogen. McDonough and Brice (1973) also noted that satellite recapture of the hydrogen ring might provide an additional loss process for the torus as well as a recycling mechanism to decrease the effective net atmospheric-gas loss rate of Titan. Later work (Hunten 1974), however, disputed the recycling idea but not the concept of a torus.

A marginal detection of Titan's hydrogen torus was made in 1976 and 1977 and reported by Barker (1977) and Barker *et al.* (1980) from Lα data obtained from the Earth-orbiting *Copernicus* satellite. These measurements suggest a Lα brightness of about 200 ± 100 rayleighs near Titan resulting from resonance scattering of sunlight by torus hydrogen atoms. Recently, a positive detection of the Titan-associated hydrogen cloud was reported by Judge, Wu, and Carlson (1980) from Lα data obtained by the ultraviolet photometer aboard the *Pioneer 11* spacecraft during its encounter with Saturn. The *Pioneer 11* measurements indicated the vertical extent of the cloud to be about 1.5 Saturn radii above and below the satellite plane and indicated an angular extent of the cloud along the satellite orbit of at least 5 Saturn radii from Titan's disk. A complete hydrogen torus may exist at a weaker signal, but the limited *Pioneer 11* data preclude a more definitive statement on the angular

extent of the cloud. The observed angular extent, however, indicates that hydrogen is definitely in orbit about Saturn since the Lagrange sphere of Titan, the region inside which the gravitational field of the satellite dominates the planetary gravitational field, has a radius of only 0.88 Saturn radii. A complete torus is therefore anticipated given the relatively long lifetime estimate of 10^7 s for hydrogen atoms in the planetary environment near Titan's orbit (Judge, Wu, and Carlson 1980). The absolute Lα intensity of the torus measured by *Pioneer 11* is difficult to determine because of sensitivity changes in the instrument during the encounter, but a preliminary estimate of 100 rayleighs has been given (Judge, Wu, and Carlson 1979).

In this paper, earlier models for the Titan torus are reviewed in § II. The new model for Titan's hydrogen torus used to interpret both the limited *Copernicus* and *Pioneer 11* measurements is presented in § III. Improved measurements of the hydrogen cloud are anticipated during the encounters of *Voyager 1* and *Voyager 2* with the Saturn system. The results presented here should be helpful in preliminary evaluation of the *Voyager* data.

II. EARLIER MODELS FOR THE TITAN TORUS

Models for Titan's toroidal gas clouds, based upon very simple, collisionless, orbital analysis of long-lived escaping gases, were first advanced by McDonough and Brice (1973) and by Dennefeld (1974). These models essentially sought to calculate an average toroidal gas density $\bar{n}$,

$$\bar{n}=\frac{Q\tau}{V},$$

by estimating the volume V of an angularly symmetric torus about Saturn, the satellite emission rate Q (atoms or molecules per second), and the lifetime τ of the orbiting gas in the planetary environment. Results of these calculations are summarized in Table 1. The emission rate may be alternatively expressed in terms of a satellite escape flux ϕ (atoms or molecules $cm^{-2}\,s^{-1}$),

$$Q=\phi S,$$

where S is the satellite surface area.

McDonough and Brice (1973) considered a range of emission rates (Trafton 1972) for the escaping gases and also different lifetime limiting processes. They estimated the toroidal volume to be of the order of the cube of Titan's orbital radius and concluded that gas densities were probably in the 1 to 10^3 atoms or molecules cm^{-3} range. Dennefeld (1974), using an assumed escape speed of 1.5 km s^{-1} to estimate the toroidal volume shown in Figure 1 and adopting reasonable lifetime and emission-rate values, determined a mean hydrogen-atom density of 15 cm^{-3}. For a smaller toroidal volume element containing Titan (about 1/15 of that estimated for V), Dennefeld (1974) determined the density to be about 3 times the mean density. Along a line of sight in the satellite plane, he then estimated that such an elevated hydrogen density would produce an optical depth of 4. Assuming, however, that one could see only up to 1 optical depth, Dennefeld (1974) then estimated the Lα brightness to be 95 rayleighs. This conversion of column density to optical depth and to solar-resonance-scattered Lα intensity can be seen to correspond to hydrogen with an effective gas temperature of 500 K from the radiative transfer results of McElroy and Yung (1975), which are shown here in Figure 2, properly scaled for Saturn's distance.

TABLE 1

MODELS FOR TITAN'S TOROIDAL GAS CLOUDS

	Emission velocity (km/sec)	Estimated torus volume V (cm^3)	Lifetime τ of H atoms (sec)	Satellite emission rate Q (atoms sec^{-1})	ϕ (atoms $cm^{-2}sec^{-1}$)	Estimated cloud density (cm^{-3})	Lyman-α brightness (Rayleighs)
McDonough and Brice (1973)	1.4	1.7×10^{33}	1.9×10^{8} †	2×10^{26}-4×10^{29}	2.5×10^{8}-5×10^{11}	10-10^5	—
	"	"	recapture	"	"	10-10^3	—
	"	"	~10^7 ‡	"	"	1-10^3	—
Dennefeld (1974)	1.5	1.5×10^{35}	1.5×10^{8} †	1.5×10^{28}	1.9×10^{10}	15	95
Fang et al (1976)	*	—	2×10^{8} †	2.4×10^{27}	3×10^{9}	0.5-2.5×10^3	~1000

† Photoionization and solar-wind charge exchange

‡ Co-rotating magnetosphere

* 100°K Maxwell-Boltzmann distribution

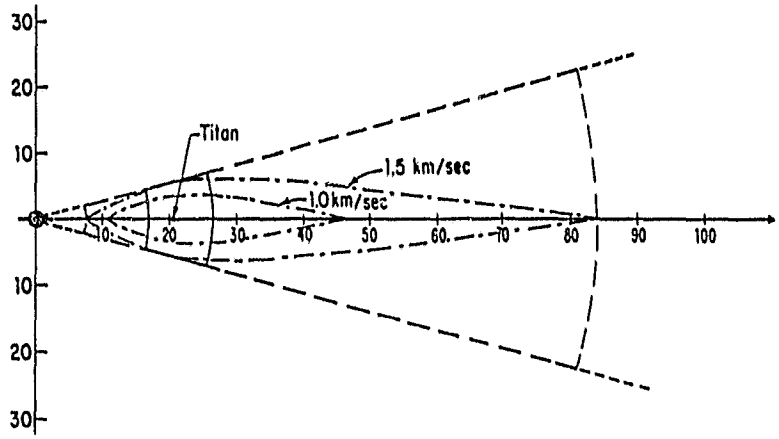

FIG. 1.—Torus Cross sections. Several cross sections of the torus volume in a plane containing Saturn and normal to Titan's orbit plane : shown, where vertical and radial coordinates are in planetary radii. Dennefeld's overestimated torus volume V and smaller adopted lume correspond to the trapezoidal-like cross sections indicated by the heavy dashed lines and solid lines, respectively. For comparison, the rrect cross sections, occupied by atoms emitted isotropically by a moving, massless, Titan point source, are calculated by the author and licated by the long-short dashed lines for the two emission speeds of 1.0 and 1.5 km s^{-1}.

An unpublished model for Titan's torus which treats : extreme high-density limit of a long-lived gas cloud .s developed by Sullivan (1973) using a collision-minated fluid description. Densities in this case were imated between 10^5 and 10^{11} cm^{-3}, depending upon : assumed details. The existence of such a dense torus unlikely, since heating supplied by absorption of solar raviolet below 800 Å will cause the torus to decay in : order of a year, while the refilling time is of the der of 2×10^4 years (Huten 1977). Densities around ^{3} cm^{-3} or less are far less objectionable.

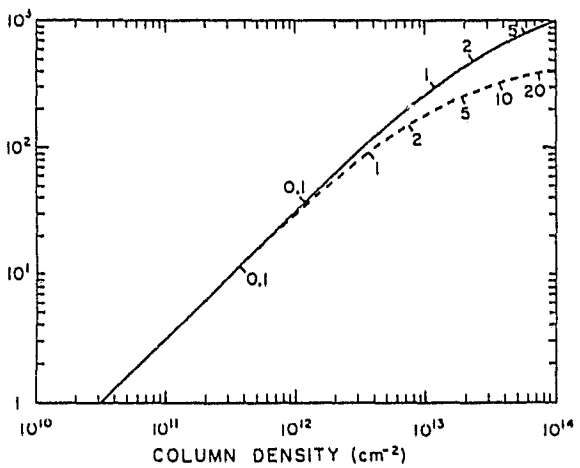

FIG. 2.—Solar-Resonance-Scattering Radiative Transfer odel for H Lα Emission. The radiative transfer results for H mputed by McElroy and Yung (1975) are shown, scaled to turn, for an effective gas temperature of 5000 K (*solid curve*) d 500 K (*dashed curve*). The optical depth of the gas is indicated labeled tick marks on each curve.

The general problem of long-lived gas clouds emitted by satellites was discussed from the orbital mechanics perspective by Fang, Smyth, and McElroy (1976). In their treatment, the gravitational field of the satellite was ignored, and a model for the cloud density was then developed within a two-body orbital mechanics context. Their paper also presented the first, detailed, three-dimensional model calculations for an angularly symmetric Titan torus. Normalized, two-dimensional, number-density profiles of hydrogen in the cross-sectional plane containing Saturn and perpendicular to the satellite plane were calculated for an effective emission temperature of 100 K. Real number densities were then obtained by multiplying the normalized number densities by the total number of particles in the cloud, which requires specification of the lifetime and satellite flux of hydrogen atoms. Results for the number density and the solar-resonance–scattered, Lα intensity of the torus are given in Table 1 for their adopted values of the satellite emission rate and lifetime. The mean density values indicated correspond to their extreme outer and inner contours. Their Lα cloud brightness of 1000 rayleighs is obtained by averaging the corresponding column density over a square area, 2 Saturn radii on a side, approximately centered on Titan, and by using the radiative transfer results of Figure 2 for an effective gas temperature of 5000 K.

All of the models discussed above have in common two simplifying physical assumptions: (1) the toroidal cloud is long-lived; and (2) the satellite may be treated as a massless point source. The first assumption restricts attention to angularly symmetric toroidal gas clouds about the central planet. The second assumption simply neglects the gravitational field of the satellite and is

strictly correct only in the limit of high gas-emission temperatures or low satellite mass. For Titan, the second assumption is approximately valid if the point source is considered to represent the velocity of the emitted gas as it escapes through the Lagrange sphere of the satellite, where the gravitational field of Titan is roughly neutralized by Saturn.

In order to define more clearly and quantitatively what is meant by a long-lived torus, Fang, Smyth, and McElroy (1976) used the concept of an angular diffusion velocity for the gas torus relative to the satellite introduced earlier by Carlson and Judge (1975). These authors noted from simple, two-body, orbital analysis that gases escaping from the satellite into a collisionless planetary environment would diffuse both ahead and behind the satellite. Gases emitted from the leading face of the satellite would have periods larger than the Titan period and, consequently, would eventually trail the satellite and populate the space outside of the satellite orbit. Gases emitted from the trailing face would have a smaller period than Titan and would eventually appear to precede Titan and populate the space within the satellite's orbit about Saturn. Assuming isotropic emission of gas from a satellite point of source with a Maxwell-Boltzmann speed distribution, Fang, Smyth, and McElroy (1976) defined an average, forward, angular diffusion velocity $\bar{\Omega}_F$ and an average, backward, angular diffusion velocity $\bar{\Omega}_B$ for the gas cloud.

For the Titan torus, these averaged, forward and backward, angular diffusion velocities are given in Figure 3 as a function of the ratio of the effective temperature of the emitted gas to the atomic weight of the emitted gas, and are compared with an approximate expression for the average angular diffusion velocity:

$$\bar{\Omega} = \frac{3}{a}\left(\frac{2kT}{\pi m}\right)^{1/2}.$$

Here a is the orbital radius of the satellite, while T is the effective temperature, and m is the mass of the atoms emerging from the Lagrange sphere with an average speed $\bar{V}$, relative to the satellite, given by

$$\bar{V} = \left(\frac{2kT}{\pi m}\right)^{1/2}.$$

For continuous emission, the forward and backward clouds will travel through an angular distance of 360° with respect to Titan in a time interval $\tau^D_{F,B}$ of the order of

$$\tau^D_{F,B} = \frac{2\pi}{\bar{\Omega}_{F,B}}.$$

Angular symmetry should be an excellent approximation for hydrogen atoms in the Titan torus if the hydrogen lifetime in the Saturn environment is long compared with either τ^D_F or τ^D_B. For an effective escape speed $\bar{V}$ of the order of 1 km s^{-1} or a temperature T of the order of 200 K for hydrogen atoms, the average, forward and backward, angular diffusion times, $\tau^D_{F,B}$, for the Titan torus are, respectively, 3.0×10^6 s (or 835 hr) and 2.9×10^6 s (or 807 hr).

To determine how angularly symmetric the Titan hydrogen torus may be, these diffusion times must be compared with the photoionization and charge-exchange lifetimes of hydrogen atoms operative near the satellite orbit. The photoionization lifetime at Saturn's distance is estimated (Gross and Rasool 1964; McDonough and Brice 1973; Carlson, Matson, and Johnson 1975) to be about $1-2\times10^9$ s. This process is, however, dominated by charge-exchange of hydrogen atoms with either solar-wind or planetary-magnetospheric protons.

Analysis prior to the *Pioneer 11* encounter with Saturn (Siscoe 1978) suggested that Titan's orbit might be contained wholly in the planetary magnetosphere, with an estimated corotating proton density of 1.7 cm^{-3} providing a proton flux of 3.4×10^7 cm^{-2} s^{-1} and a charge-exchange lifetime of 8.4×10^6 s (2300 hr). Analysis of the *Pioneer 11* data (Smith *et al.* 1980), however, has shown that the location of the Sunward boundary of the magnetosphere is sensitive to the varying, solar-wind dynamic pressure and occurred, at times, within the orbit of Titan. When the magnetopause is compressed within the orbit of Titan, the hydrogen lifetime along the unprotected orbit will be characterized by the solar-wind plasma having a bulk speed of about 500 km s^{-1}

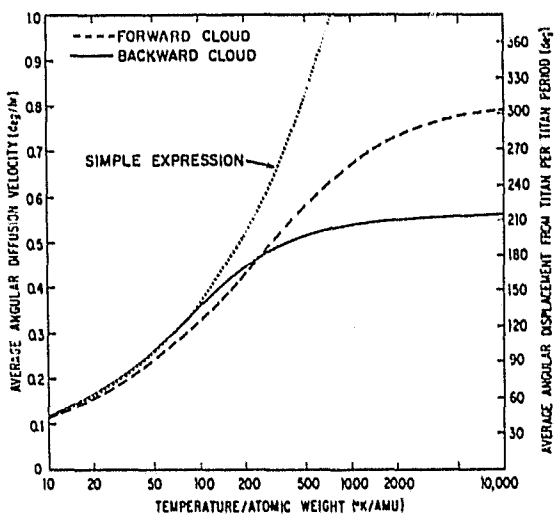

FIG. 3.—Forward and Backward, Angular Diffusion Velocities of Titan's Torus. The average diffusion velocities $\bar{\Omega}_F$ and $\bar{\Omega}_B$ are both compared with the simple expression $\bar{\Omega}$, where the ratio of the temperature to the atomic weight of the emitted atoms is the independent variable.

and a proton density fluctuating between about 0.2 to 0.3 cm^{-3} (Wolfe *et al.* 1980). This gives a lifetime varying between about $5.0-3.3\times10^7$ s. If, however, the orbit of Titan lies wholly within the magnetosphere, the hydrogen lifetime is determined by the corotating plasma ($\sim$200 km s^{-1}) with a *Pioneer 11* estimated proton density of $0.2-1.0$ cm^{-3} (Frank 1980) and has a value between $7.1-1.4\times10^7$ s.

The lifetime of hydrogen atoms in Titan's torus could thus be as short as a few of the diffusion times ($\tau_{F,B}^{\mu}$) or as long as about 25 diffusion times. For the smaller lifetime value ($\sim10^7$ s), a complete but angularly unsymmetrical torus about Saturn with an enhanced density near the satellite would be produced. Such a torus could provide an explanation for both the brighter hydrogen torus observed somewhat parallel to the satellite plane by the Copernicus satellite (Barker *et al.* 1980) and the less bright and spatially limited torus observed somewhat normal to the satellite orbit by *Pioneer 11* (Judge, Wu, and Carlson 1980). To roughly estimate the brightness of such a torus viewed parallel to Titan's orbit plane, the above smallest lifetime value of 1.4×10^7 s is used in the angularly symmetric model results of Fang, Smyth, and McElroy (1976) instead of their adopted value of 2×10^8 s. This changes their hydrogen column estimate near Titan from 1×10^{14} cm^{-2} to 7×10^{12} cm^{-2} and corresponds to a change in the optical depth from about 8 to 0.6 using the results of Figure 2 for an effective gas temperature of 5000 K. Their estimated Lα intensity of the Titan torus near the elongation point of the satellite orbit is reduced from 1000 rayleighs to about 190 rayleighs and is thus brought into good agreement with the intensity observations of Barker *et al.* (1980). Using the radiative transfer results in Figure 2 for the lower effective gas temperature of 500 K, the Lα intensity would be reduced to 145 rayleighs. The actual or appropriate temperature for the hydrogen gas is not known, but depends upon the velocity dispersion that atoms exhibit because of their orbital motion in the planetary environment. The effective gas temperature produced by this velocity dispersion varies over the spatial dimensions of the hydrogen cloud, but is likely bracketed by the high and low temperature results of Figure 2.

A lifetime value of 1×10^7 s corresponds to about 3.4 diffusion periods for hydrogen atoms in the torus and, using the calculations of Fang, Smyth, and McElroy (1976), results in a torus number density in the satellite plane ranging from a maximum value of about 125 cm^{-3} at Titan's orbit to a value of about 2.5×10^{-2} cm^{-3} at radial distances of 5 and 60 planetary radii from Saturn. The collisional mean free path of hydrogen atoms in the torus, assuming a cross section of 3×10^{-15} cm^2 and a number density of 125 cm^{-3}, is also about 3.4 Titan orbital circumferences. For lifetimes substantially longer than 10^7 s, collisions will therefore begin to be important in the center of the torus. Eventually, the collisionless assumptions adopted here will no longer be valid if the lifetime, for fixed emission conditions, is increased sufficiently. The analysis which follows lies within these permissible bounds.

III. A NEW MODEL FOR THE TITAN TORUS

To better understand the spatial distribution of hydrogen in the Titan torus, a model capable of explicitly describing its time evolution is required. Such a model is introduced here. In addition to removing the long-lived time restriction of earlier models, the assumption of a massless, satellite point source will also be relaxed by explicitly calculating the trajectories of hydrogen atoms emitted from the satellite exosphere in the combined gravitational fields of Titan and Saturn. The initial effects on the motion of hydrogen atoms and also the later effects of near encounter or actual atom recapture, which are introduced by Titan's gravitational field within the Lagrange sphere of the satellite, are therefore explicitly included. The model is similar in detail to the model developed for the extended gas clouds of Io (Smyth and McElroy 1977, 1978) and is based upon solving the well-known, circular-restricted, three-body equations of motion in three dimensions for emitted hydrogen atoms.

Key input parameters for the model are: (1) the lifetime of hydrogen atoms in the Saturn environment; (2) the escape flux of hydrogen from the satellite; (3) the exosphere radius; and (4) the mean satellite emission velocity. A value for the lifetime of the order of 10^7 s was estimated in § II. A lifetime of 2×10^7 s (5600 hr) is adopted here and represents a physically realistic value for exploring the amount of angular asymmetry in the Titan torus. The escape flux of hydrogen atoms from Titan is controlled by chemistry (Strobel 1974) and by the processes of vertical transport operative in the atmosphere (Hunten 1973). A photochemical-driven conversion of CH_4 into other heavy hydrocarbons such as C_2H_6, C_2H_4, and C_2H_2 will determine the relative abundance of H and H_2 and suggests (Strobel 1979) an escape flux ratio $H:H_2$ in the range 1:9 to 3:7. Assuming a combined escape flux for both H and H_2 of about 10^{10} cm^{-2} s^{-1}, based on the satellite surface area, provides an upper limit hydrogen-atom escape flux of 3×10^9 cm^{-2} s^{-1} and is adopted here for model calculations. Estimates of the radius of Titan's exosphere range from 4×10^3 to 10^4 km (Tabarié 1974), and a nominal value of 5000 km is adopted. A mean emission velocity of 2.0 km s^{-1} from this exosphere is assumed and provides the hydrogen atoms with sufficient energy so that they escape from the Lagrange sphere of Titan with a characteristic velocity of about 1 km s^{-1}. Hydrogen atoms escaping the Lagrange sphere with this velocity produce a visible toroidal cloud with a vertical extent

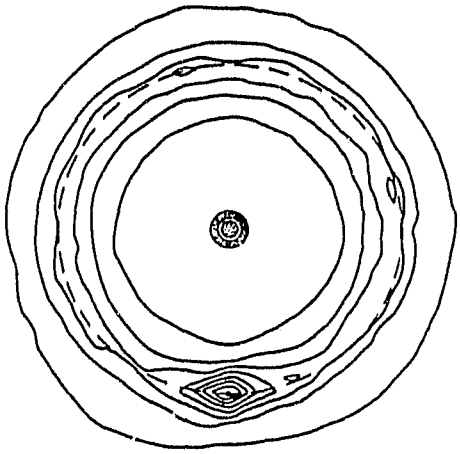

FIG. 4.—Titan H Torus. Column density contours, calculated from the cloud model for a 2.0 km s^{-1} isotropic emission velocity and a H-atom lifetime of 2×10^7 s (5600 hr), are shown as viewed from above the satellite plane.

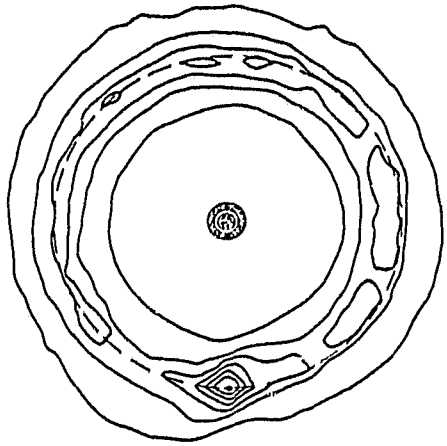

FIG. 5.—Titan H Torus. Same as Fig. 4 except for a 1×10^7 s (2800 hr) lifetime.

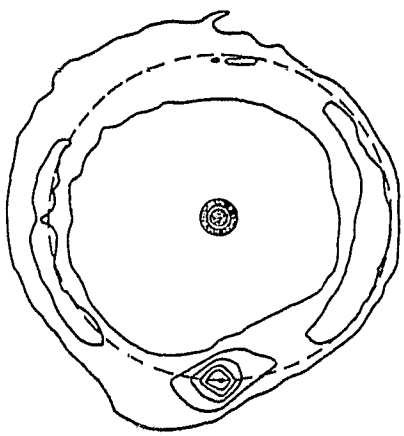

FIG. 6.—Titan H Torus. Same as Fig. 4 except for a 5×10^6 s (1400 hr) lifetime.

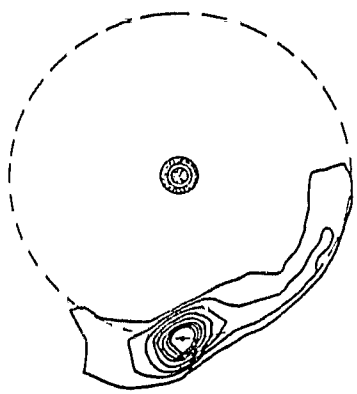

FIG. 7.—Titan H Torus. Same as Fig. 4 except for a 1.44×10^6 s (400 hr) lifetime.

comparable to the ± 1.5 Saturn radii observed by *Pioneer 11* (Judge, Wu, and Carlson 1980). The adopted emission velocity of 2 km s^{-1} may therefore be considered as an estimated value for the mean velocity associated with the yet unknown speed distribution operative at Titan's exosphere. The emission of hydrogen from the exosphere is assumed to be uniform and isotropic. More complex emission conditions could occur if, for example, there is a strong interaction between the planetary magnetosphere and Titan's atmosphere, but such possibilities are not considered here.

For these input parameters, model results showing the column density contour plot of the toroidal hydrogen cloud of Titan are given in Figure 4 as seen from above the satellite plane. The cloud is nearly circularly symmetric, except near the satellite, where the column density is peaked. The orbital-angular extent of hydrogen from Titan of 5 Saturn radii, observed by *Pioneer 11*

(Judge, Wu, and Carlson 1980), is also indicated in Figure 4 and corresponds approximately to the enhanced angular column density peak. This suggests that the UV photometer aboard the *Pioneer 11* spacecraft may have seen only the brighter portion of the hydrogen cloud near the satellite source. This enhanced column density region is more obvious for smaller lifetimes, as illustrated in Figure 5, Figure 6, and Figure 7. The enhancement will eventually diminish and become part of a cylindrically symmetric torus for lifetimes significantly longer than the adopted value of 5600 hr.

For the 2 km s^{-1} monoenergetic emission assumed in Figure 4 through Figure 7, most atoms escaping the Lagrange sphere of the satellite have velocities near 1 km s^{-1} and produce corresponding, two-body, forward and backward, average angular diffusion times of the order of 1400 hr. This is larger than the approximate diffusion times of 800 hr obtained earlier, assuming a Maxwell-Boltzmann emission velocity distribution. The actual average diffusion time will, of course, depend upon the exact velocity distribution assumed. These average diffusion times essentially represent the time it takes for the fastest half of the cloud atoms to complete 360° relative to Titan. Since the density of the torus is weighted more heavily toward the slower diffusing atoms, the apparent diffusion time for the column density from Figure 6 is seen to be more nearly equal to about 2400 hr.

The Earth-orbiting *Copernicus* satellite viewed the hydrogen torus nearly parallel to the satellite plane as shown in Figure 8, where Lα intensity contours, assuming solar-resonance scattering, are plotted. Model input parameters are identical to those of Figure 4. The brightness contours are also labeled for a reduced hydrogen atom escape flux of 1×10^{9} cm^{-2} s^{-1} as indicated by the values given in parenthesis. These labeled intensities are determined directly from model-calculated, column-density values using the radiative transfer results of Figure 2 for an effective gas temperature of 5000 K. The total vertical extent of 3 Saturn radii, suggested by *Pioneer 11* UV photometer measurements, is also indicated in Figure 8. The cloud intensity in the vicinity of the satellite orbit elongation point is in the range of 150–400 rayleighs for a flux of 3×10^{9} cm^{-2} s^{-1} and is in good agreement with the upper brightness value of 300 rayleighs estimated from the *Copernicus* satellite measurement (Barker *et al.* 1980). For the reduced flux of 1×10^{9} cm^{-2} s^{-1}, the intensity ranges from about 50–170 rayleighs and is in good agreement with the lower *Copernicus* brightness level of 100 rayleighs. If the radiative transfer of the hydrogen torus is more suitably described in Figure 2 by the lower gas temperature of 500 K, the Lα intensity of the cloud shown in Figure 8, although somewhat reduced, would still be in reasonable agreement with the *Copernicus* observation. In the vicinity of the elongation point of the satellite orbit, intensities would be in the range of 120–240 rayleighs for a flux of 3×10^{9} cm^{-2} s^{-1} and in the range 45–135 for the smaller flux of 1×10^{9} cm^{-2} s^{-1}. The actual effective gas temperature of the Titan torus will likely be bracketed by the two temperature results of Figure 2.

During the best *Pioneer 11* observation of the near Titan cloud, the spacecraft was inside of Titan's orbit and the line of sight of the UV photometer was nonradial (Judge *et al.* 1980). The spacecraft was approximately 6 Saturn radii from Titan so that the projected rectangular field of view of the photometer was about 0.1 Saturn radii along the satellite orbit and 1.0 Saturn radii perpendicular to the orbit. This viewing perspective reduces the above column densities and, hence, the

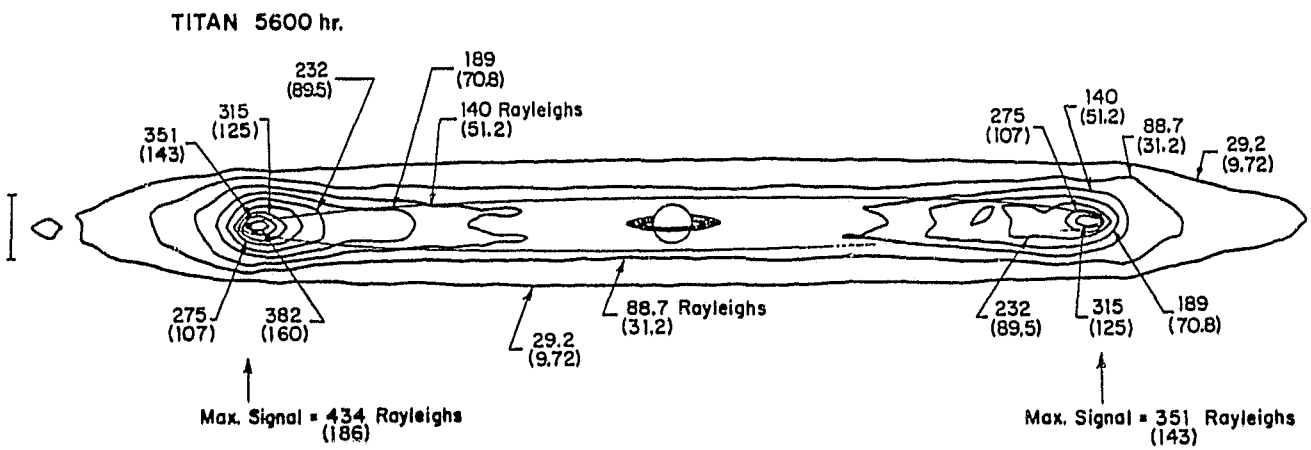

FIG. 8.—Lα Intensity of Titan's H Torus. Intensity contours, calculated assuming resonance scattering of sunlight, are shown for the satellite plane tilted by 3.25°. An isotropic emission of H atoms with an initial speed of 2.0 km s^{-1}, a satellite flux of 3×10^{9} cm^{-2} s^{-1} and the indicated lifetime were assumed. Brightness contour values in parenthesis are for a reduced flux of 1×10^{9} cm^{-2} s^{-1}.

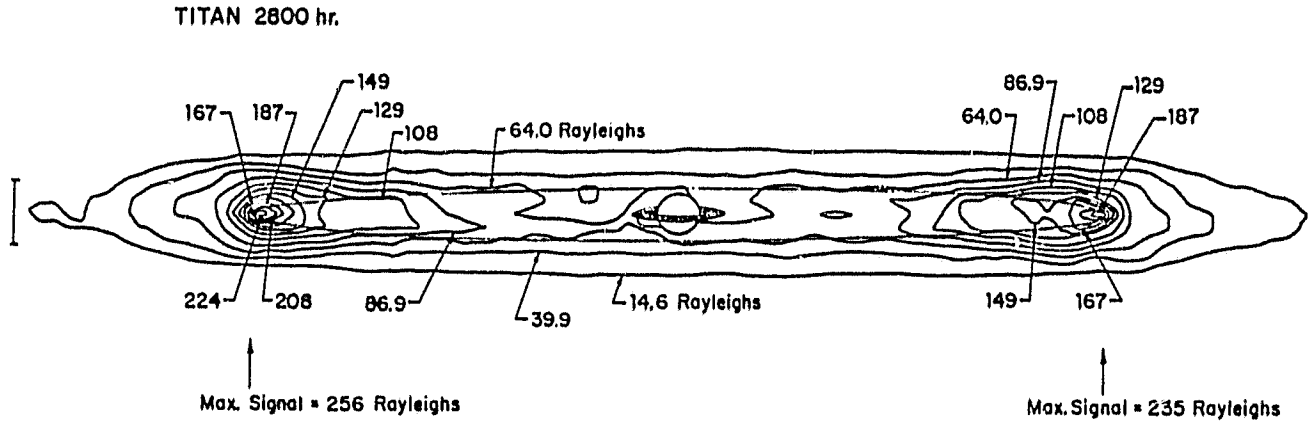

FIG. 9.—Lα Intensity of Titan's H Torus. See legend to Fig. 8.

observed intensities near the satellite by about a factor of 3. Estimated maximum intensities for the *Pioneer 11* viewing geometry would then vary between about 130–155 rayleighs for a hydrogen flux of 3×10^9 cm^{-2} s^{-1} and 49–56 rayleighs for a flux of 1×10^9 cm^{-2} s^{-1}, using the lower and higher temperature results of Figure 2, respectively. This is in excellent agreement with the 100 rayleigh estimate given by Judge, Wu, and Carlson (1979).

In the event that the lifetime of hydrogen atoms near Titan's orbit is smaller than the adopted 5600-hour value, a more asymmetric or even a partial toroidal cloud could exist. This is illustrated in Figure 9, Figure 10, and Figure 11 for a lifetime of 1×10^7 s (2800 hr), 5×10^6 s (1400 hr), and 1.44×10^6 s (400 hr), respectively, for a hydrogen atom flux of 3×10^9 cm^{-2} s^{-1}. This might occur if the plasma densities are sufficiently enhanced by solar wind compression. Labeled contour intensities in Figures 9–11 correspond to the higher gas temperature radiative transfer results of Figure 2. If, however, the atoms live longer than the 5600-hour estimate of Figure 8, the column density of the hydrogen cloud would increase approximately in proportion to the increased lifetime value. The Lα intensity would increase less rapidly. Near the elongation point of the satellite orbit, where, for example, the optical depth in Figure 8 is already between 1 and 2 for the 3×10^9 cm^{-2} s^{-1} flux value and an effective gas temperature of 5000 K, a tenfold increase in the column density would only increase the intensity to values slightly in excess of 1000 rayleighs. The model calculation would at this point, however, cease to be valid since collisional redistribution of hydrogen in the torus would then be important.

Eventual loss of hydrogen atoms from the torus through ionization may provide a significant ion source for the outer magnetosphere. An average radial distribution of hydrogen atoms in the torus may be calculated by integrating over the angular and vertical dimensions

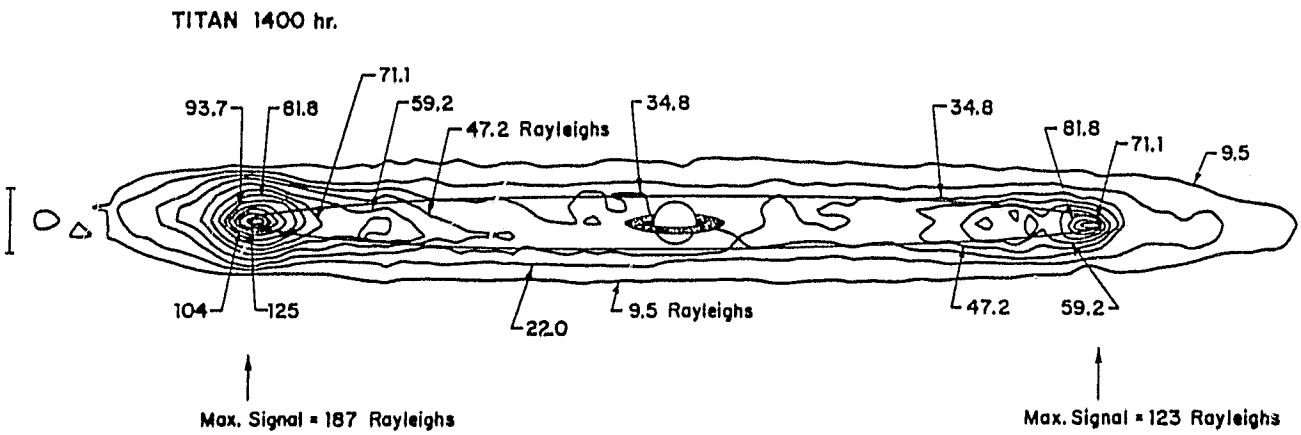

FIG. 10.—Lα Intensity of Titan's H Torus. See legend to Fig. 8.

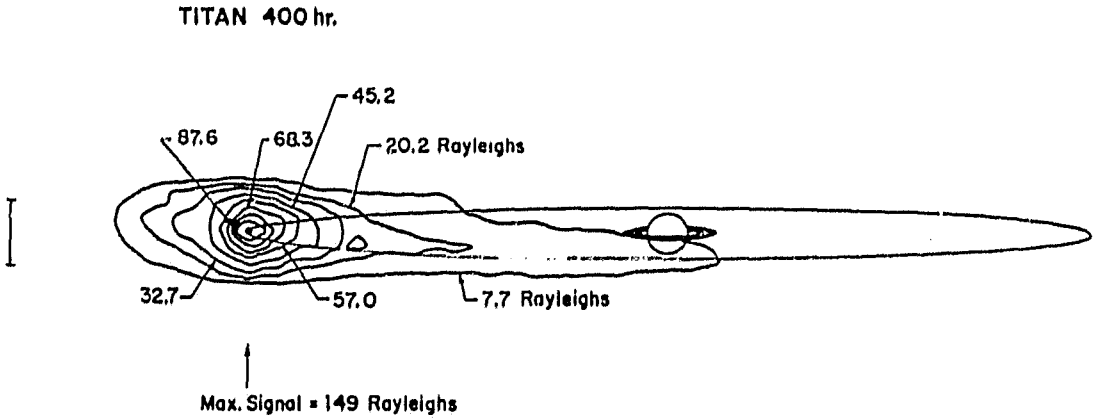

FIG. 11.—Lα Intensity of Titan's H Torus. See legend to Fig. 8.

of the cloud. Dividing this distribution by the lifetime of cloud atoms provides an average radial distribution for the loss rate of hydrogen atoms (given in Fig. 12). Assuming a steady-state cloud this hydrogen-atom loss rate is the rate at which new protons are introduced into the rotating planetary magnetosphere. Since the introduction of a new proton requires the loss of an old proton, for the charge-exchange lifetime process dominant in Titan's torus, only the energy distribution, not the number of protons is changed. Most of the neutral hydrogen atoms released from the charge-exchange process are on gravitational escape orbits from the planet. A net production of protons will, however, result from electron impact ionization of torus hydorgen atoms, with a rate of approximately 10^{-2} times the charge-exchange rate, and also from photoionization. Such a signature in either the energy or the abundance of protons near Titan's orbit may be present in the *Pioneer 11* data or in anticipated *Voyager* ion data.

IV. CONCLUDING REMARKS

Observations of Titan's hydrogen torus and earlier modeling efforts are reviewed. Estimated lifetimes for hydrogen atoms near Titan's orbit of the order of 10^7 s based upon recent *Pioneer 11* measurements suggest that the torus completely encircles Saturn and is angularly unsymmetric, having an enhanced gas density near the satellite. New model calculations presented confirm this hypothesis and, furthermore, provide an explanation for

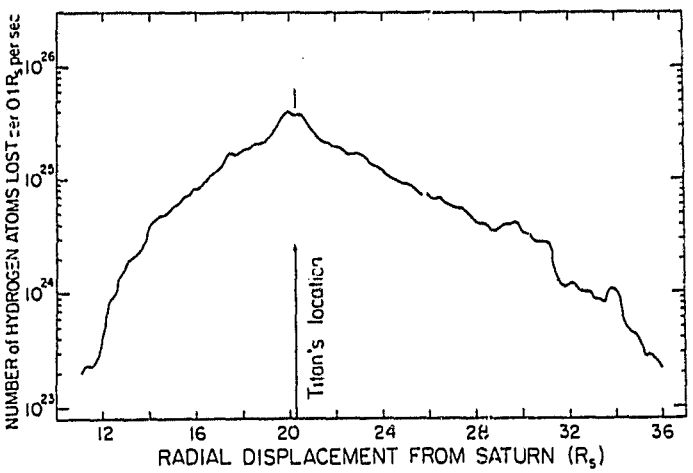

FIG. 12.—Torus H-Atom Loss Rate. Model results for the average radial distribution of the loss rate of H atoms from the Titan torus by charge-exchange processes are shown. The total atom population and overall loss rate are 4.6×10^{34} atoms and 2.3×10^{27} atoms s^{-1}, respectively. Model parameters are the same as those adopted for Fig. 8. Radial displacement is in units of Saturn radii.

the torus detected both by the Earth-orbiting *Copernicus* satellite and the UV instrument of *Pioneer 11*. Agreement between calculated and observed Lα intensities suggests a hydrogen escape flux between 1×10^{9} cm^{-2} s^{-1} and 3×10^{9} cm^{-2} s^{-1} should be operative at Titan. This produces a torus containing some 10^{34} hydrogen atoms.

The average rate at which hydrogen atoms are lost from the torus is calculated. This loss occurs mainly through charge-exchange, which modifies the energy distribution but not the abundance of the planetary ions. A radial profile for this ion injection rate is presented. Loss of hydrogen atoms through electron-impact ionization will, however, provide a net source of magnetospheric protons, as will photoionization. The actual spatial distribution of satellite magnetospheric ions will, of course, depend upon the balance established between the ion injection rate of the Titan torus and the ion loss rates provided both by ion diffusion inside the magnetosphere and solar-wind ion capture outside of the magnetosphere. The capture loss rate may be substantial since the solar wind/magnetosphere boundary is variable and can occur at times within Titan's orbit.

The Titan hydrogen torus model presented should be useful in preliminary evaluation of both the UV and charged-particle data anticipated from the *Voyager* mission during the next year. Future modeling of these new measurements should make it possible to refine our knowledge of the local Titan atmosphere as well as of the supply and diffusion of ions in the planetary magnetosphere.

The author would like to thank R. Goody and D. M. Hunten for helpful comments. This research was supported by the Planetary Atmospheres program of the National Aeronautics and Space Administration under grant NASW-3174. Acknowledgement is also made to the National Center for Atmospheric Research, which is sponsored by the National Science Foundation, for the computing time used in model computations.

REFERENCES

Barker, E. S. 1977, Presentation at 8th Annual Meeting of AAS/DPS, January 19–22, Honolulu, Hawaii.
Barker, E., Cazes, S., Emerich, C., Vidal-Madjar, A., and Owen, T. 1980, *Ap. J.*, **242**, 383.
Carlson, R. W., and Judge, D. L. 1975, *Icarus*, **24**, 395.
Carlson, R. W., Matson, D. L., and Johnson, T. V. 1975, *Geophys. Res. Letters*, **2**, 469.
Dennefeld, M. 1974, in *IAU Symposium 65, Exploration of the Planetary System*, ed. A. Woszczyk and C. Iwaniszewska (Dordrecht: Reidel), p. 471.
Fang, T-M., Smyth, W. H., and McElroy, M. B. 1976, *Planet. Space. Sci.*, **24**, 577.
Frank, L. A. 1980, private communication.
Gillett, F. C., Forrest, W. J., and Merrill, K. M. 1973, *Ap. J. (Letters)*, **184**, L93.
Gross, S. H., and Rasool, S. I. 1964, *Icarus*, **3**, 311.
Hunten, D. M. 1973, *J. Atmos. Sci.*, **30**, 726.
_____. 1974, in *The Atmosphere of Titan*, ed. D. M. Hunten NASA SP-340, p. 110.
_____. 1977, in *Planetary Satellites*, ed. J. A. Burns (Tucson: University of Arizona Press), p. 420.
Judge, D. L., Wu, F-M., and Carlson, R. W. 1979, Presentation at 1979 Fall AGU Meeting, December 3–7, San Francisco, California.
_____. 1980, *Science*, **204**, 431.
Kuiper, G. P. 1944, *Ap. J.*, **100**, 378.
McDonough, T. R., and Brice, N. M. 1973, *Icarus*, **20**, 136.
McElroy, M. B., and Yung, Y. L. 1975, *Ap. J.*, **196**, 227.
Münch, G., Trauger, J. T., and Roesler, F. L. 1977, *Ap. J.*, **216**, 963.
Pollack, J. B. 1973, *Icarus*, **19**, 43.
Sagan, C. 1973, *Icarus*, **18**, 649.
Siscoe, G. L. 1978, in *The Saturn System*, ed. D. M. Hunten and D. Morrison, NASA CP-2068, p. 265.
Smith, E. J., Davis, L., Jones, D. E., Coleman, P. J., Colburn, D. S., Dyal, P. and Sonett, C. P. 1980, *Science*, **207**, 407.
Smyth, W. H., and McElroy, M. B. 1977, *Planet. Space Sci.*, **25**, 415.
_____. 1978, *Ap. J.*, **226**, 336.
Strobel, D. F. 1974, *Icarus*, **21**, 466.
_____. 1979, private communication.
Sullivan, R. J. 1973, preprint.
Tabarié, N. 1974, in *The Atmosphere of Titan*, ed. D. M. Hunten, NASA SP-340, p. 123.
Trafton, L. 1972, *Ap. J.*, **175**, 283.
Wolfe, J. H., Mihalov, J. D., Collard, H. R., McKibban, D. D., Frank, L. A., and Intriligator, D. S. 1980, *Science*, **207**, 403.

WILLIAM H. SMYTH: Atmospheric and Environmental Research, Inc., 872 Massachusetts Avenue, Cambridge, MA 02139

APPENDIX B

MODELING OF NEUTRAL SATELLITE GAS CLOUDS - RECENT ADVANCES

MODELING OF NEUTRAL SATELLITE GAS CLOUDS - RECENT ADVANCES

by

William H. Smyth

presented before the

American Astronomical Society
Division for Planetary Science

Tucson, Arizona

October 14-17, 1980

Introduction

Recent advances made in modeling Titan's hydrogen torus, Io's sodium cloud and Io's oxygen cloud will be presented.

Model results for these neutral satellite gas clouds are based upon following the trajectories of many atom orbits emitted by the satellite.

This involves solving the equations of motion of each atom in three-dimensions, for prescribed initial conditions, and including proper weight factors along each orbit to simulate both ionization and excitation phenomena.

Slide 1 Titan's Hydrogen Torus

Slide 2 A model calculation for Titan's hydrogen torus is shown in the first two slides.

On the left, Lyman-α intensity contours for the hydrogen torus, produced by resonance scattering of sunlight, are shown as they would appear to the Earth-orbiting Copernicus satellite.

On the right, column density contours are shown as viewed normal to the satellite plane, revealing a complete torus about Saturn.

Values assumed for model parameters are indicated in the box.

The density of the torus is limited by the lifetime of H atoms in the Saturn environment, here estimated from Pioneer 11 plasma data to be about 2×10^7 sec.

The Lyman-α intensity of 200 ±100 Rayleighs, observed near the elongation points of Titan's orbit by the Copernicus

satellite, is in agreement with the model calculation if the satellite escape flux is between 1×10^9 and 3×10^9 atoms cm^{-2} sec^{-1}.

The angular extent of the hydrogen torus about Titan of ±5 Saturn radii, observed by the UV photometer of Pioneer 11, is indicated in the right slide and corresponds to the enhanced hydrogen density near the satellite source.

Io Oxygen Torus

A model calculation for the Io atomic oxygen torus,
Slide 3 recently discovered by Brown, is shown in the next two slides
Slide 4 The viewing perspective shows Io as it appeared at the mid-point of Brown's measurements.

On the left, brightness contours calculated for the 6300 Å oxygen line, assuming electron impact excitation, are indicated in Rayleighs and assume a satellite escape flux of 10^{10} atoms cm^{-2} sec^{-1}.

On the right, column density contours are shown as viewed normal to the satellite plane, revealing that the torus occurs mainly ahead of the satellite and inside of Io's orbit.

This shape is determined primarily by the Io plasma torus, which provides a spatially non-uniform sink for atomic oxygen, through electron impact ionization.

Plasma conditions assumed here, reflect the Voyager 1 encounter conditions, and were recently calculated by Shemansky using both Voyager UVS and plasma data.

The two locations of Brown's observing aperture are indicated by the shaded rectangles, and his average measured value of 8 ±4 Rayleighs is in agreement with this model calculaton, if a slightly reduced satellite escape flux of 5×10^9 oxygen atoms cm^{-2} sec^{-1} is adopted.

For the cooler plasma torus conditions of the Voyager 2 encounter, the model calculated oxygen densities are larger by about a factor of two.

Under these conditions, the satellite escape flux, necessary for agreement with Brown's observation, is reduced to about 3×10^9 atoms cm^{-2} sec^{-1}.

Io's Sodium Cloud

Faint linear-like features of the Io sodium cloud, recently detected by Pilcher, suggest that localized regions of the satellite may eject enhanced high-speed streams of sodium atoms.

Preliminary modeling to explore this suggestion is presented.

Slide 5
Slide 6

The next two slides show column density contours of the sodium cloud viewed normal to the satellite plane for two different model calculations.

These results were obtained by adding to our standard region B sodium cloud model, a localized jet 10° x 10° in size and centered 20° above the satellite plane.

The jet is emitted radially from Io with a speed of 9 km sec^{-1} and its vector direction, projected onto the satellite plane, is indicated on each slide by the heavy arrow.

Viewed from the Earth, with Io near the elongation point of its orbit, the brighter portions of these two jets look somewhat alike and are similar to a recurring transient feature observed by Pilcher.

However, if Io is 45° ahead of its western elongation point, the two jet features may easily be distinguished by
Slide 7 an Earth observer as illustrated in the last two slides.

Slide 8 Future comparison of data and model results are required to understand and hopefully identify localized sodium jet emissions.

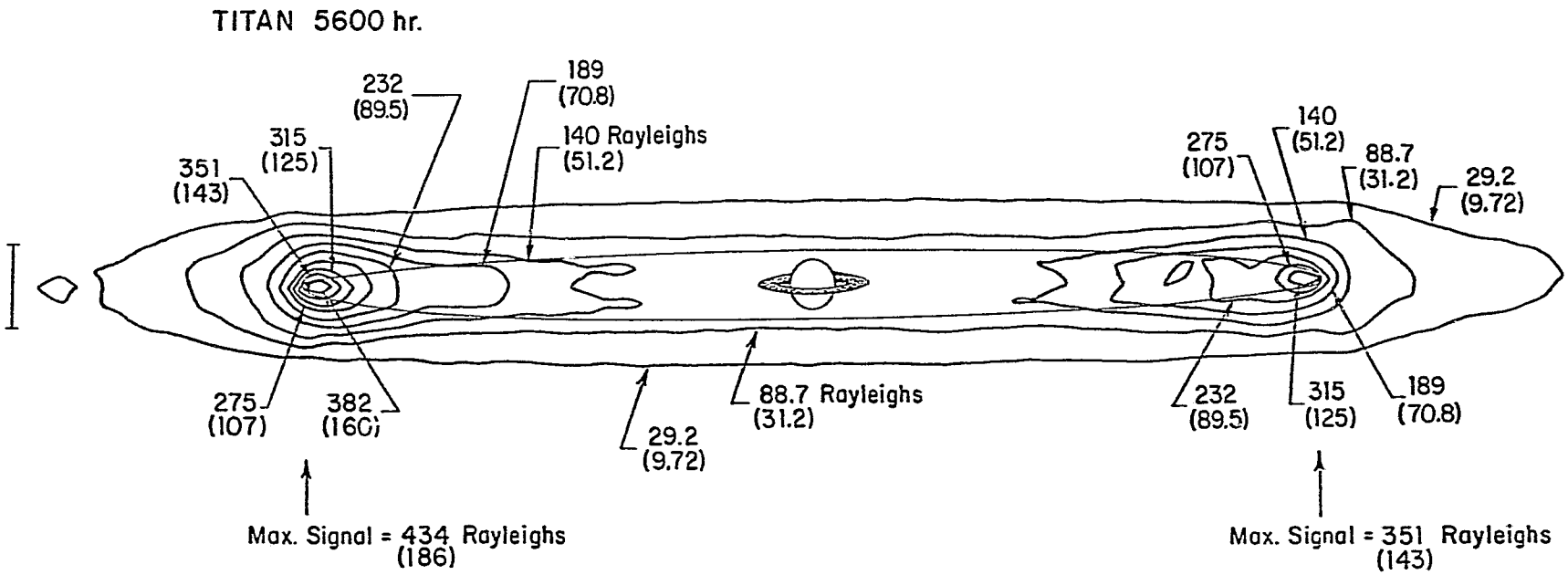

Slide 1

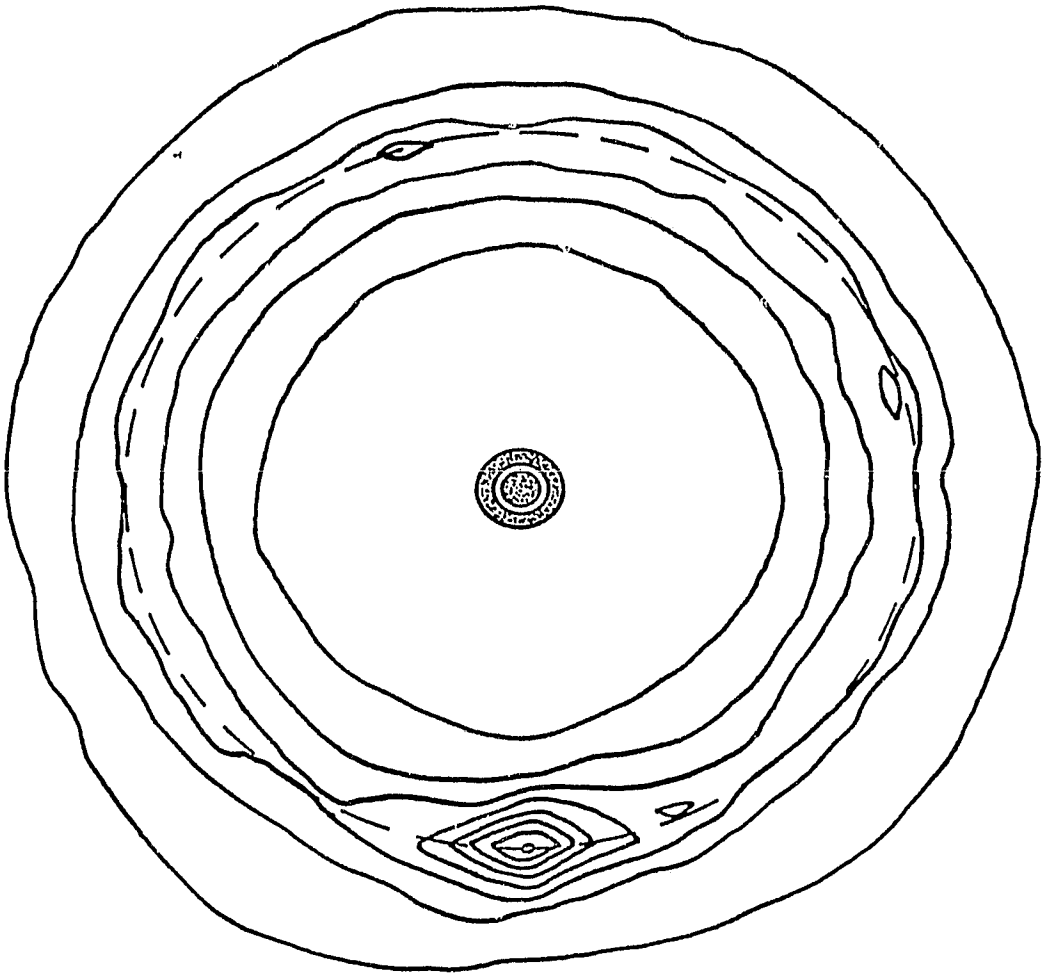

Slide 2

Io OXYGEN TORUS 6300 Å EMISSION INTENSITY

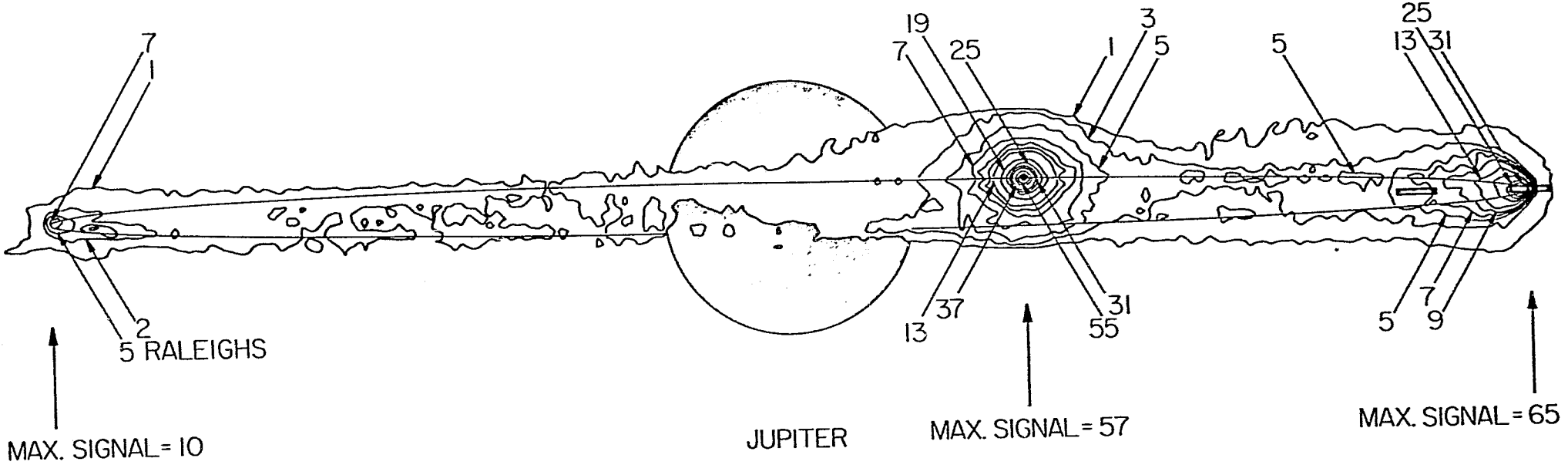

Io: Atomic Oxygen Torus

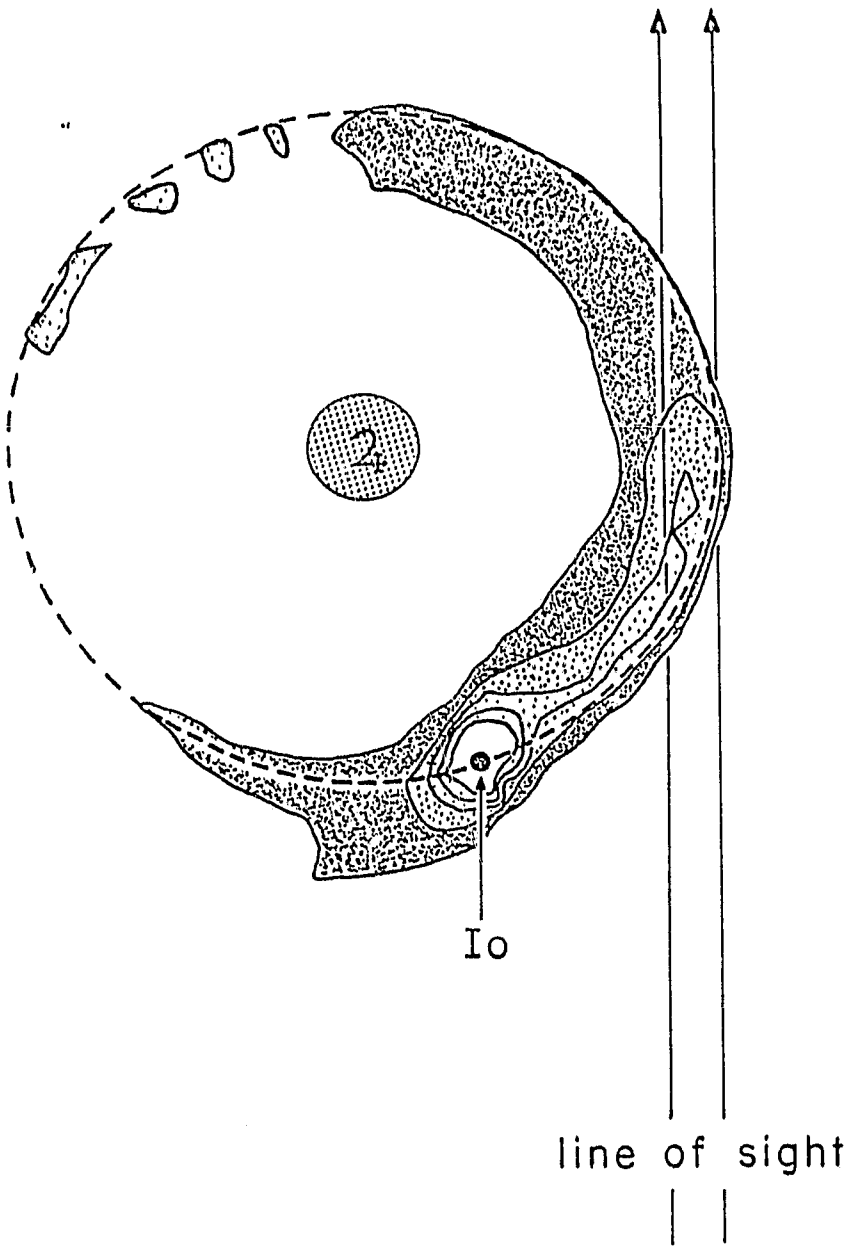

Sodium Cloud with Jet Feature

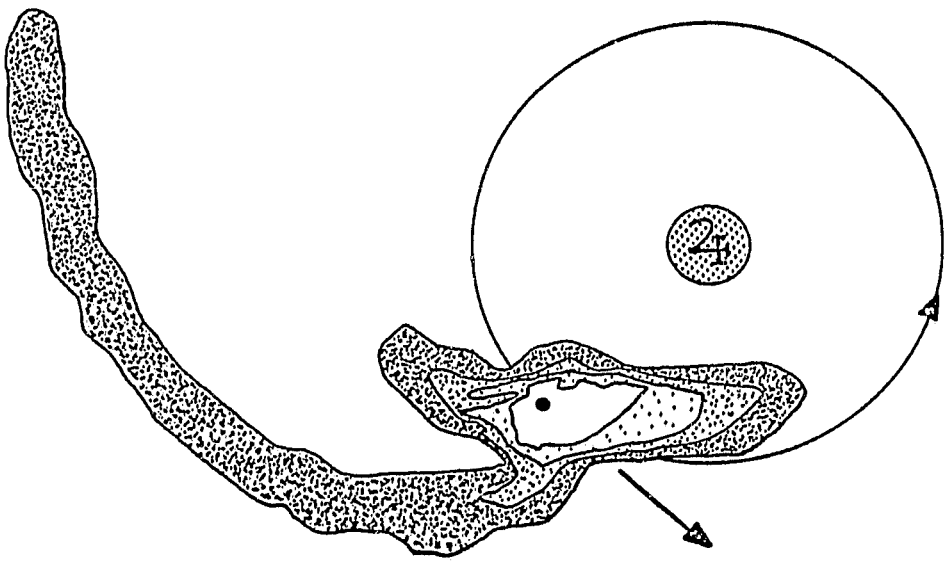

Sodium Cloud with Jet Feature

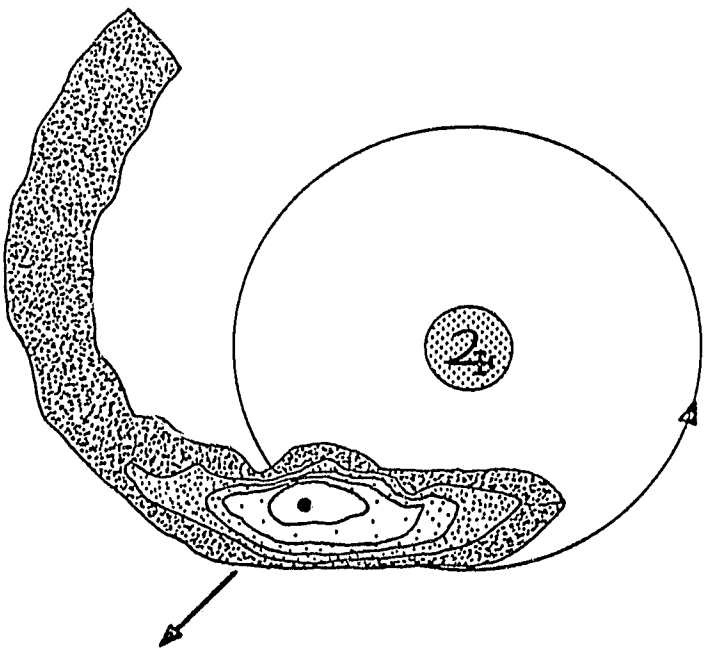

Slide 7

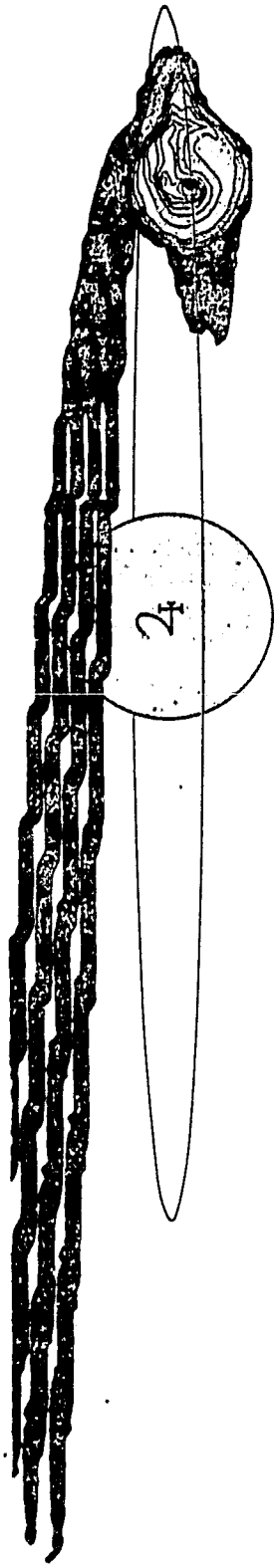

Slide 8

APPENDIX C

IO'S SODIUM CLOUD:
EXPLANATION OF THE EAST-WEST ASYMMETRIES. II

IO'S SODIUM CLOUD: EXPLANATION OF THE EAST-WEST ASYMMETRIES. II

William H. Smyth

Atmospheric and Environmental Research, Inc.
840 Memorial Drive
Cambridge, Massachusetts 02139

submitted for publication in
The Astrophysical Journal

Abstract

A new model has been developed for the sodium cloud of Io capable of describing its phase-angle dependent interaction with the solar radiation pressure arising from resonance scattering of sunlight in the D_1 and D_2 lines. This model was developed to more quantitatively explore the hypothesis, originally presented in Paper I (Smyth, 1979), that solar radiation pressure provides a mechanism for explaining the east-west cloud distribution asymmetry discovered by Goldberg et al. (1978) and the east-west cloud intensity asymmetry discovered by Bergstralh et al. (1975). Model calculations presented here confirm the original hypothesis and uncover explicit mechanisms responsible for the two observed east-west asymmetries. Model results presented for the cloud intensity did not include the spatially and time dependent sodium lifetime produced by oscillation of the Io plasma torus about the orbital plane of the satellite. Modifications to these results anticipated upon inclusion of the Io plasma torus in the model were, however, discussed and represent the only major improvement to the model required before proper inversion of the east-west asymmetry data may be undertaken.

1. Introduction

In an earlier paper (Smyth, 1979; hereinafter referred to as Paper I), an explanation of the observed east-west asymmetries of the Io Sodium cloud, based upon the effects of solar radiation pressure, was presented. These asymmetries were discovered by Bergstralh et al. (1975, 1977) and Goldberg et al. (1978) when Earth-based observations of the D-line emissions of the sodium cloud were compared for diametrically opposite satellite phase angles east and west of Jupiter. In Paper I, the force experienced by sodium atoms as they resonantly scatter sunlight in the D-lines and the ability of this force to alter the cloud atom orbits were explored. Orbit calculations presented showed that this solar radiation pressure has two major effects on the cloud. First, it acts in a time-dependent fashion, compressing the cloud near eastern elongation and expanding the cloud near western elongation, thereby providing the correct behavior to explain the east-west intensity asymmetry observed by Bergstralh et al. (1975, 1977). Second, it causes the sodium cloud to tilt closer to Jupiter when Io is near western elongation, thereby providing an explanation for the east-west cloud distribtuion asymmetry observed by Goldberg et al. (1978). An illustration from Paper I showing these two effects is given in Figure 1.

The major objective of Paper I was to simply demonstrate, using orbit calculations restricted to the satellite plane,

that solar radiation pressure provides a mechanism to qualitatively explain the observed east-west asymmetry features. The object of this second paper is to further test this mechanism by providing quantitative and more realistic three-dimensional model calculations for the sodium cloud. To accomplish this, a sodium cloud model, including the inherent time dependent effects of solar radiation pressure on the cloud atom orbits, has been developed. This model represents a substantial modification of the earlier sodium cloud model of Smyth and McElroy (1977, 1978) and is presented in Section 2.

In addition to solar radiation pressure, the actual intensity distribution of the observed sodium cloud will depend upon the initial velocity dispersion of sodium ejected from Io and also upon the spatial and time variations of the sodium lifetime in the Jovian environment. Knowledge of this velocity dispersion should be obtained from a careful inversion of the sodium data using the above described cloud model into which the lifetime information had been properly incorporated. The emphasis of the three dimensional modeling presented in this paper will not, however, be data inversion. It is rather to provide the preliminary and necessary step of documenting the physical changes that occur in the sodium cloud intensity because of solar radiation pressure. In this documentation, the effects of solar radiation pressure on those components of velocity that would make up the actual initial velocity dispersion of the ejected sodium atoms and that would

also contribute dominantly to the cloud intensity are investigated. Changes in the cloud density, introduced because sodium atoms are lost by ionization in a spatially non-uniform manner through electron impact with the Io plasma torus, have not been included. These changes represent a further numerical tailoring of the cloud density and D-line intensities within the three-dimensional sodium envelope which has already been altered by the action of solar radiation pressure. It is the altered intensity distribtuion within this sodium envelope, without this additional numerical tailoring, that is the subject of this paper. The additional effects of this tailoring are currently under evaluation and will be considered in a future publication. A brief discussion of the anticipated effects of this tailoring is, however, included in the following section.

2. Sodium Cloud Model

An improved model for the Io sodium cloud is presented for calculation of its density and solar resonance scattered D-line intensities. The model is based upon following the trajectories of many atom orbits emitted by the satellite, subject to the combined gravitational fields of Jupiter and Io and the acceleration produced by resonance scattering in the D-lines. This involves numerically solving the equations of motion of each atom in three-dimensions, for prescribed initial conditions, and including proper weight factors along each orbit to simulate both ionization and excitation phenomena. A description of the equations of motion and the resulting sodium cloud model, when the acceleration produced by solar resonance scattering is not included, was previously considered in detail by Smyth and McElroy (1977, 1978). Similar approaches have also been adopted in other sodium cloud modeling efforts (Matson et al., 1978; Goldberg et al., 1980). In these earlier papers, the motion of sodium atoms in the Io-Jupiter system required numerical solution of the circular restricted three-body problem in three dimensions. The present account provides an extension of these earlier papers by explicitly including the acceleration of sodium atoms produced by solar resonance scattering in the D-lines.

The trajectories of sodium atoms in the improved model are governed by what will be called the modified circular restricted three-body equations of motion, given as follows:

$$\ddot{x} - 2\dot{y} = \frac{\partial \Phi}{\partial x} + \vec{b} \cdot (\hat{i}_\xi \cos t + \hat{i}_\eta \sin t) \tag{1}$$

$$\ddot{y} + 2\dot{x} = \frac{\partial \Phi}{\partial y} + \vec{b} \cdot (-\hat{i}_\xi \sin t + \hat{i}_\eta \cos t) \tag{2}$$

$$\ddot{z} = \frac{\partial \Phi}{\partial z} + \vec{b} \cdot \hat{i}_\zeta \tag{3}$$

with

$$\Phi(x,y,z) = -\tfrac{1}{2}z^2 + \tfrac{1}{2}[\mu r_1^2 + (1-\mu) r_2^2] + \frac{\mu}{r_1} + \frac{1-\mu}{r_2} \tag{4}$$

$$r_1^2 = (x_1 - x)^2 + y^2 + z^2 \tag{5}$$

$$r_2^2 = (x_2 - x)^2 + y^2 + z^2 \tag{6}$$

$$x_1 = 1 - \mu \tag{7}$$

$$x_2 = -\mu \tag{8}$$

and

$$\mu = \frac{m_1}{m_1 + m_2} \tag{9}$$

$$\vec{b} = b\, \hat{i}_{sun} \tag{10}$$

where b is the acceleration experienced by sodium atoms because of resonance scattering in the D-lines, expressed in dimensionless form. The normal circular restricted three-body equations of motion are recovered when b is equal to zero (see Smyth and McElroy, 1977).

The coordinates (x,y,z) measure the displacement of the sodium atoms with respect to the center of mass of the Jupiter-Io system in units of the constant separation distance between the planet and satellite. Velocities $(\dot{x},\dot{y},\dot{z})$, accelerations $(\ddot{x},\ddot{y},\ddot{z})$ and time t are defined in dimensionless fashion using the reciprocal of the angular frequency for motion of the planet and satellite around their center of mass as a characteristic time. Satellite and planet masses are denoted by m_1 and m_2 respectively.

The coordinates (x,y,z) are defined in a non-inertia frame which rotates in such a manner to maintain the planet and satellite at fixed positions on the x-axis as shown in Figure 2. These rotating coordinates are related to a dimensionless inertia frame coordinate (ξ,η,ζ), with right handed unit vectors $(\hat{i}_\xi,\hat{i}_\eta,\hat{i}_\zeta)$, by the transformation

$$\begin{pmatrix} \xi \\ \eta \\ \zeta \end{pmatrix} = \begin{pmatrix} \cos t & -\sin t & 0 \\ \sin t & \cos t & 0 \\ 0 & 0 & 1 \end{pmatrix} \begin{pmatrix} x \\ y \\ z \end{pmatrix} \qquad (12)$$

The inertia frame, also with origin at the center of mass of the Jupiter-Io system, is positioned with its ζ-axis normal to the satellite orbit plane and its ξ-axis in the plane defined by the Earth-Jupiter line and the ζ-axis. The direction of positive ξ is away from the Earth toward Jupiter when the tilt angle of the satellite plane view from the Earth is zero. The units vector $\hat{i}_{sun}$ is directed away from the sun along the Sun-Jupiter line.

The acceleration b is given by

$$b = (b_1 + b_2) \Big/ \left[\frac{G(m_1 + m_2)}{a^2}\right] \qquad (12)$$

where b_1 and b_2 are the contributions to the acceleration of a sodium atom by resonance scattering in the D_1 and D_2 lines respectively, where G is the gravitational constant and where a is the constant separation distance between the planet and satellite. The acceleration b is made nondimensional by the characteristic acceleration given in brackets, which is effectively the gravitational acceleration experienced by a sodium atom in circular orbit of radius a about Jupiter. The magnitude of the acceleration b, as discussed in detail in Paper I, is as large as 0.01 to 0.02 and depends upon the radial velocity v of the sodium atom with respect to the sun in the following manner:

$$b_i = \frac{h\nu_i}{m_0 c} J_i \qquad (13)$$

where

$$J_i = \gamma_i(v)\left(\frac{\pi e^2}{m_e c}\right)\left(\frac{\pi F_{\nu_i}}{h\nu_i}\right) f_i R^{-2} \qquad (14)$$

Here $\frac{h\nu_i}{c}$ is the momentum change experienced by a sodium atom of mass m_0 upon absorbing a photon of energy $h\nu_i$ in the D_1 line (i=1) or D_2 line (i=2) and J_i is the corresponding rate at which photons are absorbed. In the expression for J_i, R is the Sun-Jupiter distance in astronomical units, f_i is the oscillator strength of the i^{th} line,

πF_{ν_i} is the solar continuum-level photon energy flux between the D_1 and D_2 lines at R = 1, and $\gamma_i(v)$ is the fraction of this solar continuum flux available to the sodium atom as it is Doppler shifted out of the bottom of the solar D-line Fraunhofer absorption feature by the instantaneous radial velocity v of the sodium atom relative to the Sun. The velocity v is the sum of the radial component of the velocity of the center of mass of the Jupiter-Io system $\vec{u}_{cm}$ and the velocity of the sodium atom $\vec{u}_{atom}$ in the inertia frame with respect to the Sun:

$$v = (\vec{u}_{cm} + \vec{u}_{atom}) \cdot \hat{i}_{sun} \qquad (15)$$

where

$$\vec{u}_{atom} = \sqrt{\frac{G(m_1 + m_2)}{a}}\,(\dot{\xi},\dot{\eta},\dot{\zeta}) \qquad (16)$$

and where $(\dot{\xi},\dot{\eta},\dot{\zeta})$ is given in terms of (x,y,z) and $(\dot{x},\dot{y},\dot{z})$ by differentiation of (11) with respect to t:

$$\begin{pmatrix} \dot{\xi} \\ \dot{\eta} \\ \dot{\zeta} \end{pmatrix} = \begin{pmatrix} -\sin t & -\cos t & 0 \\ \cos t & -\sin t & 0 \\ 0 & 0 & 0 \end{pmatrix} \begin{pmatrix} x \\ y \\ z \end{pmatrix} + \begin{pmatrix} \cos t & -\sin t & 0 \\ \sin t & \cos t & 0 \\ 0 & 0 & 1 \end{pmatrix} \begin{pmatrix} \dot{x} \\ \dot{y} \\ \dot{z} \end{pmatrix} . \qquad (17)$$

The presence of the solar radiation acceleration in the equation of motion (1) - (3) makes the differential

equations explicitly time dependent in two ways. First there is the obvious explicit time dependence in the (x,y,z) frame of the changing vector direction of $\vec{b}$ indicated in equations (1)-(3). Second there is the complex time-dependent modulation of the magnitude of the acceleration vector b as described by (13) - (17). The value of b varies more than an order of magnitude and is strongly dependent upon the satellite phase angle through the first term in (17) and is also dependent upon the instantaneous velocity of the sodium atom $(\dot{x},\dot{y},\dot{z})$ relative to Io through the second term of (17). These two sources of explicit time dependence severely complicate the solutions of the equations of motion (1) - (3). The natural circular symmetry of the gravitational problem, that exists in the (x,y,z) frame when $b=0$, is destroyed, thus causing each atom orbit, ejected from Io with the same initial conditions, to have a different trajectory for different initial locations of the satellite on its circular orbit. This breakdown of the natural circular symmetry of the gravitational problem caused by the introduction of the acceleration b gives rise to east-west differences in the cloud atom orbits dicussed in Paper I and provides a mechanism to explain the east-west asymmetries observed in the sodium cloud.

Model calculations of the density and intensity of the sodium cloud are based upon determining the locus of cloud atoms in space and their instantaneous velocities resulting from continuous ejection of sodium from Io. This locus of atom positions

for each individual initial conditions used to describe this ejection process, cannot be obtained by simply integrating the equations (1) - (3) once over the effective lifetime of the atom in the Jovian environment for one orbital location of Io as was accomplished in earlier modeling efforts where b is zero. In the present case, as the satellite is moving around its orbit continuously emitting sodium, the atoms ejected at different satellite orbital locations experience a different force and therefore have different trajectories even though their initial conditions relative to the satellite are identical. The determination of the desired locus of atom positions in the (x,y,z,) coordinates and their corresponding velocities therefore must be constructed, for each initial condition, from the solutions of the equations of motion (1) - (3) for a succession of different locations of the satellite along its orbit. The length of the angular section, over which these successive solutions are required, is determined by the effective lifetime of the sodium atoms, and this angular section must be properly pre-positioned along the satellite orbit to correctly define the cloud history at the time of observation. The number of satellite locations chosen within a given angular sector will be determined by the spatial resolution of the cloud density and intensity required in the model calculation.

The equations of motion (1) - (3) may be taken to define

a set of coupled first order differential equations which defines the time evolution of $(x,y,z,\dot{x},\dot{y},\dot{z})$. These equations are solved numberically using a fourth order Runge-Kutta method. The equations (1) - (3) exhibit no integrals of motion. Accuracy of the numerical solution is achieved by using carefully constructed sets of small time steps for integrating each atom orbit. In performing these integrations, properly constructed weight factors along each orbit to simulate both ionization and D-line excitations of the sodium cloud atoms may also be calculated and used to compute the column density, D-line intensities, and D-line emission profiles of the cloud.

In the model the ejection of sodium by Io is described by atoms emitted radially from a spherical exobase taken to lie at an altitude of 780 km above the satellite surface. This three dimensional model contains 1298 source points distributed uniformly over the exobase surface. Model calculations considered in this paper are however restricted to monoenergetic ejection of sodium from the inner hemisphere of the satellite and involve only 685 of these exobase points. The inner hemisphere is selected, since earlier modeling efforts (Smyth and McElroy, 1978; Matson et al., 1978; Macy and Trafton, 1980) have shown it to be the dominant emission hemisphere to explain the two-dimensional intensity features of the sodium cloud.

Ionizations of the sodium atoms along their orbits in

the following model calculations are limited to the simplest description of a constant cutoff lifetime of 20 hours and no attempt is made, as discussed earlier, to address the more complex spatially non-uniform and time-dependent tailoring of the sodium cloud produced by its interaction with the Io plasma torus. The small lifetime for sodium atoms of order one hour in the warm inner region of the Io plasma torus, estimated from Voyager plasma data (Bagenal and Sullivan, 1981), is in marked contrast to the lifetime estimates of 15 to 20 hours (Smyth and McElroy, 1978) and 28 hours (Matson et al., 1978) obtained from earlier modeling efforts and to the 20 hour value to be adopted here. In these earlier modeling studies, where no spatial variation of the sodium lifetime was assumed, the value of the lifetime was essentially determined by properly modeling the spatial extent of the forward sodium cloud observed in Earth-based measurements. With the presence of the plasma torus since established, it is now clear that the forward extent of the sodium cloud is determined by ionization of these cloud atoms upon their second encounter with the plasma torus, somewhat ahead of Io (as illustrated in Figure 3), which occurs for flight times of order 20 hours. During the first encounter of the cloud atoms with the plasma torus (i.e., as they escape Io initially) the abundance of sodium atoms in the cloud is reduced in a manner which depends critically upon the time history of the atom orbits and their location in the plasma

torus, which oscillates about the satellite plane. This spatial and time dependent destruction of the sodium density within the 20 hour cloud envelope will not be treated in this paper. The value of 20 hours for the sodium lifetime is adopted, however, in order to preserve the correct dimensions for the forward sodium cloud.

From Figure 3, it is relatively easy, however, to anticipate three effects of including the spatially nonuniform ionization of the Io plasma torus on the model calculations presented here. First note that the forward cloud, as determined by the Io plasma torus, will be significantly more elongated for western phase angles than for eastern phase angles, when cloud images are compared for diametrically opposite satellite locations about Jupiter. This more elongated behavior of the western cloud has been confirmed in very recent measurements of Goldberg et al., (1981). The actual flight times in Figure 3 for which sodium atoms traveling along the inner edge of the east and west clouds would have their second encounter with the plasma torus are, however, nearly equal being about 26 and 24 hours respectively. Second note that the density and D-line intensity of the outside portion of the sodium cloud will be reduced, relative to the inside portion of the sodium cloud, because of its prolonged spatial interaction with the Io plasma torus. This may cause the east-west cloud distribution asymmetry calculated in this paper to be modified in such a way as to reduce the predicted

values of the east critical phase angle more than the predicted value of the west critical phase angles. The critical phase angles are the satellite phase angles for which the sodium cloud on the sky plane appears to be distributed approximately symmetrically about Io. Third note that because of the first ionization encounter of the forward cloud atoms with the Io plasma torus, the density and D-line intensities of the sodium cloud near Io will be more enhanced, in comparison to the forward portion of the sodium cloud, than in the present calculation. This will cause the east-west intensity asymmetry effects that originate near Io to be enhanced and will also require that a larger flux of sodium atoms be emitted from Io in order to properly populate the elongated portion of the forward cloud.

Initial velocities of atoms emitted from the staellite exobase in the following model calculations are limited to values less than 3 km sec^{-1}, since these lower velocity components are those that will contribute dominantly, in the actual velocity dispersion, to the cloud intensity for brightness levels greater than about 1000 rayleigh (see Smyth and McElroy, 1978). It is these larger intensity values which are observed in the data of Bergstralh et al. (1975, 1977) and Goldberg et al. (1978). Velocity components greater than about 3 km sec^{-1} will, however, contribute significantly to the two-dimensional intensity of the sodium cloud for lesser brightness levels, such as the peculiar directional features seen

by Picher (1980) and Goldberg et al. (1981), and to the asymmetric wings of the sodium line profile shape, such as has been noted by Trafton (1975), Trauger et al. (1976) and Carlson et al. (1978).

3. Model Results: Goldberg's Cloud Distribution Asymmetry

The sodium cloud has been observed by Goldberg et al. (1978) to exhibit an east-west asymmetry in the spatial distribution of the D-line intensities with respect to the phase angle location of the satellite. Their observations showed that the projected intensity pattern of the cloud on the sky plane did not produce a mirror image for satellite orbital phase angles separated by 180 degrees. To initially quantify and characterize one of the differences observed in comparison of these east and west cloud images, the critical phase angles were selected as parameters. The cloud exhibits two critical phase angles which occur for those satellite phase angles where the sodium cloud on the sky plane appears nearly symmetric about Io as the satellite approaches either the eastern or western elongation points of its orbital (i.e., 90 degrees or 270 degrees, respectively).

The first estimates of the eastern and western critical phase angles were originally reported by Goldberg et al. (1978) as 65 degrees and 230 degrees respectively. These values were defined quantitatively by measuring the intensity seen in two simulated slits, applied to the two-dimensional cloud image and located 9 arc sec on either side of Io, and by determining that satellite phase angle for which the ratio of the two slit intensities was unity. This method led to a rather well defined value for the critical phase angle in the

west, but resulted in a large amount of scatter in determining the critical phase angle in the east. The less distinct behavior of the data in the east seemed to reflect a fundamental east-west difference in the sodium cloud, not a difference in the quality of the east and west data. Later estimates made with additional observations (Goldberg, 1979) indicated that the critical eastern phase angle might even be as large as 70 to 75 degrees. This then suggested that in the east the central axis of the forward sodium cloud was inclined only about 15 to 20 degrees with respect to the line drawn tangent to the satellite orbit at Io, whereas in the west this inclination angle was about 40 degrees. The sodium cloud would then have an east-west phase lag asymmetry of about 20 to 25 degrees.

The accuracy of these estimates for the east and west critical phase angles and hence for the east-west phase lag asymmetry has been, however, somewhat difficult to determine with exactness from the data of Goldberg et al. (1978) and Goldberg (1979), since their 2 to 3 hour long measurements introduced an orbital smear of 17 to 25 degrees into the cloud images. To rectify this situation, Goldberg et al. (1981) have recently made several new measurements using an improved instrument with an integration time of about 10 minutes. Their preliminary analysis of these new measurements, based upon visual comparisons, indicates that the western critical phase angle is distinct and occurs near 235 degrees, whereas the eastern critical phase angle is significantly

less distinct and occurs somewhere in the angular interval from 55 to 70 degrees. The exact value of the east-west phase lag asymmetry at present, therefore, remains undetermined and may or may not be as large as initially suggested. The one significant east-west asymmetric cloud feature that does occur both in these new measurements and in their older observations is the obvious presence of a distinct critical western phase angle and the noticeable visual absence of a distinct critical eastern phase angle. Quantitative analysis of existing data and acquisition of new data will be required to better determine the critical eastern phase angle and to understand possible variations of its value introduced by the oscillating Io plasma torus. Further analysis of these data should also be useful in identifying and characterizing other salient features of the east-west cloud distribution asymmetry, such as the greater elongation of the forward portion of the sodium cloud observed for western phase angles by Goldberg et al. (1981). To provide a step forward, based upon our current understanding, modeling analysis in this section will be restricted to exploring and documenting the east-west phase lag asymmetry introduced by the solar radiation pressure, excluding the spatially non-uniform and time-dependent ionization of sodium atoms by the Io plasma torus.

The preliminary results of calculations in the satellite plane, originally present in Paper I and repeated here in Figure 1, demonstrate that solar radiation pressure in the

D-lines causes the envelope of the sodium cloud to behave in a manner similar to the observations of Goldberg et al. (1978). Changes in the cloud shape in Figure 1 suggest an east-west phase lag of about 15 degrees. It is clear, however, that such an estimate is only preliminary and that the actual three dimensional distribution of sodium atoms within the cloud envelope must be calculated in order to determine a more accurate phase lag angle. Suitable three-dimensional model calculations for this purpose are presented below.

Three-dimensional model calculations, illustrating the effects of solar radiation acceleration on the D_2 intensity distribution of the sodium cloud viewed parallel to the satellite plane, are given for satellite phase angles of 55 and 235 degrees in Figure 4 and Figure 5, respectively. In these model calculations, which may be compared directly with the simpler results of Figure 1, sodium was emitted radially from the inner hemisphere of Io's exobase (2600 km radius) with a velocity of 2.6 km sec^{-1} and with a cutoff lifetime of 20 hours in the Jovian environment. Each outer contour value is 916 Rayleighs for a surface flux of 10^8 atoms cm^{-2} sec^{-1}, with contours spaced by 367 Rayleighs, increasing inward toward Io. The results of Figure 4 and Figure 5 show that changes in the D_2 intensity pattern of the sodium cloud are not very sensitive to the illumination angle of the sun relative to the Earth-Jupiter line of sight. The sun angle is confined to values between about 167 and 193 degrees as

the earth moves about the Sun. For a sun angle of 180 degrees, the Earth-Jupiter line of sight and the Sun-Jupiter axis of Figure 1 are identical. For a satellite phase angle of 55 degrees, note that in Figure 4 the effect of solar radiation is to rotate the central axis of the forward elongated sodium cloud further away from Jupiter as anticipated in the results of Figure 1. With solar radiation acceleration included in the model calculation, the inner edge of the cloud (right portion) in Figure 4 is therefore closer to Io while the outer edge (left portion) is extended further from Io. For a phase angle of 235 degrees, note that in Figure 5 the solar radiation pressure has effectively rotated the sodium cloud axis more toward Jupiter, as anticipated in Figure 1. With solar radiation acceleration included, the outer edge of the cloud (right portion) in Figure 5 is therefore closer to Io while the inner edge of the cloud (left portion) clearly reveals that the axis of the forward elongated sodium cloud has already begun to swing through our line of sight.

The model calculations of Figure 4 and Figure 5 indicate that solar radiation pressure introduces an east-west phase lag asymmetry into the spatial distribution of the sodium cloud. This can be illustrated more clearly as follows. In the absence of solar radiation acceleration, model calculations of the D_2 intensity pattern of the sodium cloud for diametrically opposite satellite phase angles are presented in Figure 6, where the sun angle is 180 degrees and the other model

parameters and contour levels are the same as in Figure 4 and Figure 5. Note that the east and west intensity patterns are effectively mirror images of each other, and that the axis of the forward elongated cloud can be seen to swing through our line of sight at a phase angle of about 55 degrees in the east and 235 degrees in the west, yielding no phase lag. The observed changes in the intensity pattern of the cloud with satellite phase angle are almost completely due to the changing geometric viewing perspective of the cloud projected onto the plane of the sky. In Figure 7, the D_2 intensity patterns of the sodium cloud, where the effects of solar radiation acceleration have been included, are presented for the identical diametrically opposite satellite phase angles, model parameters, and contour levels used in Figure 6. Near eastern elongation, note that the outer contour of the sodium cloud appears symmetric about Io near a satellite phase angle of between 60 and 65 degrees, whereas near western elongation the cloud appears symmetric at a phase angle of 230 degrees. This produces an east-west phase lag asymmetry between 10 and 15 degrees. The distribution of the D_2 intensity within the outer contour in Figure 7 is approximately symmetric for a phase angle of 65 degrees in the east and 235 degrees in the west. Using this as a criteria, the east-west phase lag asymmetry is then about 10 degrees. Note that in Figure 7, the passage of the forward cloud axis through our field of view is much less distinct in the east than in the west. This makes it more difficult to accurately determine the eastern critical

satellite phase angle, a persistent characteristic noted in the observational data of Goldberg et al. (1978, 1981).

The results Figure 6 and Figure 7 are calculated assuming a monoenergetic emission velocity of 2.6 km sec^{-1}. Results for lower emission velocity components that would be included, if a more realistic initial emission velocity distribution were adopted, have also been calculated. For emission velocities of 2.0 km sec^{-1}, 2.2 km sec^{-1} and 2.4 km sec^{-1}, the intensity patterns on the sky plane are again essentially mirror images, in the absence of solar radiation pressure, when the east and west clouds are compared for diametrically opposite satellite phase angles. The critical phase angles increase with decreasing emission velocity, having a value, in the absence of solar radiation pressure, in the east between 55 and 60 degrees for an initial velocity of 2.4 km sec^{-1} and a value of about 60 degrees for initial velocities of both 2.2 km sec^{-1} and 2.0 km sec^{-1}. With solar radiation pressure included, these model calculations have the same general east-west character as the results presented in Figure 7. Based upon the outer contour criteria, the critical eastern phase angle is about 65 degrees for the emission velocities of 2.4 km sec^{-1} and below, while the critical western phase angle is between 230 and 235 degrees. This provides an east-west phase lag asymmetry of about 10-15 degrees. Based upon the distribution of intensity within the outer contour, the critical eastern phase angle is about 70 degrees while

the critical western phase angle is about 235 degrees for emission velocities of 2.4 km sec^{-1} and lower, producing a 15 degree east-west phase lag asymmetry.

Model results for emission velocities of 2.2 km sec^{-1}, 2.4 km sec^{-1} and 2.6 km sec^{-1} are compared in Figure 8 and Figure 9 for diametrically opposite phase angles east and west of Jupiter. These D_2 intensity images include the effects of solar radiation pressure and are calculated for the same contour levels, emission conditions, and lifetime conditions chosen in Figures 4-7. As the emission velocity decreases, the cloud is more closely confined near Io and provides a rapidly increasing contribution to the intensity of the cloud near the satellite. The exact east and west critical phase angles and corresponding east-west phase lag asymmetry predicted from these model calculations will then depend to some extent upon the shape of the initial velocity distribution. From the above calculations, however, it is clear that a phase lag of about 10 to 15 degrees would be present even if an initial velocity distribution were adopted. For such an adopted distribution, the passage of the cloud through its eastern critical phase angle would also appear to occur slower than the passage of the cloud through its western critical phase angle. The critical phase angle in the east should be within the angular range from 55 to 70 degrees, while in the west it should be between 230 and 235 degrees.

The presence of a distinct critical western phase angle and of a significantly less distinct critical eastern phase angle in the observations of Goldberg et al. (1981) suggests that the non-uniform ionization of sodium introduced by the Io plasma torus oscillating about the satellite plane may tailor and modify, but will not eliminate, the basic characteristics of the east-west cloud distribution asymmetry determined by the model calculations in this section. Further quantitative analysis of the recently acquired data of Goldberg et al. (1981) and future analysis of additional sodium data anticipated during next apparition by Goldberg (1981) is warranted. These data should provide the necessary information for detailed modeling of the east-west cloud distribution asymmetry as well as the alternating north-south asymmetry discovered by Trafton and Macy (1975) and discussed further by Trafton (1980). Improvements in the present sodium cloud model to include the non-uniform ionization of the Io plasma torus are now in progress. The improved model should provide the necessary tool for interpretation of both the east-west and the north-south asymmetric phenomena and, thereby, lead to a better understanding of the local atmosphere of Io and its complex interactions with the Jovian magnetosphere.

4. Model Results: Bergstralh's Intensity Asymmetry

The sodium cloud has been observed by Bergstralh et al. (1975,1977) to exhibit an east-west asymmetry in its absolute intensity. In their observations, the intensity of the sodium cloud was measured as a function of phase angle through a 3" x 8" slit centered on the satellite with the long dimension of the slit oriented approximately perpendicular to the projection of Io's orbital plane. This observational geometry is illustrated in Figure 10. The long dimension of the slit is only slightly larger than the diameter of the Lagrange sphere of Io, within which the gravitational field of the satellite dominates the planetary gravitational field. The spatial region of the cloud sampled by the slit is therefore composed of a mixture of the dense sodium that likely exists within the Lagrange sphere and the somewhat less dense sodium that occurs, along the line of sight, in the foreground and background of this sphere.

The D-line intensities of the cloud, measured through this observing slit, were shown by Bergstralh and colleagues to be correlated with Io's orbital position around Jupiter. This correlation made it possible for them to identify resonance scattering of sunlight by sodium atoms as the dominant excitation mechanism for the cloud. In addition, the measured intensity of the cloud with the satellite east of Jupiter was shown, in their initial paper (Bergstralh, Matson and Johnson, 1975), to be consistently about 50% greater than the measured

intensity with the satellite west of Jupiter. In their second paper Bergstralh et al., 1977), which included additional observations and a presentation of more select data, this east-west intensity asymmetry was more accurately estimated to be 20 to 25%.

In paper I, this intensity asymmetry was associated with the ability of solar pressure to compress the east cloud and expand the west cloud envelope, as illustrated in Figure 1. To more fully investigate how solar radiation pressure provides a mechanism to explain this intensity asymmetry, a number of three-dimensional model calculations have been performed and are presented here. The D_1 and D_2 intensities seen through a 3" x 8" slit centered on Io have been calculated as a function of both the satellite phase angle and the initial speed of sodium atoms emitted from the inner hemisphere of Io's exobase. In all of these model computations, the two-dimensional distributions of both the column density and the intensity of the cloud on the sky plane, as well as the shape of the sodium D-line profiles, have also been simultaneously calculated, both excluding and including solar radiation pressure, to more fully understand the basic phenomena.

Model calculations for the relative D_2 intensity seen through the 3" x 8" viewing slit, taken here to have nominal dimensions of 9×10^3 km by 2.4×10^4 km, are presented in Figure 11 and compared with the observations of Bergstralh

et al. (1975). The relative D_2 intensity of the model calculations is shown as a function of the satellite phase angle for four different monenergetic emission velocities spanning the range from 2.0 km sec^{-1} to 2.6 km sec^{-1}. In each monoenergetic model calculation, the same number of atoms were emitted from Io's exobase. These relative intensities were calculated for sodium atoms emitted from the inner hemisphere of the exobase and include the shadow effect of the disk of Io blocking the cloud behind it. The tilt angle of the satellite plane is assumed to be zero relative to the observer. The sun, observer and Jupiter are assumed to be along the same straight line. Intensities calculated for a satellite-plane tilt angle of a few degrees, differ only slightly.

The model calculations of Figure 11 clearly show that solar radiation pressure introduces a large east-west intensity asymmetry for the initial emission velocity of 2.0 km sec^{-1} and a somewhat less pronounced asymmetry for the 2.1 km sec^{-1} emission velocity. The asymmetry is present only in small amounts for the higher emission velocities of 2.4 km sec^{-1} and 2.6 km sec^{-1}. The maximum intensity of the 2.0 km sec^{-1} results is 4.38 times larger than the 2.6 km sec^{-1} results in the east and 3.48 times larger in the west. The contributions to the intensity for the different velocities have a maximum value near 60 degrees in the east and near 230 degrees in the west. In both the east and west, these

peak intensities correspond to the enhancement of the sodium cloud density produced by the forward portion of the cloud as it passes through the line of sight of the viewing slit. The peak intensity is larger and more pronounced for the lower emission velocities since the forward cloud is then much more narrow and is much more tightly confined near Io. This spatial behavior of the forward cloud, in the absence of solar radiation pressure, was discussed earlier by Smyth and McElroy (1977), who at that time noted a similarity between their calculated column density peaks and the peaks in the data of Bergstralh et al. (1975). This similarity is also present in the results of Figure 11, although before an accurate comparison can be made with the observations, the additional modifications introduced by the spatially non-uniform lifetime of the Io plasma torus must be included in the model calculations.

The east-west ratio of the relative D_2 intensity for the 2.0 km sec^{-1} and 2.1 km sec^{-1} emission velocities is presented in Figure 12, where the results of including and excluding the effects of Io's shadow are both indicated. For an emission velocity of 2.0 km sec^{-1} the ratio provides a minimum east-west asymmetry of 17 percent over most of the angular range when the shadow is included, and at a 70 degree phase angle the ratio has a peak value of over 1.8. The 2.1 km sec^{-1} ratio is less pronounced, but still provides a significant east-west symmetry over much of the phase angle interval. The general qualitative behavior of the D_2 intensity ratio exhibited in

Figure 11 can be simply understood in terms of the action of solar radiation pressure upon the sodium atom orbits. This qualitative explanation will now be discussed in some detail.

In Figure 12, the D_2 intensity ratio is greater than unity for east/west phase angles in the range from 0/180 to 40/220 because the column density of the east cloud in the viewing slit is larger than that of the west cloud by approximately 20% from an emission velocity of 2.0 km sec^{-1}. The radial velocity v of most sodium cloud atoms with respect to the sun is larger, however, in the west cloud than in the east cloud, for this phase angle interval, so that the D_2 intensity ratio is reduced somewhat from this column density ratio through the factor $\gamma_i(v)$ in equation (14). This larger velocity of sodium atoms in the west cloud is also evident in sodium line profiles when model results are compared for diametrically opposite satellite phase angles. For an east/west phase angle near 50/230 in Figure 12, the D_2 intensity of the west cloud in the viewing aperature has reached its maximum value, because of the phase lag asymmetry alignment of the forward cloud. The east cloud, however, reaches its maximum D_2 intensity value about 10 degrees later and maintains intensity values near this maximum level over a longer phase angle interval, beyond the peak, than does the west cloud (see the model calculation in Figure 11). This gives rise in Figure 12 to the dramatic increase in the

C-2

D_2 intensity ratio within the east/west phase angle range from 50/230 to 120/300, and to the asymmetric slope of the D_2 intensity ratio about its peak value located at a phase angle of 70/250.

For larger east/west phase angles between 120/300 and 165/345, the D_2 intensity ratio decreases and eventually becomes less than unity. In this angular range, most atoms now seen in the viewing slit are near Io and not in the forward cloud. Solar radiation pressure, in this angular range, so acts on these cloud atoms to elevate the column density of the west cloud by as much as 18% for the 2.0 km sec^{-1} emission velocity and as much as 4% for the 2.1 km sec^{-1} emission velocity. In the west cloud, the radial velocity v of most atoms with respect to the sun is also enhanced over the east cloud and, through the factor $\gamma_i(v)$ in equation (14), causes the D_2 intensity ratio to be reduced ever further.

The significant enhancement of the calculated column density of the east cloud relative to the west cloud within the phase angle range 0/180 to 40/220 in Figure 12, may be attributed to two factors. The first one is that solar radiation pressure produces an east cloud that is spatially more tightly confined near Io and hence has elevated densities. The second and more important factor is that solar radiation pressure modifies the escape process of atoms from Io so that the total number of atoms within the east cloud is larger.

This modification of the escape process is also largely responsible for the elevation of the column densities of the west cloud relative to the east cloud within the east/west phase angle range form 135/315 to 170/350.

With regard to the first factor, the density enhancements of the east cloud and the density reductions of the west cloud within the phase angle range 0/180 to 40/220 in Figure 12 are more pronounced for atom emission velocities near 2.0 km sec^{-1}. This occurs because many of these atoms, shortly after emission from the exobase, experience a near balance between the effective gravitational field of Jupiter and Io. This near balance causes the relative magnitude of the solar radiation acceleration experienced by the sodium atom to be favorably amplified. The vector direction of the solar radaiation acceleration, being oppositely oriented in the east and west cloud, then asymmetrically and somewhat abruptly alters the cloud atom orbits. Future evolution of these altered atom orbits then produces the density enhancement of the east cloud and density reduction of the west cloud. For the higher emission velocities of 2.4 km sec^{-1} and 2.6 km sec^{-1}, this amplification effect is much smaller since the sodium atoms, moving more rapidly away from Io, spend less time near the Lagrange sphere. The resulting east-west density changes for these higher emission velocities are therefore much less pronounced and result primarily from the smooth and continuous action of solar radiation pressure over the 20 hour lifetime of the atoms.

In the case of the higher emission velocities, the compression of the east cloud and the expansion of the west cloud, as shown in Figure 1, are, in fact, to first order compensated by the column integration along the line of sight and contribute little to the intensity asymmetry.

With regard to the second and more important factor, the ability of solar radiation pressure to modulate the total number of sodium atoms within the cloud occurs essentially for those emission velocities near 2 km sec^{-1} where the escape of atom orbits is energetically possible only from a limited surface area of the satellite exobase. This energetically possible areas of the exobase defines the window in the Lagrange sphere surrounding Io through which the atoms escape. It is this effective exospheric area, from which the emitted atoms are able to escape from the satellite, that is modulated by the action of solar radiation.

The Lagrange window in Io's orbital plane for atoms emitted from the exobase of the satellite has been discussed, in the absence of solar radiation pressure, by Smyth and McElroy (1977). One of their illustrations is shown in Figure 13 for radial emission velocities of 1.8 km sec^{-1}, 2.0 km sec^{-1}, and 3.0 km sec^{-1}. For a 1.8 km sec^{-1} velocity, the Lagrange window is closed except near the center of the inner satellite hemisphere (i.e. at 180°) and near the center of the outer satellite hemisphere (i.e. at 0°). The window is preferentially open in

this direction because it is the easiest direction for escape of atoms, since the two collinear Lagrange points, L_1 and L_2, nearest to Io lie along the line connecting Io and Jupiter (see Figure 2). For an emission velocity of 2.0 km sec^{-1}, the Lagrange window is closed on a small sector of the leading inner quadrant and a small sector of the trailing outer quadrant of the exobase. For a velocity of 3.0 km sec^{-1}, the Lagrange window is completely open, since all atoms emitted radially from the exobase now have sufficient energy to escape Io regardless of their initial surface location. In the absence of solar radiation pressure, the percentage of atoms emitted from the inner hemisphere of the exobase that do not escape Io is determined by model calculations to be 60.3, 28.6, 9.6, 1.8, and 0.19 for monoenergetic emissions velocities of 1.8 km sec^{-1}, 1.9 km sec^{-1}, 2.0 km sec^{-1}, 2.1 km sec-1 and 2.2 km sec^{-1}. These percentage values are of course independent of the phase angles at which the satellite is observed.

The ability of solar radiation pressure to modulate, as a function of the satellite phase angle, the percentage of atoms not escaping from Io, having been initially emitted radially from the inner hemisphere of the exobase, is illustrated in Figure 14. Model results, where solar radiation pressure has been both included and excluded, are compared for monoenergetic emission velocities of both 2.0 km sec^{-1} and 2.1 km sec^{-1}. The functional behavior exhibited is essentially similar in nature for both emission velocities.

Solar radiation pressure enhances the escape of sodium atoms for smaller satellite phase angles in the east (i.e. between 0 and 68 degrees for 2.0 km sec^{-1} and between 0 and 98 degrees for 2.1 km sec^{-1}) and for larger phase angles in the west (i.e. between 208 and 360 degrees for 2.0 km sec^{-1} and between 291 and 360 degrees for 2.1 km sec^{-1}). This behavior accounts, in Figure 12, for the earlier noted enhancement of the column density of the east cloud relative to the west cloud in the east/west phase angle range of 0/180 to 40/220, and of the west cloud relative to the east cloud in the east/west phase angle range of 135/315 to 170/350. The general behavior exhibited by the effect of solar radiation pressure in Figure 14 may also be anticipated on geometrical grounds by simply considering, as a function of the observed phase angle of the satellite, the 20 hour time history of the orientation of the solar radiation acceleration vector and that portion of the inner hemisphere exobase from which atom escape is modulated.

The maximum observed D_2 intensity reported by Bergstralh et al. (1977) using their best data base was 241 k Rayleighs. This was measured for a satellite phase angle near eastern elongation and assumed that only a 3 x 3 second portion of their observing slit was uniformly illuminated. If the complete 3 x 8 arc second slit is considered, this uniform intensity is reduced to about 90 k Rayleighs. If this

intensity were produced by the maximum D_2 intensity given by the 2.0 km sec^{-1} calculation of Figure 11, a satellite flux of order 1 x 10^8 atoms cm^{-2} sec^{-1} would be required, in agreement with an earlier estimate by Smyth and McElroy (1978). This flux value of 1 x $10^8 cm^{-2} sec^{-1}$ will, however, be revised upward, as noted by Brown (1981), upon inclusion in the model calculation of the highly spatially, non-uniform ionization of sodium atoms by the Io plasma torus.

For the results in Figure 11 and Figure 12 to explain the observed east-west intensity asymmetry, the relative importance of the emission velocity components near 2.0 km sec^{-1} must be significant in the actual initial velocity distribution of sodium atoms in the Io atmosphere. For velocity components of 1.8 km sec^{-1} and lower, ballistic orbits are dominant, and the cloud becomes less bright and is mostly confined inside the Lagrange sphere, where the asymmetric mechanism is not operative. For velocity components of 2.4 km sec^{-1} and higher, essentially all the cloud atoms escape the Lagrange sphere in a sufficiently short time to render the asymmetric mechamism ineffective, and the cloud becomes less bright near Io and more spatially extended. Inversion of the sodium data of Bergstralh et al. (1975, 1977) should therefore be sensitive to the velocity components near 2.0 km sec^{-1}. This inversion is clearly a desirable modeling goal and will be critically dependent upon the calculated results presented in Figure 11. The results of Figure 11, however,

must first be recalculated so as to include the non-uniform spatial lifetime of sodium atoms produced by the presence of the Io plasma torus. With these new results, which are currently under evaluation, such an inversion process would be meaningful.

Some of the modifications to the results of Figure 11 and Figure 12 that will be produced by including the presence of the Io plasma torus in the new model calculations may be anticipated on simple geometrical grounds. The atoms emitted from the inner hemisphere of the satellite exobase with a velocity of 2.0 km sec^{-1} will create a forward cloud that is almost completely confined between the inner and outer boundaries of the plasma torus shown in Figure 3. The continual exposure of this sodium to the ionization of the plasma torus will cause the atom population in the forward cloud to be significantly diminished relative to the atom population near Io. As the emission velocity increases, however, less and less of the forward cloud will be confined within the plasma torus, as illustrated for an emission velocity of 2.6 km sec^{-1} in Figure 3. The ability of the plasma torus to diminish the relative number of atoms in the forward cloud will therefore be less severe as the emission velocity increases. The relative values of the calculated intensity curves in Figure 11 for different emission velocities will thus be altered.

The dramatic increases in the calculated D_2 intensities in Figure 11 near 60 degrees and 230 degrees for the emission

velocities of 2.0 km sec^{-1} and 2.1 km sec^{-1}, which occur because of the passage of the forward cloud through the field of view of the observing slit, will also be reduced by this ionization of the plasma torus. The extent of this reduction will depend upon the mean plasma conditions, which have been observed to change over a time period of several months (Sandel et al., 1979), and may also depend upon the time modulation of these mean conditions by the oscillation of the Io plasma torus about the satellite plane. The resulting peak of the east/west intensity ratio in Figure 12 at an east/west angle of 70/250 will therefore be reduced. The new model predicted east-west intensity asymmetry should then be more strongly dependent upon the ability of solar radiation pressure to modulate, as a function of phase angle, the percentage of atoms escaping from Io, which was illustrated earlier in Figure 14.

5. Concluding Remarks

A three-dimensional model for Io's sodium cloud incorportating the full effects of solar radiation acceleration associated with solar resonance scattering of atoms in the D_1 and D_2 lines has been developed. The model has been applied to interpret two different east-west asymmetries exhibited by the Io sodium cloud in data obtained from ground-based telescopes. The major objective of the modeling analysis presented was not to invert the sodium data and deduce information about the escape mechanism of gases from Io. It was rather to provide the preliminary step of documenting the physical changes produced in the sodium cloud by the solar radiation acceleration, as a function of the satellite phase angle, and to further clarify, beyond the efforts of Paper I, how these changes provide an explanation of the observed east-west asymmetries. To provide model results appropriate for inversion of the east-west asymmetry data, the present calculations would have to be upgraded to include the spatially non-uniform and time variable ionization of cloud atoms by the Io plasma torus. Such an effort to improve the model is in progress.

Model results for the observed east-west cloud distribution asymmetry of Goldberg et al, (1978), Goldberg (1979) and Goldberg et al. (1981) were presented in Section 3. The observations indicated that the projected intensity patterns

of the sodium cloud on the plane of the sky did not produce mirror images at orbital phase angles separated by 180 degrees. When the satellite was west of Jupiter, the central axis of the forward portion of the sodium cloud was observed to pass through the line of sight of the observer at a distinct critical phase angle between 230 and 235 degrees. When the satellite was east of Jupiter, however, the passage of the central axis of the forward cloud through the line of sight of the observer was significantly slower and less distinct. The critical phase angle in the east at present remains uncertain within the angular range of 55 to 70 degrees. The east-west phase lag asymmetry associated with the east and west critical phase angles therefore remains uncertain and may or may not be as large as 15 to 20 degrees. Model results, calculated for different monenergetic emission velocities, reproduced the correct phase angle behavior of the observations, indicating a distinct critical phase angle in the west between 230 and 235 degrees and a significantly less distinct critical phase angle in the east between 55 and 70 degrees. These results, which have excluded the effects of the spatially nonuniform ionization of sodium by the plasma torus, suggest an east-west phase lag asymmetry of 10 to 15 degrees.

The behavior of the cloud distribution asymmetry and the value of the phase lag asymmetry predicted by the model calculations are not critically dependent upon the exact distribution of the emission velocity chosen between 2 km sec^{-1}

and 3 km sec^{-1}, because these effects depend primarily upon the simple geometrical orientation of Io's orbit and the solar radiation force vector. In brief, cloud atoms observed at eastern satellite phase angles are initially emitted at western phase angles where the solar radiation force acts in a direction to enhance either the angular or outward radial component of velocity of most atoms over much of their 20 hour lifetime. This increases the kinetic energy of these atoms relative to Jupiter and produces a cloud that remains more distant from Jupiter and closer to Io than would occur in the absence of the solar radiation acceleration (see Figure 1). Conversely, cloud atoms observed at western satellite phase angles are initially emitted at eastern phase angles where the solar radiation force acts in a direction to initially decrease the angular component and later to decrease the outward radial component of velocity of most atoms during much of their 20 hour lifetime. This initial energy loss relative to Jupiter and the later inward directed force will produce a cloud which lies closer to Jupiter and more distant from Io than would occur in the absence of the solar radiation acceleration (see Figure 1).

Model results for the observed east-west intensity asymmetry of Bergstralh et al. (1975, 1977) were presented in Section 4. The observations indicated that the intensity of the cloud seen through a 3 x 8 arc second viewing slit centered on Io was about 20 to 25 percent brighter for

eastern satellite phase angles than for western satellite phase angles. Model calculations exhibited a somewhat similar east-west intensity asymmetry, but only for a narrow range of the emission velocities, unlike the model results for the east-west cloud distribution asymmetry. Those emission velocities which contribute significantly to the intensity asymmetry have speeds very near the escape velocity of atoms emitted from the satellite exobase.

The east-west intensity asymmetry predicted by the model calculations is critically dependent upon those atoms which have emission velocities near the satellite escape speed, because these atoms spend a significant amount of time in their orbits close to the Lagrange sphere of the satellite, where the effective gravitational fields of Jupiter and Io are nearly balanced. This near balance amplifies the relative importance of the solar radiation force, which then acts in two distinct ways to produce the intensity asymmetry. First there is a significant enhancement of the normal compression of the east cloud and the expansion of the west cloud, illustrated in Figure 1, and an additional geometrical amplification provided by the phase lag asymmetry. Second and more importantly, for a constant emission flux from the exobase, there is a periodic modulation with respect to the satellite phase angle of the total number of sodium atoms that escape the satellite, and hence, that populate the extended sodium cloud. The combination of these enhancement and modulation processes

produces an elevated D_2 intensity in the east cloud relative to the west cloud over a significant east-west phase angle interval.

In summary, the model predicted changes in the shape and spatial orientation of the sodium cloud envelope and in the intensity distributions within the envelope, provide a simple explanation for the east-west cloud distribution asymmetry and for the east-west intensity asymmetry. These results follow directly from the lack of circular symmetry about Jupiter of the forces acting on the cloud atoms. The lack of this circular symmetry is introduced by the presence of the solar radiation force in the model calculations.

The identification of the east-west asymmetry in the model calculations with sodium atoms emitted within a somewhat narrow range of the velocities near the satelllite escape speed is significant. It both provides an explicit and simple mechanism to explain the observed east-west intensity asymmetry, and suggests that if there are no other major contributors to the intensity asymmetry, this narrow portion of the velocity dispersion must be well represented in the actual initial velocity distribution of sodium atoms operative in the Io atmosphere. Careful model inversion of the east-west intensity data would then be sensitive to accurately determining the relative weights for the contributing velocity components in the 1.8 km sec^{-1} to 2.2 km sec^{-1} velocity interval. This analysis would be somewhat complementary to the inversion of the two-dimensional intensity data for the sodium cloud on the

sky plane (such as the phase lag asymmetry data), which is primarily sensitive to the emission velocities between 2 km sec^{-1} and 3 km sec^{-1}, and to the line profile data of the sodium cloud, which is particularly sensitive to higher emission velocities, up to 15 km sec^{-1} or 20 km sec^{-1}. A consistent and simultaneous analysis of all three types of sodium data should provide the necessary overlapping constraints to deduce the real initial velocity distribution function for sodium atoms escaping from Io.

Acknowledgement

This research was supported by the Planetary Atmospheres program of the National Aeronautics and Space Administration under grant NASW-3174 and NASW-3387. Acknowledgement is also made to the National Center for Atmospheric Research, which is sponsored by the National Science Foundation, for the computing time used in model computations.

REFERENCES

Bagenal, F., and Sullivan, J.D. (1981), J. Geophys. Res. Preprint (to appear in JGR, special Voyager Issue).

Bergstralh, J.T., Matson, D.L., and Johnson, T.V. (1975), Ap. J. Lett., 195, L 131.

Bergstralh, J.T., Young, J.W., Matson, D.L., and Johnson, T. V. (1977), Ap. J. Lett., 211, L 51.

Brown, R.A. (1981), Cospar 1980 Space Research, XXI, (article, in press).

Carlson, R.W., Matson, D.L., Johnson, T.V., and Bergstralh, J.T. (1978), Ap. J., 223, 1082.

Goldberg, B.A., Carlson, R.W., Matson, D.L., and Johnson, T. V. (1978), Bull. AAS 10, 579.

Goldberg, B.A., Mekler, Yu, Carlson, R.W., Johnson, T.V., and Matson, D.L. (1980), Icarus 44, 305.

Goldberg, B.A. (1979), private communication.

Goldberg, B.A. (1981), private communication.

Goldberg, B.A., and Carlson, R.W., Johnson, T.V., Lorre, J. J., Matson, D.L., and Young, J.W. (1981), EOS 62, 316. Presented May 25, 1981 at the AGU meeting, Baltimore, Md.

Macy, W. and Trafton, L. (1980), Icarus 41, 131.

Matson, D.L., Goldberg, B.A., Johnson, T.V., and Carlson, R. W. (1978), Science 199, 531.

Pilcher, C. (1980) Bull. Amer. Astron. Soc., 12, 675.

Sandel, B.R. et al. (1979), Science, 206, 962.

Smyth, W.H., and McElroy, M.B. (1977), Planet. Space Sci., 25, 415.

Smyth, W.H., and McElroy, M.B. (1978), Ap. J., 226, 336.

Smyth, W.H. (1979), Ap. J., 234, 1148.

Trafton, L. (1975), Ap. J. Lett., 202, L 107.

Trafton, L., and Macy, W., Jr. (1975), Ap. J. Lett., 202, L 155.

Trafton, L. (1980), Icarus, 44, 318.

Trauger, J., Roesler, F., and Münch, G. (1976), Bull. AAS, 8, 468.

FIGURE CAPTIONS

Figure 1. East-West Changes in the Sodium Cloud. Calculations performed in Paper I for the solar radiation perturbed cloud shape, indicated by the shaded area, and for the unperturbed cloud shape, indicated by the dashed boundary, are compared for diametrically opposite satellite phase angles.

Figure 2. Dimensionless Coordinate System for the Modified Circular Restricted Three Body Problem in Io's Orbital Plane. The locations of the five classical Lagrange points at L_1, L_2, L_3, L_4 and L_5, the satellite at x_1, and the planet at x_2 in the (x,y)-plane are indicated.

Figure 3. Interaction of the Sodium Cloud and the Plasma Torus. The spatially projected overlap in the satellite plane of the Io plasma torus with the solar radiation perturbed cloud shape (solid boundary with heavy shading) and with the unperturbed cloud shape (heavy dashed boundary) of Figure 1, is indicated for the diametrically opposite satellite phase angles.

Figure 4. Effects of Solar Radiation Pressure in the East Cloud. Calculated D_2 intensity contours of the sodium cloud are compared, with and without the effects of solar radiation pressure, for the indicated phase and sun angles. The outer dashed lines are for reference in comparison of the left and right cloud boundaries, and the center dashed line is for vertical alignment of the satellite location.

Figure 5. Effects of Solar Radiation Pressure in the West Cloud. See legend to Fig. 4.

Figure 6. East-West Comparison of the Sodium Cloud. Model calculations for the D_2 intensity contours of the sodium cloud, excluding the effects of solar radiation pressure, are shown for diametrically opposite satellite phase angles east and west of Jupiter. No east-west phase lag asymmetry is evident. See text for discussion.

Figure 7. East-West Comparison of the Sodium Cloud. Model calculations for the D_2 intensity contours of the sodium cloud, including the effects of solar radiation pressure, are shown for diametrically opposite satellite phase angles east and west of Jupiter. A distinct east-west phase lag asymmetry is evident. See text for discussion.

Figure 8. Dependence of the Sodium Cloud on Emission Velocity. Model calculated D_2 intensity contours for the sodium cloud, including solar radiation pressure effects, are shown for diametrically opposite satellite phase angles and compared for emission velocities of 2.2 km sec^{-1}, 2.4 km sec^{-1} and 2.6 km sec^{-1}. See text for discussion.

Figure 9. Dependence of the Sodium Cloud on Emission Velocity. See legend to Fig. 8.

Figure 10. Observational Slit for the Intensity Asymmetry Measurements. The rectangular observational slit of Bergstralh et al. (1975, 1977), centered on Io, is shown in relation to the sodium cloud, the satellite orbit and the planet.

Figure 11. Comparison of Observation and Model Results for the East-West Intensity Asymmetry. The observations of Bergstralh et al. (1975) are compared to model calculations for the relative D_2 intensity seen through their rectangular viewing slit. Model calculations for four different monoenergetic values of the emission velocity are shown. See text for discussion.

Figure 12. Model Results for the East-West Intensity Ratio. The east to west D_2 intensity ratio of Figure 11 is shown as a function of the east to west phase angles for emission velocities of 2.0 km sec^{-1} and 2.1 km sec^{-1}.

Figure 13. Lagrange Window in Io's Orbital Plane for Atoms Emitted from the Exobase of the Satellite. Io, surrounded by its exobase (the dashed circle), is shown as depicted in an original illustration of Smyth and McElroy (1977). The radial coordinate indicates the flight time of an atom emitted radially from the exosphere at the angular orientation about the satellite shown. Upon capture by Io, the 5° angular-resolution radial sector containing that orbit is blackened for all later time. Ballistic orbits are indicated for a capture time of 50 hr. For greater capture times, blackening indicates that atoms, initially on an escape trajectory, have been recaptured because of a close encounter with Io.

Figure 14. Solar Radiation Pressure Modulation of the Sodium Atom Escaping from Io. The percentage of sodium atoms not escaping Io, which are emitted uniformly and at a constant rate from the inner hemisphere of the satellite exobase with monoenergetic emission velocities of 2.0 km sec^{-1} and 2.1 km sec^{-1}, are compared as a function of the Io phase angle for model calculation excluding (dashed curve) and including (solid curve) the effects of solar radiation pressure. See text for discussion.

William H. Smyth
Atmospheric and Environmental Research, Inc.
840 Memorial Drive
Cambridge, Massachusetts 02139

Figure 1

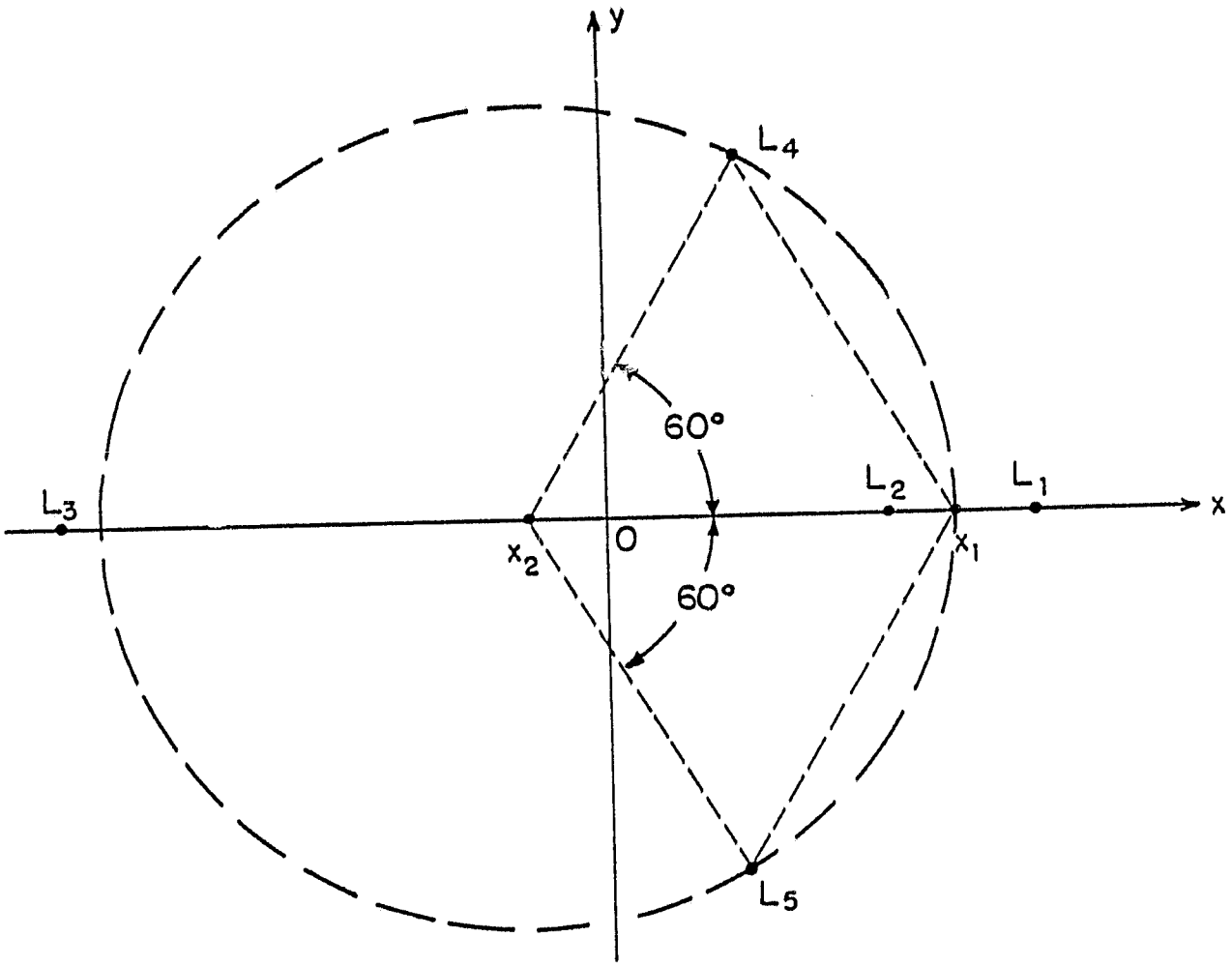

Figure 2

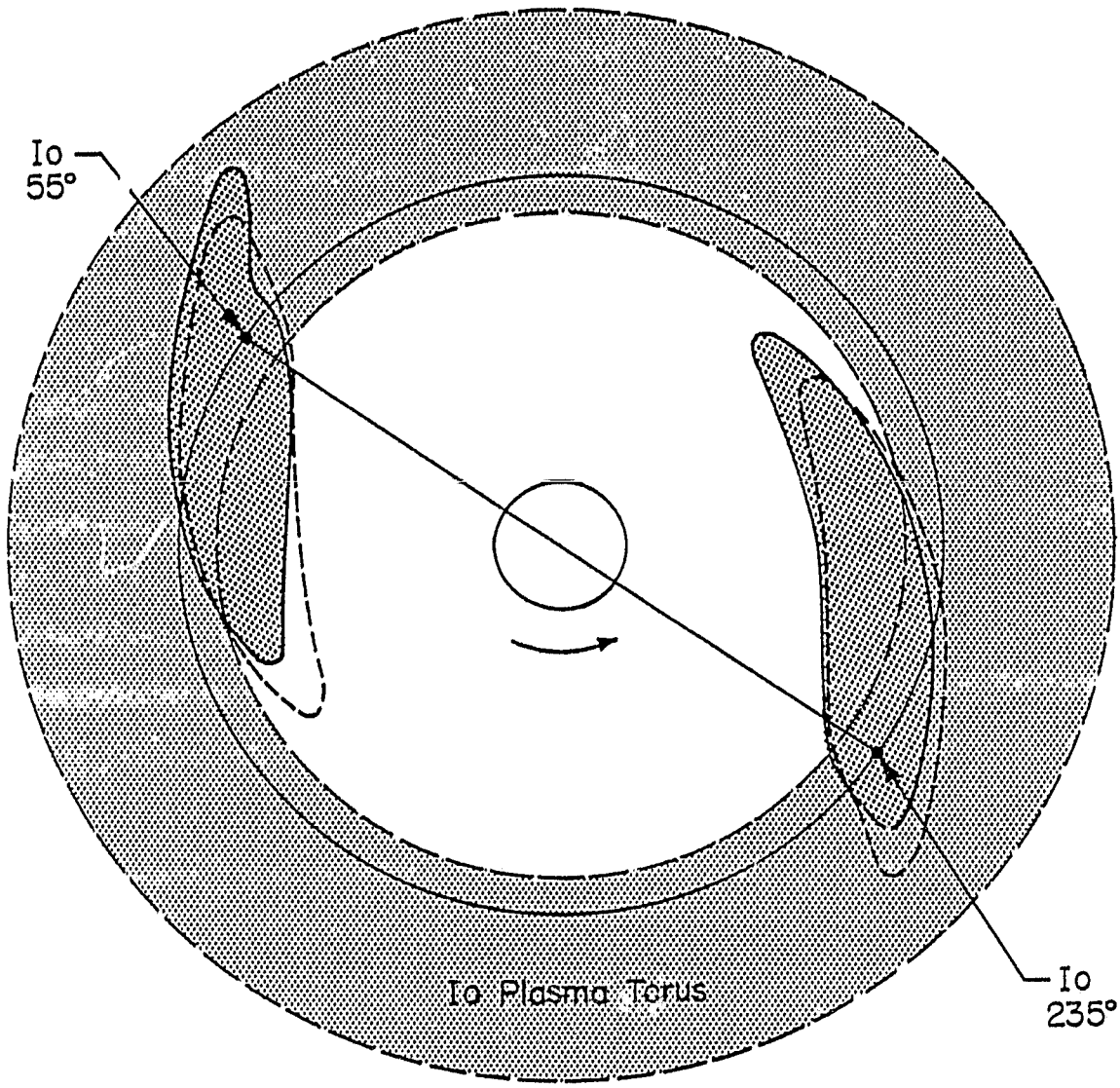

Figure 3

IO'S SODIUM CLOUD FOR A SATELLITE PHASE ANGLE OF 55°

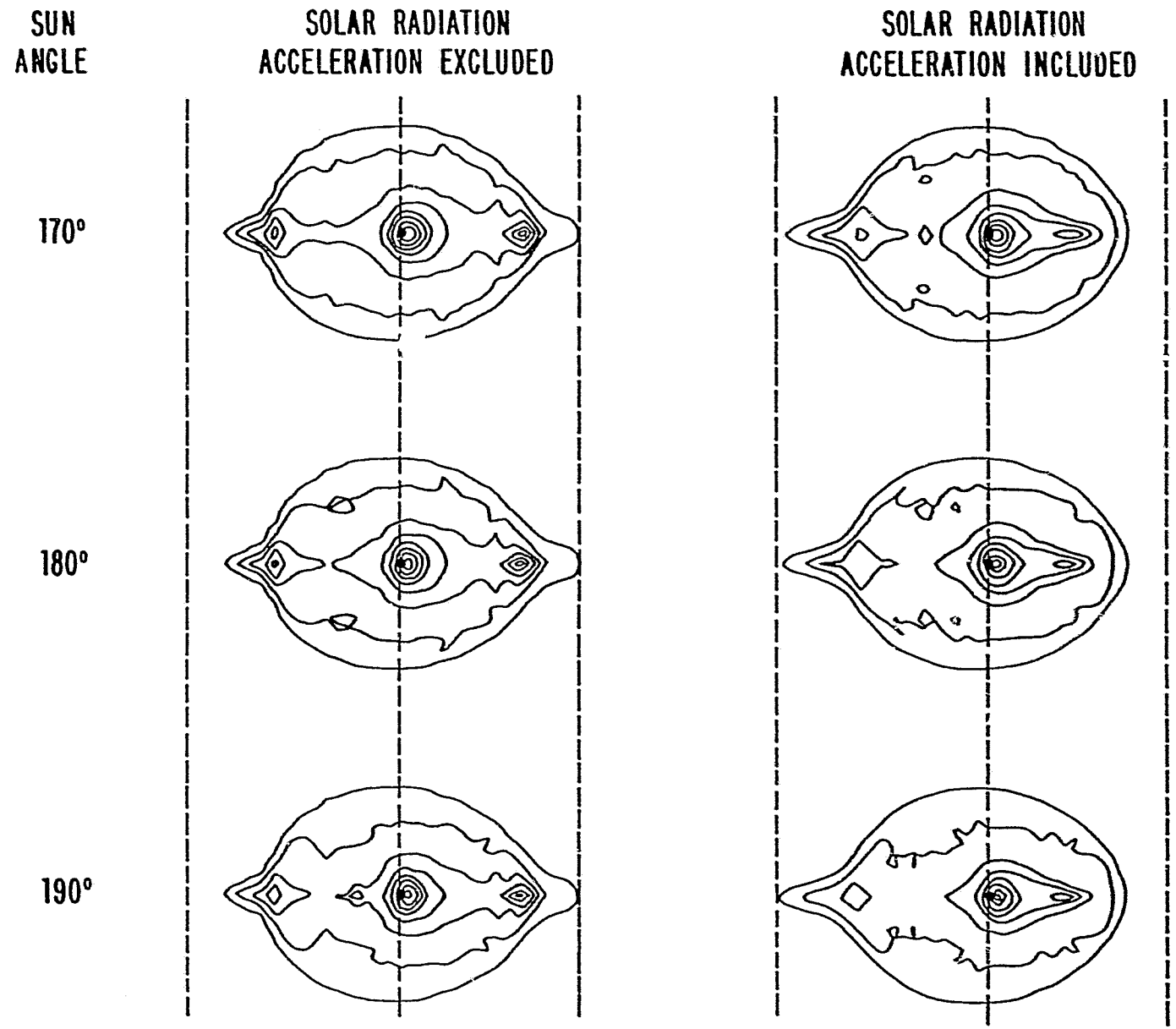

Figure 4

IO'S SODIUM CLOUD FOR A SATELLITE PHASE ANGLE OF 235°

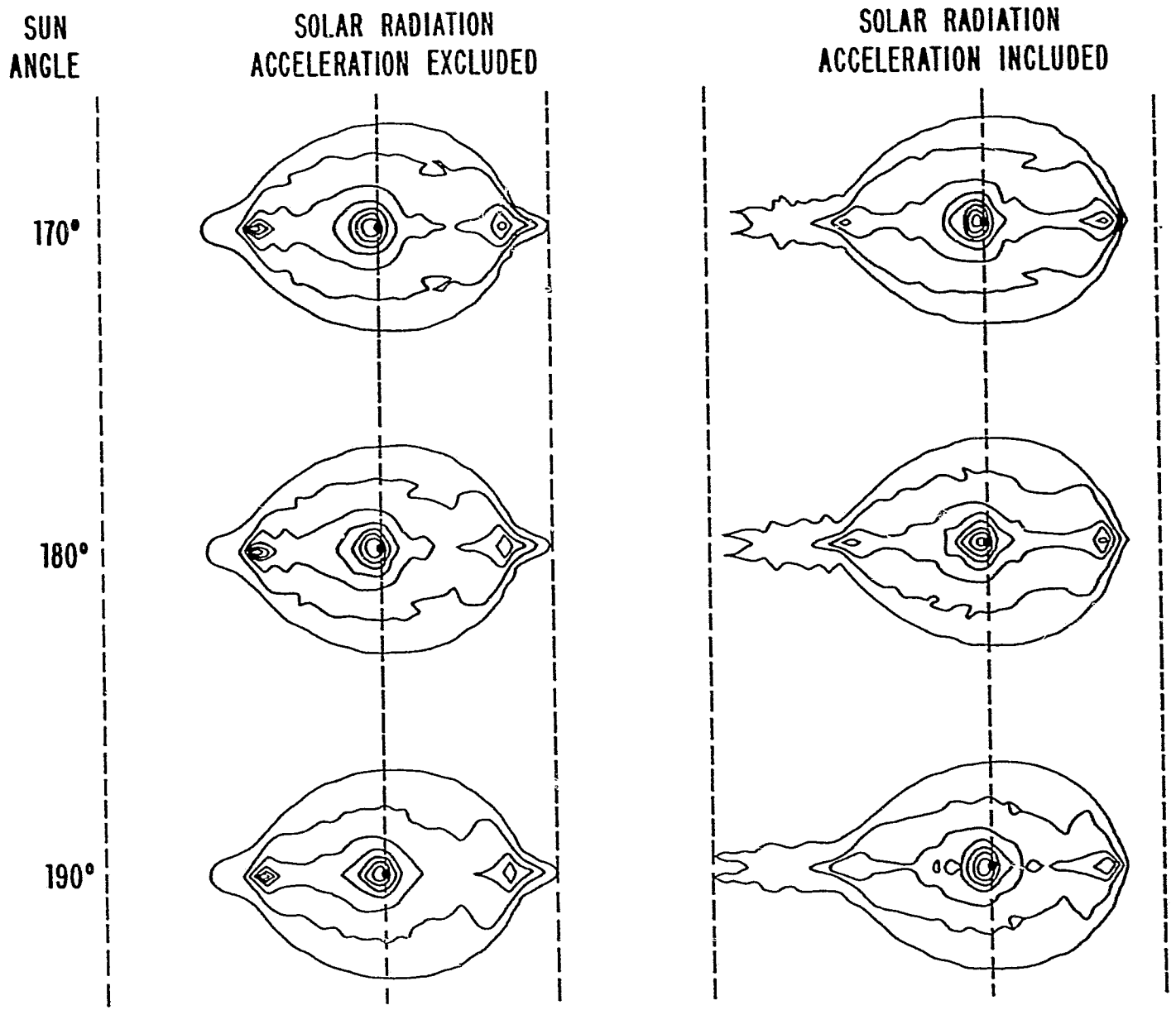

Figure 5

SODIUM CLOUD OF Io

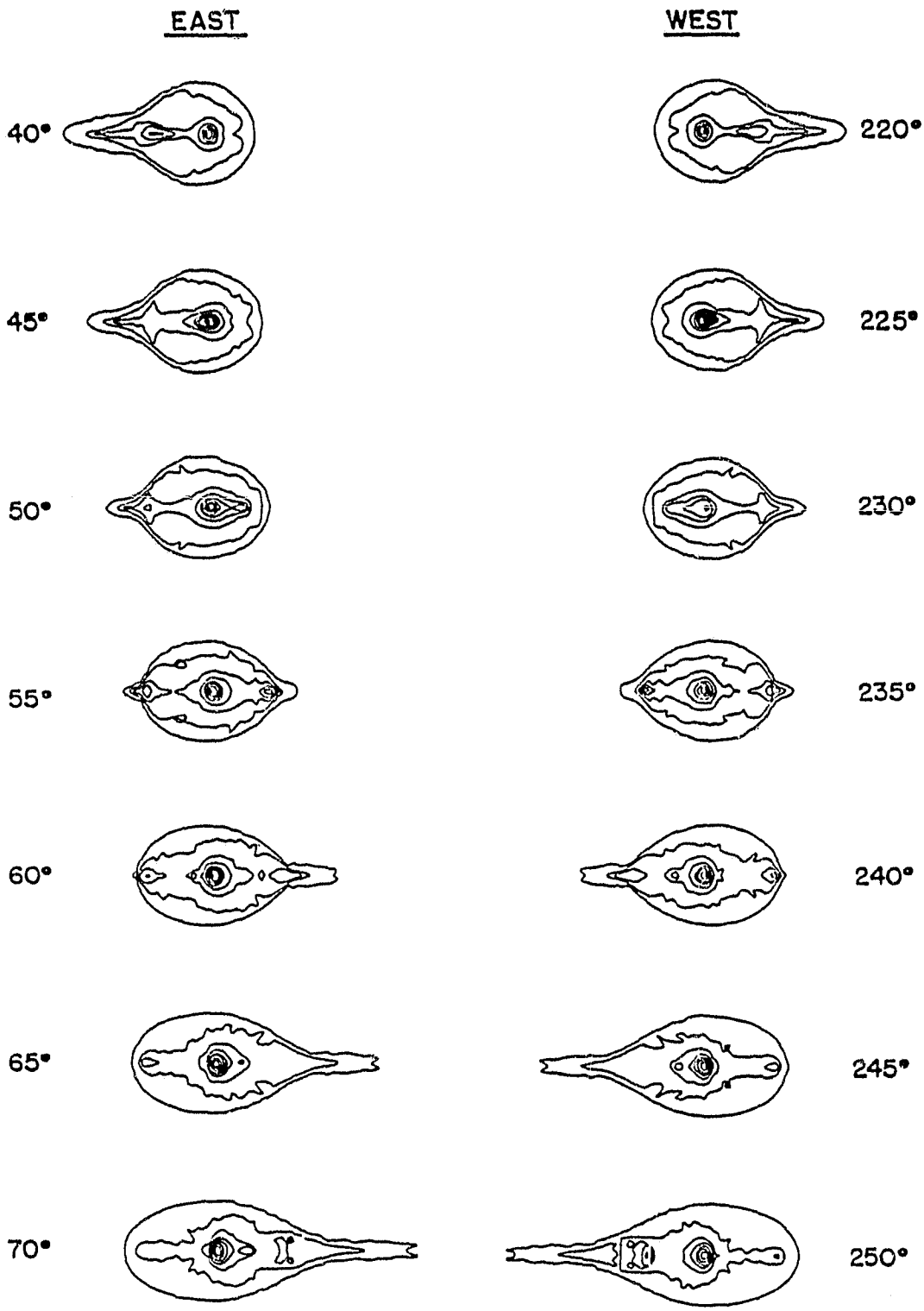

Figure 6

SODIUM CLOUD OF Io

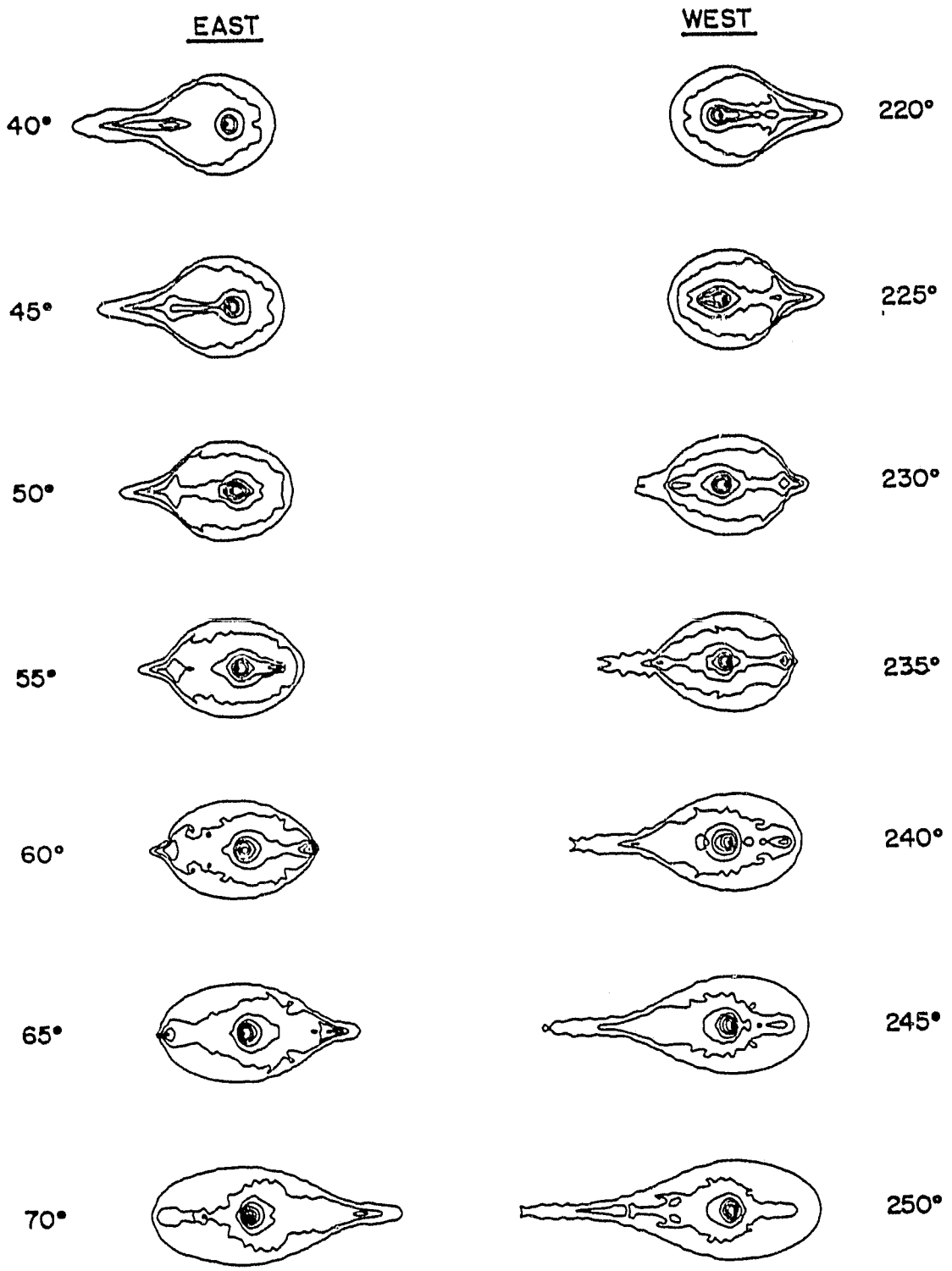

Figure 7

Figure 8

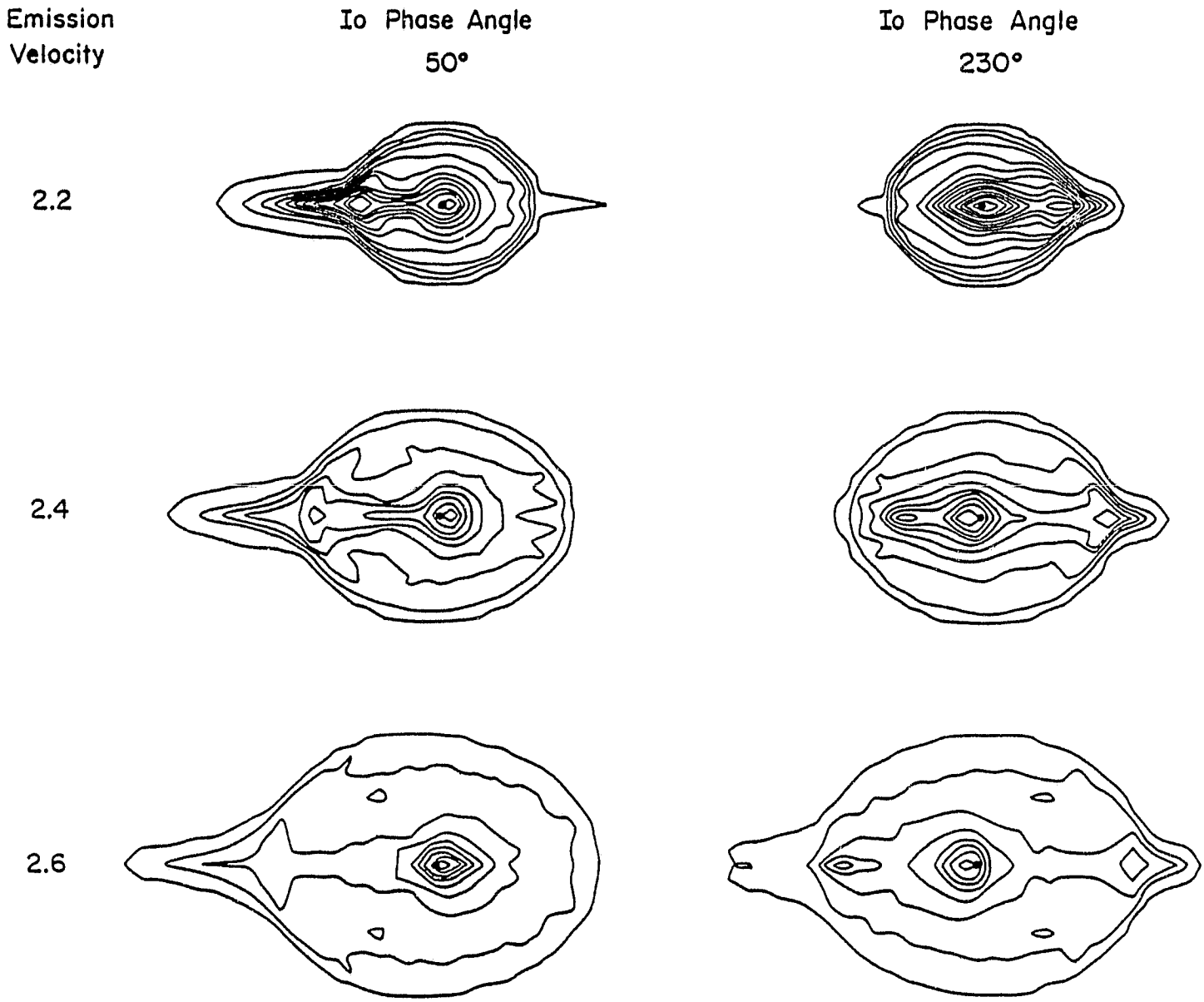

Figure 9

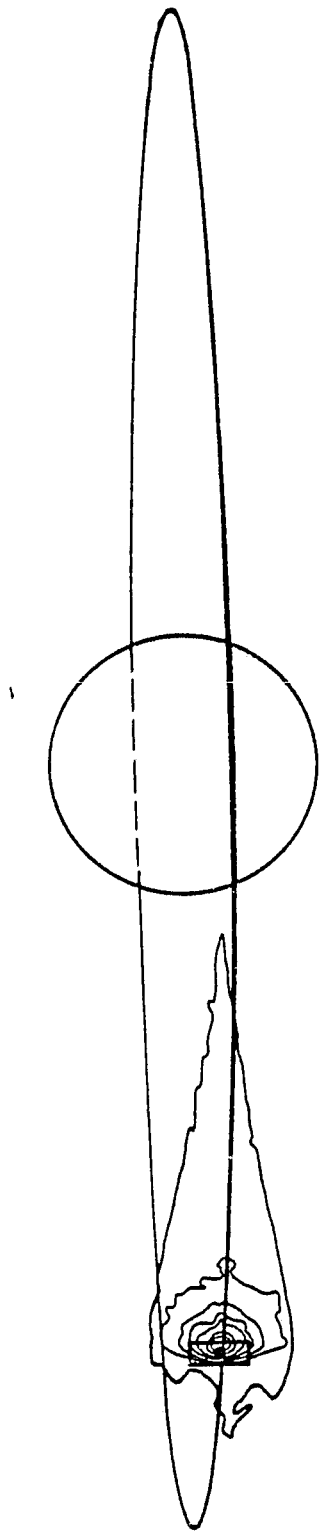

Figure 10

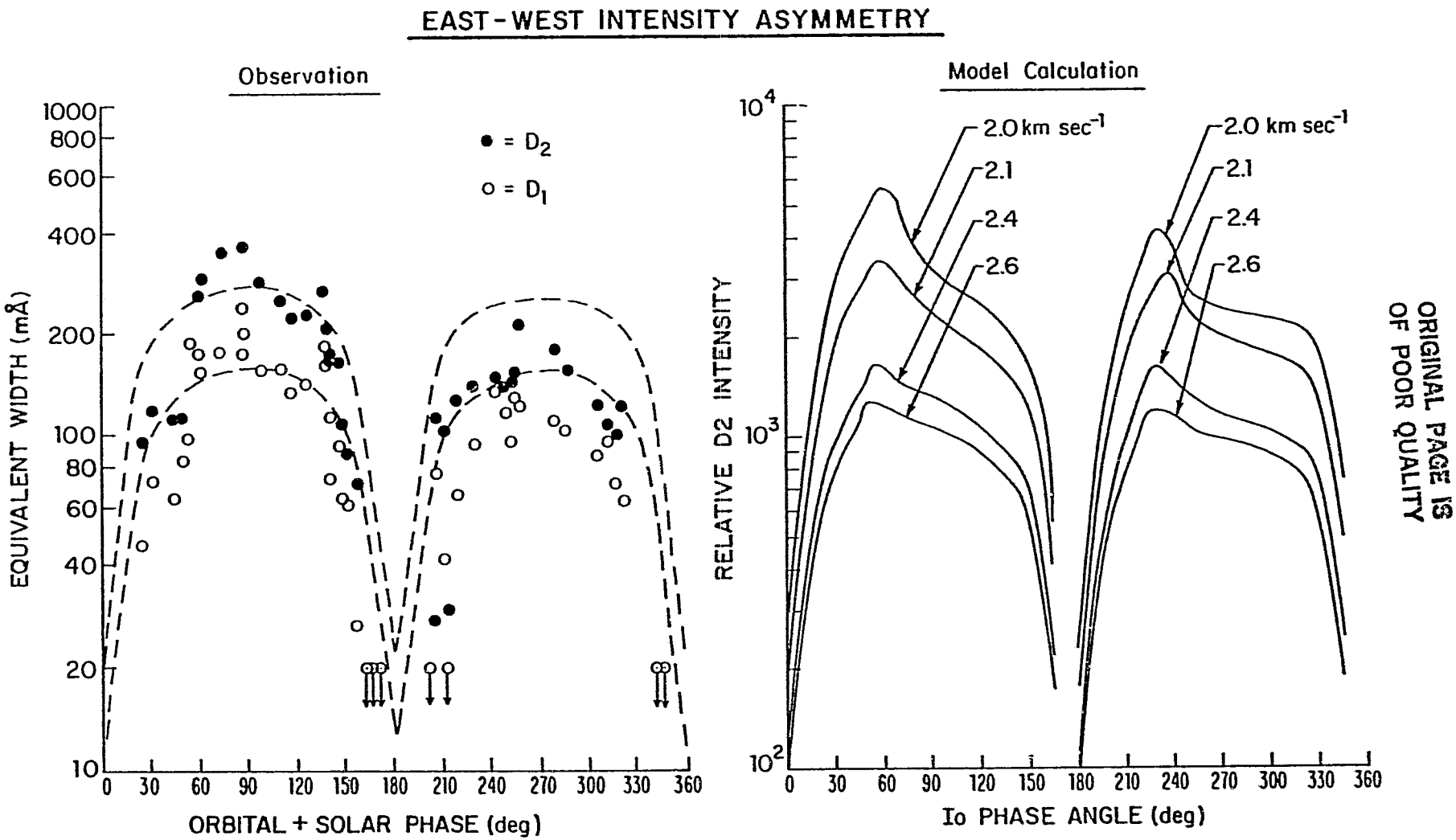
EAST-WEST INTENSITY ASYMMETRY
Observation
Model Calculation
EQUIVALENT WIDTH (mÅ)
1000
800
600
400
200
100
80
60
40
20
10
● = D2
○ = D1
0 30 60 90 120 150 180 210 240 270 300 330 360
ORBITAL + SOLAR PHASE (deg)
RELATIVE D2 INTENSITY
10^4
10^3
10^2
2.0 km sec^-1
2.1
2.4
2.6
2.0 km sec^-1
2.1
2.4
2.6
0 30 60 90 120 150 180 210 240 270 300 330 360
Io PHASE ANGLE (deg)
ORIGINAL PAGE IS
OF POOR QUALITY

Figure 11

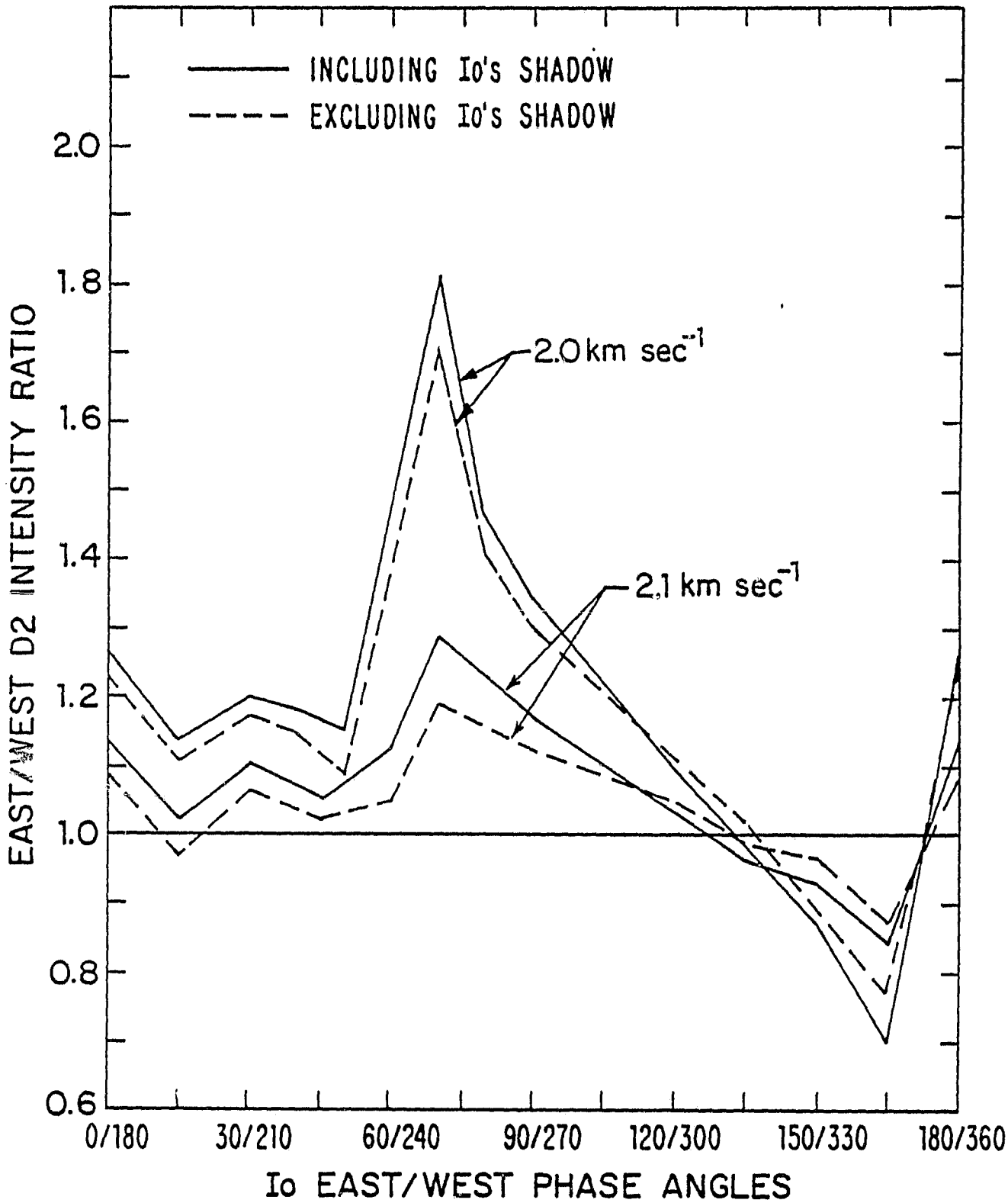

Figure 12

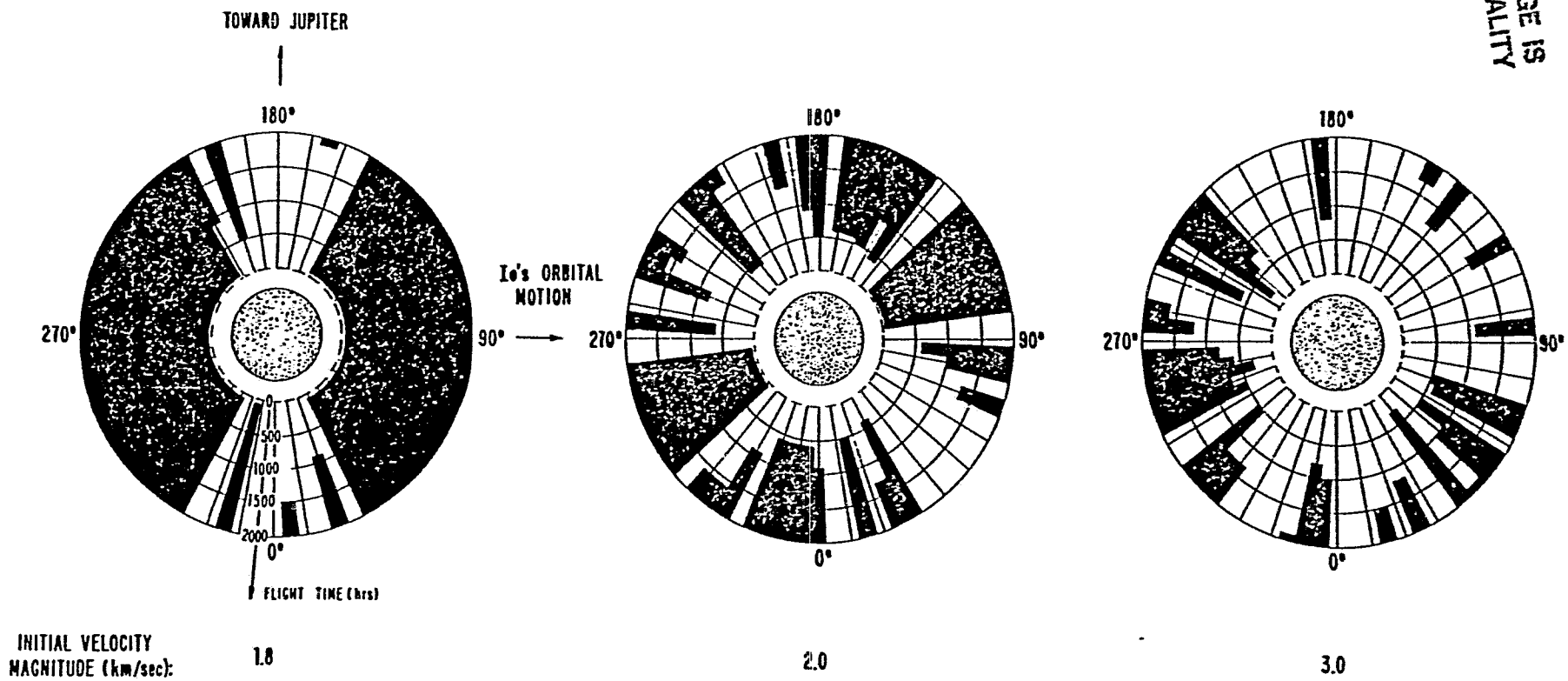

Figure 13

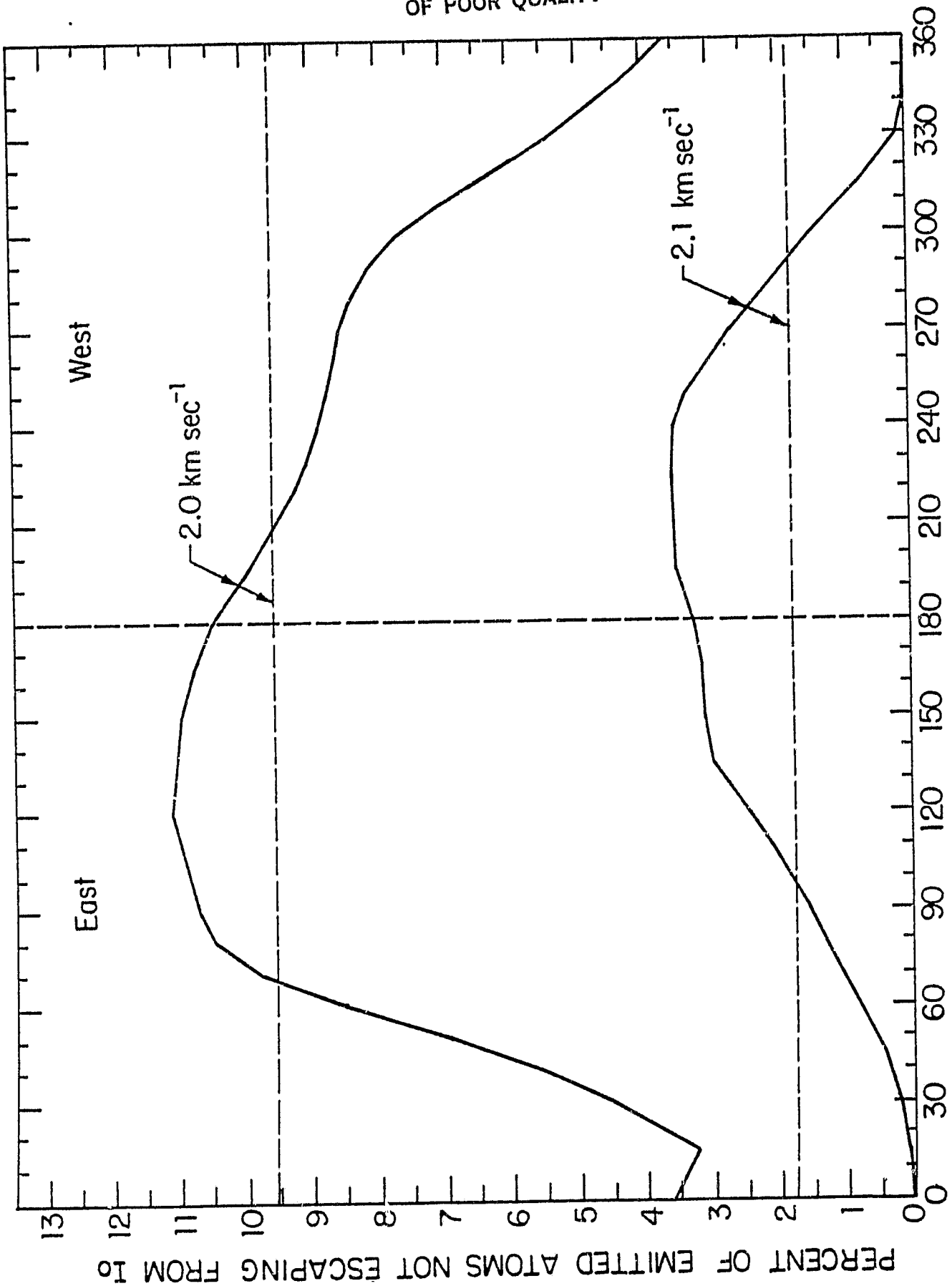

Figure 14